University of
South-Eastern Norway

www.usn.no

FMH606 Master's Thesis 2021
Process Technology

Improved Oil Recovery through Advanced Control

University of
South-Eastern Norway

Ashish Bhattarai

Faculty of Technology, Natural Sciences and Maritime Sciences
Campus Porsgrunn

University of
South-Eastern Norway

www.usn.no

Course: FMH606 Master's Thesis 2021
Title: *Improved Oil Recovery through Advanced Control*
Pages: *116*
Keywords: *uncertainty analysis, oil reservoir model, PI controller, MPC*

Student: *Ashish Bhattarai*
Supervisor: *Bernt Lie*
External partner: *Equinor ASA, Juan Videla*
Availability: ***Confidential***

Summary:

Norway is one of the major suppliers of oil and gas to the world market. Revenues from sales of oil and gas have played an important role in building modern Norwegian society. Oil and gas are trapped in the subsurface formation of relatively thin slabs of porous rock. The oil wells are drilled into the subsurface with an oil rig to extract the oil and gas from the reservoir. The production of oil can be increased by predicting and managing the future performance of the oil reservoir. However, because of the subsurface complexity and limited data, numerous uncertainties are present in oil reservoir characterization. These uncertainties should be considered for better future prediction of oil reservoir performance. In this paper, a simplified 2D control relevant model for a slightly slanting wedge-shaped black oil reservoir as in Zhang (2013) is made more realistic by incorporating model uncertainty. Furthermore, based on this model with uncertainty, a Proportional Integral (PI) controller is implemented to increase the oil production while minimizing the water production. The model in Zhang (2013) is re-implemented in Julia programming language. A standard package called *DifferentialEquations.jl*, available in Julia, is used to solve the model. A *Tsit5()* solver under this package solves the ODE problems with variable time steps which reduce the computational time and improve the performance. Furthermore, the uncertainty in the model is predicted via a parallel Monte Carlo simulation. A parallel Monte Carlo simulation is performed using *EnsembleProblem* in Julia. Finally, a PI controller is implemented in the model with uncertainty to control the valve opening of the Inlet Control Valves (ICVs) in the production well. The implementation of a PI controller improved the total oil production in 1000 days by 1.7873%. However, the effect is not very significant due to the limited capability of a PI controller. In this case, a more effective controller, such as a model predictive controller (MPC) is required.

The University of South-Eastern Norway accepts no responsibility for the results and conclusions presented in this report.

Preface

This thesis was performed as a part of the course work FMH606 in the department of Process, Energy, and Environmental Technology of the University of South-Eastern Norway (USN). This work is a part of a new research project at the University of South-Eastern Norway in *Digital wells for optimal production and drainage(DigiWell)*, funded by the Norwegian Research Council, project no. 308817, as well as energy company Equinor ASA, and USN. Also, this work was a continuation of a previous master's thesis *Improved oil recovery through advanced control* by Jianghui Zhang. The work was performed under the supervision of Professor Bernt Lie and external partner Juan Videla from Equinor ASA. I would like to express my gratitude to my supervisors for their continuous support and assistance throughout this work.

This thesis investigates the dynamics of a simplified 2D control relevant model for a slightly slanting wedge-shaped black oil reservoir. It is of interest to predict the uncertainty in the model via Monte Carlo simulation and to implement control strategies to enhance oil production.

Porsgrunn, May 19, 2021

Ashish Bhattarai

Contents

Preface 5

Contents 9
- List of Figures 12
- List of Tables 13

1 Introduction 17
- 1.1 Background 17
- 1.2 Previous Work 17
- 1.3 Scope and Outline 18

2 Overview of Fields 21
- 2.1 Oil Reservoir 21
- 2.2 Oil Wells 23
  - 2.2.1 Horizontal wells 24
  - 2.2.2 Coning of gas and water 24
    - 2.2.2.1 Water coning and heel-toe effect 26
    - 2.2.2.2 Water coning due to heterogeneity 26
  - 2.2.3 Inflow control strategies 27
    - 2.2.3.1 Inflow control devices (ICDs) 27
    - 2.2.3.2 Smart wells 28

3 Basic Concepts in Reservoir Simulation 31
- 3.1 Darcy's law 31
- 3.2 Rock properties 32
  - 3.2.1 Porosity 33
  - 3.2.2 Absolute permeability 33
    - 3.2.2.1 Permeability variation and permeability averages 34
  - 3.2.3 Fluid saturation and constraints 35
  - 3.2.4 Wettability 35
  - 3.2.5 Capillary pressure 35
  - 3.2.6 Effective and relative permeability 36
- 3.3 Fluid properties 38
  - 3.3.1 Formation volume factors 38
  - 3.3.2 Physical classification of crude oils 38

3.3.3 Classification of reservoir fluids 39
3.3.4 Important measurement terms in multi-phase fluid flow 39
3.3.4.1 Water cut 40
3.3.4.2 Gas liquid ratio 40
3.3.4.3 Well productivity index 40

4 Model Uncertainties, Advanced Control Strategies, and State Estimation 41
4.1 Model uncertainties 41
4.2 Advanced control strategies 41
4.2.1 Model predictive controller 42
4.2.1.1 Subspace identification 43
4.2.2 PI controller 44
4.2.2.1 Discretization and tuning of a PI controller 44
4.3 State estimation 46

5 Model Overview 47
5.1 Two-phase flow in a Porous Media 47
5.2 Model objective 47
5.3 Model development 49
5.3.1 Step 1: Introduction to the relevant balance laws 49
5.3.2 Step 2: Relate the quantities in the balance law to the inputs and outputs 50
5.3.2.1 Representation of the Well: 54
5.3.2.2 Assumptions and Model Simplification 57
5.3.2.3 Mobility determination at the integration points 62
5.3.2.4 Representation of valve and pipe 62
5.3.3 Numerical Solution 63
5.3.3.1 Boundary conditions 65
5.3.3.2 Pressure Equation For Incompressible Immiscible flow 66
5.4 Model summary 67

6 Implementation of model 75
6.1 Implementation of oil reservoir and well model in Julia 75
6.1.1 Simulation setup 75
6.1.2 Curve fitting for the relationship between saturation and relative permeability 75
6.1.3 Simulation results and discussion 75
6.1.3.1 Fluid flow rates at the well and water cut 77
6.1.3.2 Bottom hole pressure 78
6.1.3.3 Pressure profile 79
6.1.3.4 Saturation profile 80
6.1.3.5 Total oil and water production 81
6.1.4 Implementation of Monte Carlo Simulation 83

6.2 Implementation of PI controller 89
6.2.1 Implementation of PI controller based on model with uncertainties . . 92

7 Conclusion 97

8 Future work 99

Bibliography 99

A Master's Thesis Task Description 105

B List of Codes and Additional Results 109
B.1 Implementation of model with fully open ICVs 109
B.2 Implementation of PI controller in the model 109
B.3 Implementation of Monte Carlo simulation in model with fully open ICVs 109
B.4 Implementation of Monte Carlo simulation in model with PI controller 109
B.5 Calculation of fluid flow distribution at the production well 110
B.6 Curve fitting for the water saturation and relative permeability data 110
B.6.1 Pressure and water saturation profiles after implementation of PI controller. 113
B.6.2 Water saturation and permeability data 113

List of Figures

2.1 Equinor Peregrino oil field in Brazil (Editor 28th jun 2016). 22
2.2 Oil reservoir geographical view (Crotogino 2016). 22
2.3 Schematic view of water flooding oil reservoir with horizontal well (Völcker et al. 2011). 23
2.4 Schematic of oil well (Hasan 2015). 25
2.5 Categories of horizontal well (Jahn et al. 2008). 26
2.6 Heel-toe effect in a horizontal well (Salamander 2021). 27
2.7 Production well with ICDs and without ICDs (Chammout et al. 2017). . 28
2.8 Intelligent well completion (Barreto & Schiozer 2015). 29

3.1 Darcy's experiment (Ringrose & Bentley 2015). 32
3.2 Types of flow (Ringrose & Bentley 2015). 34
3.3 Water saturation (S_w)versus relative permeability (k_rel) (*Oil and water wet permeabilities* 2014). 37

4.1 Smart wells expressed as a closed loop model-based control process (Zhang 2013). 42
4.2 Block diagram of PID controller (Zhang 2013). 44

5.1 (a) Schematic view of the reservoir and (b) geometrical characteristics of the reservoir (Zhang 2013). 48
5.2 Model functional diagram. 48
5.3 A single cell of the reservoir (Zhang 2013). 49
5.4 2D diagram of horizontal well in a single cell. 56
5.5 The block-centered grid system and a five-point stencil scheme (Zhang 2013). 57
5.6 Single cell of the reservoir in (i_r, i_ℓ) coordinate (Zhang 2013). 58

6.1 Relation between water saturation S_w and relative permeabilities. 77
6.2 Water cut at the well at different positions along the well length. 78
6.3 Total flow rates of oil and water, respectively at the well. 79
6.4 Bottom hole pressure at the well heel. 80
6.5 Pressure profiles at different radius and different length after 400 days. . . . 81
6.6 Pressure profiles after different days of production. 82
6.7 Average pressure profile at different radius. 83
6.8 Water saturation profiles after different days of production. 84

6.9 Average water saturation profile at different radius. 85
6.10 Total production of oil in 1000 days. 85
6.11 Total production of water in 1000 days 86
6.12 Monte Carlo simulation for production of oil in 1000 days. 87
6.13 Monte Carlo simulation for production of water in 1000 days. 87
6.14 Monte Carlo simulation for water cut at $\ell = 0.5L$. 88
6.15 Monte Carlo simulation for flow rate of oil. 88
6.16 ICVs control signals. 90
6.17 Comparison of total production of oil in 1000 days with and without PI controller. 91
6.18 Comparison of total production of water in 1000 days with and without PI controller. 91
6.19 Comparison of total volumetric flow rates of oil and water with and without PI controller. 92
6.20 Comparison of water cut at the well at $\ell = 0.5L$ with and without PI controller. 93
6.21 Comparison of bottom hole pressure at the well heel with and without PI controller. 93
6.22 Comparison of Monte Carlo simulation for production of oil in 1000 days with PI controller (green dot lines) and without PI controller (maroon solid lines). 94
6.23 Comparison of Monte Carlo simulation for production of water in 1000 dayswith PI controller (red dot lines) and without PI controller (blue solid lines). . 95

B.1 Pressure profile for model with PI controller. 111
B.2 Saturation profile for model with PI controller. 112

List of Tables

2.1 Description of the value range for a different types of horizontal wells (PetroWiki 2018). 24

3.1 Classifications of wettability (Dandekar 2013). 36
3.2 Classification of crude oils based on API (Wikipedia 2021). 39
3.3 Basic characteristics of different types of reservoir fluids (Dandekar 2013). 39

5.1 Descriptions of the inputs and outputs of the oil reservoir model. 72
5.2 Description of parameters, the algebraic variables, and the differential variables used in oil reservoir model. 73

6.1 Operating conditions for black oil model. 76
6.2 Water cut and volumetric flow rate of oil, and water. 78
6.3 Total oil and water production in 1000 days. 81
6.4 Monte Carlo simulation setup. 83
6.5 Simulation results based on model with uncertainties. 86
6.6 Total oil and water production and average water cut in 1000 days after implementing PI controller. 94

Nomenclature

Symbol	**Explanation**
∇	Gradient operator
C_{rock}	Rock compressibility
C_{η}	Fluid compressibility
η	Fluid phase
J	Well productivity index

1 Introduction

Hydrocarbons are trapped in the subsurface formation of relatively thin slabs of porous rock. The oil wells are drilled into the sub-surface with an oil rig to extract the hydrocarbons from the reservoir (Wikipedia 2020). After drilling of wells into the subsurface with several single or multi-branch pipes, holes are made in the base of the well to enable hydrocarbons to pass into the bore from the reservoir. The hydrocarbons are then transported to the surface through the pipe system (Zhang 2013).

1.1 Background

To maximize the economic value of an oil field in oil production, it is essential to maximize the flow rate of oil from an oil reservoir to the surface while minimizing the water fraction in the oil. Various technologies have been developed to optimize the production of oil from a reservoir. These technologies are typically installed within the well and can be operated remotely. A well equipped with these types of technologies is generally referred to as a smart well. Wells with a controllable downhole inflow device coupled with advanced control technologies is one of them. Controllable downhole inflow devices like ICV[1] coupled with advanced control strategies help to improve the oil recovery factor by manipulating the inflow rate and bottom hole pressure of the production well (Nævdal et al. 2006).

An advanced controller like model predictive controller (MPC), Proportional-Integral-Derivative (PID) controller should be developed to control the fluids inflow at the well. A simplified reservoir model with pipes and completion should be developed to predict the future performance of a reservoir.

1.2 Previous Work

A computer model can be developed based on seismic investigations, geological data, and physical laws (Darcy's law, two-phase flow). Various commercial oil reservoir simulators such as ECLIPSE, MRST[2], INTERSECT, MEERA, ReservoirGrail, etc are in use.

---

[1] Inflow control valves

The control relevant model for slightly slanting wedge-shaped black oil reservoir was developed in Zhang (2013). Geological features like rock permeabilities and porosities were assumed to be homogenous in a black oil reservoir model. The model was based on mass conservation of oil and water, and dispersive flow described by Darcy's law. In Zhang (2013), it was found that the use of PI controller in remotely controlled ICVs in combination with a simplified reservoir model with pipes improved the oil production rate by up to 7%.

In Völcker et al. (2011), gradient-based optimization methods in a nonlinear MPC control framework were implemented in a smart well in combination with a reservoir model to increase the oil recovery and economic value of the reservoir.

1.3 Scope and Outline

In this work, a simplified 2D control relevant model for a slightly slanting wedge-shaped black oil reservoir as in Zhang (2013) is made more realistic by incorporating model uncertainty. Furthermore, based on this model with uncertainty, a Proportional Integral (PI) controller is implemented to increase the oil production while minimizing the water production. Initially, it was planned to implement MPC instead of a PI controller. However, this task could not be performed because of the time constraint.

In Chapter 2, some basic concepts in reservoir engineering, such as the description of the oil reservoir and oil wells, types of oil wells, etc., are given. Moreover, the disadvantages of horizontal wells such as water, and gas coning are given. Finally, a brief introductions of inflow control strategies and smart wells are given.

In Chapter 3, basic concepts in reservoir engineering, such as introduction to Darcy's law, introduction to rock and fluid properties, etc., are given.

In Chapter 4, first, an overview of uncertainties in the oil reservoir model is given. Then, an introduction to advanced control strategies like MPC, and PI controller is given. Finally, the need for state estimation in the oil reservoir model is described.

In Chapter 5, a model overview of two-phase flow in a porous media is given. Then, the overview of a simplified 2D control relevant model for a slightly slanting wedge-shaped black oil reservoir model development is given.

In Chapter 6, first, a model developed in Chapter 5 is implemented in Julia. Second, the simulation setup and boundary conditions are described. Finally, results from the simulation and their discussion are given. Chapter 7 will be for concluding remarks. Also, in Chapter 8, possible future works are described.

---

[2] MATLAB Reservoir Simulation Toolbox by SINTEF

The task description of this thesis work is given in Appendix A. Appendix B contains a list of related codes and additional results obtained after implementing the PI controller in the model.

2 Overview of Fields

An oil field consists of a reservoir in a shape that will trap hydrocarbons and that is covered by impermeable rock. Numerous wells are drilled into the subsurface of an oil field region for the production of petroleum/crude oil. An oil reservoir usually extends up to several hundred kilometers across thus, multiple wells are required to be drilled across the oil field area. There are more than 65,000 oil fields scattered around the world (Li 2011). Statoil Peregrino oil field with the platform is shown in Figure 2.1.

Oil is transported to floating production storage and offloading vessel unit (FPSO) after the production from offshore production platforms. The oil is then transported to land by pipeline or tanker (Zhang 2013).

2.1 Oil Reservoir

An oil reservoir is a subsurface pool of hydrocarbons trapped in formations of relatively thin slabs of porous rock. They are found at a depth of hundreds to thousands of meters (Zhang 2013). Oil reservoirs are generally categorized into conventional and unconventional reservoirs. In conventional reservoirs, the hydrocarbons are trapped by overlying rock formations with lower permeability. While in unconventional reservoirs, hydrocarbons are trapped in the rocks with high permeability and high porosity. The geographical view of a typical oil reservoir is shown in Figure 2.2.

Oil extraction from the oil reservoir is divided into three stages: primary recovery, secondary recovery and, tertiary recovery or enhanced recovery. During the primary stage of oil recovery, the hydrocarbon naturally flows into the oil production well. The natural flow of hydrocarbons is due to (a) natural water displacing oil downward into the oil production well, (b) expansion of the petroleum gas and other gases dissolved in the crude oil (c) drainage of oil caused by gravity (Wikipedia 2020). Recovery factor, the percentage of hydrocarbon in place that can be produced, ranges from 5% to 15% during the primary recovery stage (Tzimas et al. 2005). The pressure in the oil reservoir falls over time. When the pressure in the oil reservoir is insufficient to naturally drive the oil to the surface, secondary oil recovery is required. The fluids like water or gas are injected externally to increase the oil reservoir pressure during the secondary oil recovery method as shown in Figure 2.3. The recovery factor after primary and secondary oil recovery

Figure 2.1: Equinor Peregrino oil field in Brazil (Editor 28th jun 2016).

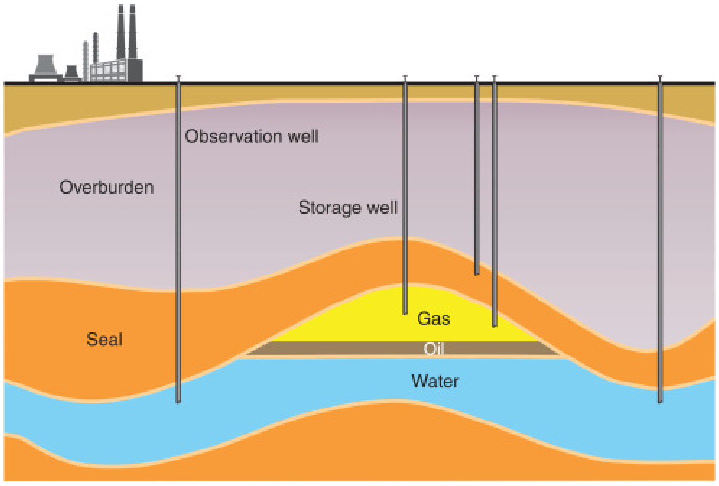
Observation well
Overburden
Storage well
Gas
Seal
Oil
Water

Figure 2.2: Oil reservoir geographical view (Crotogino 2016).

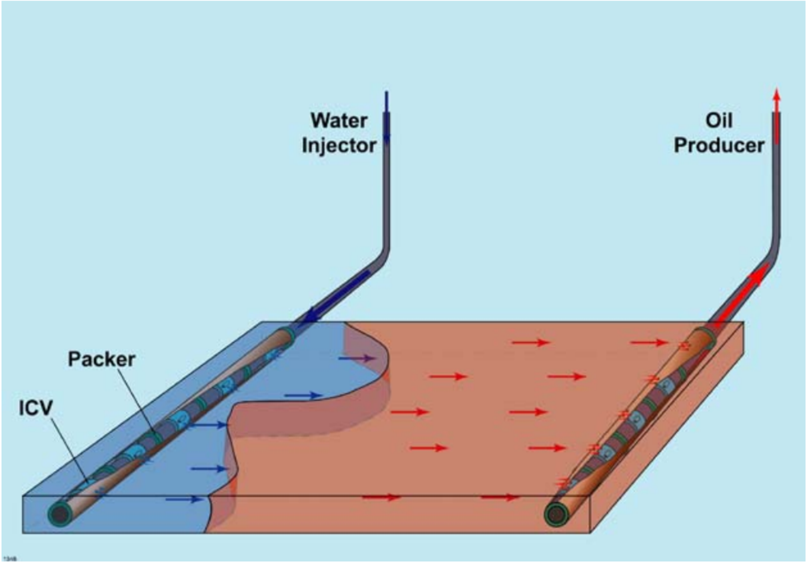

Figure 2.3: Schematic view of water flooding oil reservoir with horizontal well (Völcker et al. 2011).

stages is between 35% to 45% (Tzimas et al. 2005). Finally, tertiary recovery or enhanced oil recovery involves increasing the mobility of oil to enhance oil extraction. Oil mobility increases with a decrease in its viscosity. The tertiary oil recovery technique consists of TEOR[1] methods to heat the oil in the reservoir, injection of surfactants into the reservoir to alter the surface tension between water and the oil, reduction of oil viscosity by CO_2 flooding (Wikipedia 2020). Further 5% to 15% increase in recovery factor can be achieved after the tertiary recovery stage (Tzimas et al. 2005).

2.2 Oil Wells

An oil well is a hole dug into the sub-surface to bring oil or other hydrocarbons to the surface. There are several different ways that an oil well can be drilled to maximize the well output. The most common way of drilling a well today is conventional well drilling. In conventional well drilling, the drilling location is chosen above the oil reservoir and the well is drilled vertically downward. However, in horizontal well drilling, wells are drilled and steered to enter a reservoir nearly horizontally. These wells are more effective in hitting the targets and stimulate the reservoir compared to the vertical well. Offshore wells are another type of wells that are drilled in the water instead of onshore. Multilateral wells are wells that have several branches off of the main borehole that drain a separate part of the reservoir (Wikipedia 2020).

---

[1] Thermally enhanced oil recovery

Well type	Radius [ft]	Build rate [°/100 ft]	Average Lateral section [ft]
Long-radius	$1000-3000$	$2-6$	up to 8000
Medium-radius	$125-1000$	$6-50$	3000
Short-radius	$20-40$	$0.015-0.03$	$200-900$

Table 2.1: Description of the value range for a different types of horizontal wells (PetroWiki 2018).

Oil wells are drilled into the sub-surface with the help of a drilling rig. Drilling bores the hole through many layers of dirt until it reaches the oil and gas reservoir. The size of the borehole ranges from 12.5 to 90 centimeters wide. The drill is pushed down by the weight of the piping above it to cut through the rocks. A thick fluid known as drill mud is continuously pumped into the well as shown n Figure 2.4. This mud helps in the drilling process by maintaining pressure below ground in the well as well as by collecting the debris created from drilling. To lengthen the well, piping sections are attached as the drilling digs deeper. After the drilling, the well is completed and cased. Well casing is the lining inserted between the edge of the well and the well itself. It helps to support the well structurally. Cement is used to fill the annulus between the casing and the borehole for stability and to prevent groundwater contamination from seepage. Small holes called perforation are drilled in each segment of the casing to offer a way for the oil from the reservoir to flow into the production tubing[2].

2.2.1 Horizontal wells

Horizontal wells are characterized based on their build rate. The build rate of a horizontal well is the positive change in inclination over a normalized length. Horizontal wells are classified into three categories based on the build rate: long-radius, medium-radius, and short-radius as shown in Figure 2.5 (Moradi 2020).

The typical value range for build rate, radius, and average lateral section length of different types of wells are shown in Table 2.1.

2.2.2 Coning of gas and water

Coning of gas and water is one significant reason for the decrease in efficiency of a horizontal well. Water and gas coning happen because of the movement of gas and water zone up towards the wellbore as a cone. This can altogether decrease the well profitability. Deferring water and gas advancement is one of the primary estimates that should be taken to augment the efficiency of an oil field (D.G. Hatzignatiou 1994).

---

[2] https://en.wikipedia.org/wiki/Oil_well

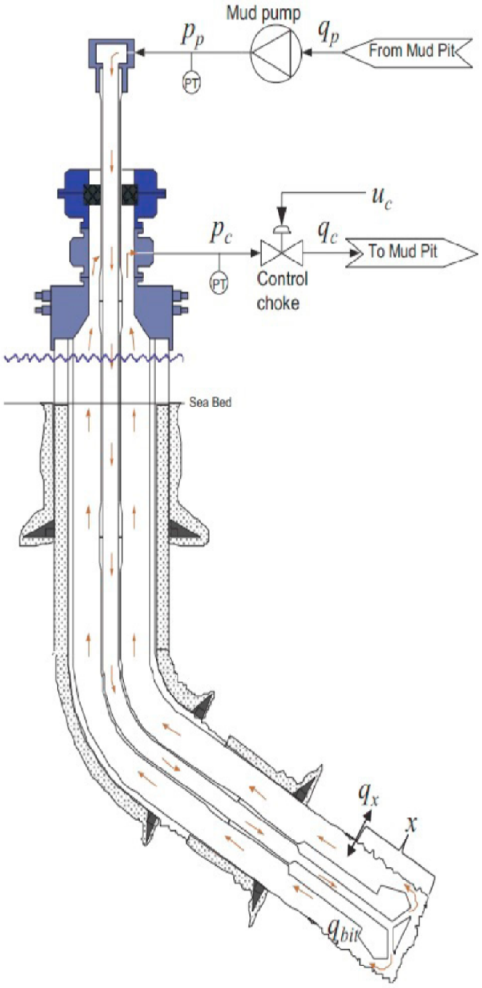
Mud pump
p_p
q_p
From Mud Pit
PT
u_c
p_c
q_c
To Mud Pit
PT
Control
choke
Sea Bed
q_x
x
q_{bit}

Figure 2.4: Schematic of oil well (Hasan 2015).

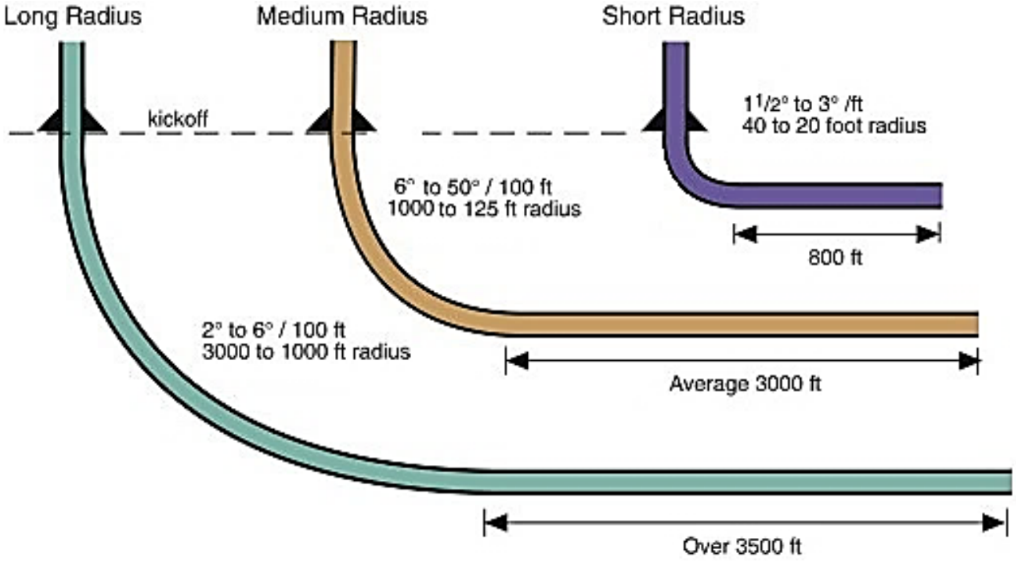
Long Radius
Medium Radius
Short Radius
kickoff
1 1/2° to 3° /ft
40 to 20 foot radius
800 ft
6° to 50° / 100 ft
1000 to 125 ft radius
Average 3000 ft
2° to 6° / 100 ft
3000 to 1000 ft radius
Over 3500 ft

Figure 2.5: Categories of horizontal well (Jahn et al. 2008).

2.2.2.1 Water coning and heel-toe effect

In a horizontal well, pressure drawdown, the pressure difference between the reservoir and well, will be unequal because of the frictional pressure drop in the well. The pressure drawdown will be maximum at the heel of the well while it is comparatively low at the toe of the well. The higher the pressure drawdown, the higher the driving force for moving the reservoir fluids towards the well. Thus, the water cone will reach sooner at the heel compared to the toe of the well. This is called the heel-toe effect and is shown in Figure 2.6 (Salamander 2021).

2.2.2.2 Water coning due to heterogeneity

In the case of heterogeneous reservoirs, the characteristics such as permeability of the reservoir change with the position along the oil reservoir. This difference in permeability within the oil reservoir has a significant effect on the production of oil. For horizontal well, the permeability varies along the well. Since the flow resistance is lower in the high permeable zones, inflow to the well is higher in the low permeable zones compared to other zones. This phenomenon causes an uneven inflow profile along the well. The water cone grows faster in the zones with high inflow causing early water breakthrough (Aakre 2017).

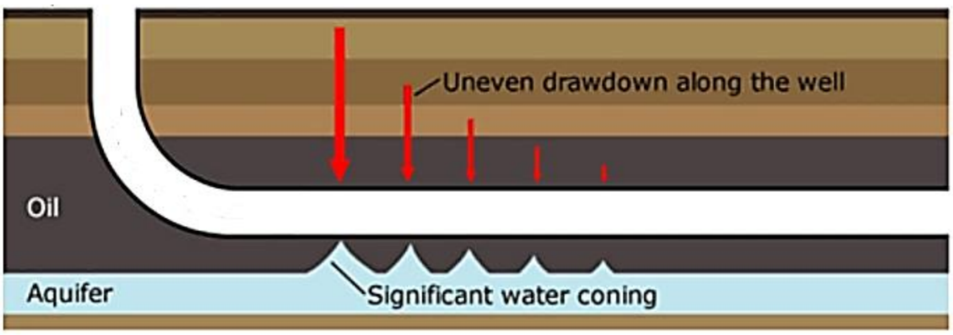

Figure 2.6: Heel-toe effect in a horizontal well (Salamander 2021).

2.2.3 Inflow control strategies

Inflow control strategies are applied to overcome the early water coning due to the heel-toe effect and heterogeneity along the horizontal well. Some of the inflow control strategies are as follows.

2.2.3.1 Inflow control devices (ICDs)

A passive inflow control device (ICD) is a device that restricts the flow and has no moving parts. They are used for choking the flow by adding the extra pressure drop and thereby helps to maintain homogeneity along the horizontal well. Passive inflow control valves are classified as Channel-type ICD, Nozzle-type ICD, Orifice-type ICD (Ouyang et al. 2009).

In horizontal wells, many ICDs are distributed along the well length. The pressure drop across the ICD depends upon the flow rate, geometry of ICD, and fluid density. Initially, the oil production is lower in a well with ICD completion compared to an open-hole well. However, ICDs can delay the early water breakthrough by balancing the inflow along the well thereby increasing the oil production in the long term. The effect of ICD in a horizontal can be seen in Figure 2.7. The main disadvantage of passive ICDs is that they are not able to choke the water back after the water breakthrough. Thus, after the water breakthrough, the well must be shut down to avoid increasing the water cut more than the capacity of the separation facilities (Moradi 2020).

.

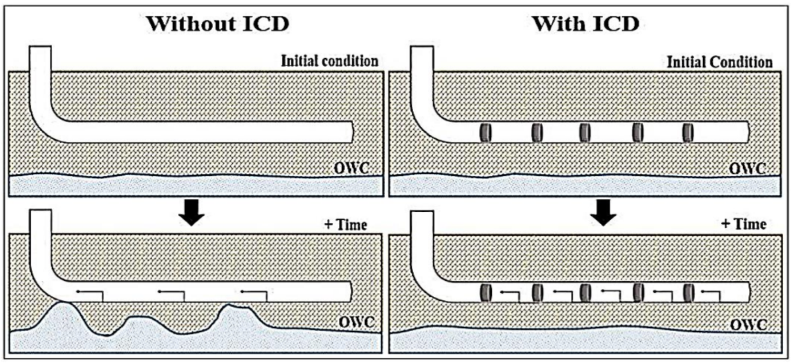
Without ICD
With ICD
Initial condition
Initial Condition
OWC
OWC
+ Time
+ Time
OWC
OWC

Figure 2.7: Production well with ICDs and without ICDs (Chammout et al. 2017).

2.2.3.2 Smart wells

Intelligent or smart well applications are widely developed nowadays. Wells equipped with a variety of down-hole sensors and remotely controlled ICVs are considered smart-wells. ICVs are active sliding valves, operated remotely utilizing a controlling system. The valves are shut off when the water cut is higher than the specified minimum water cut. The main objective of a smart-well system is to maximize increased production, improved reservoir recovery, minimize capital cost, etc. An example of intelligent-well completion is shown in Figure 2.8.

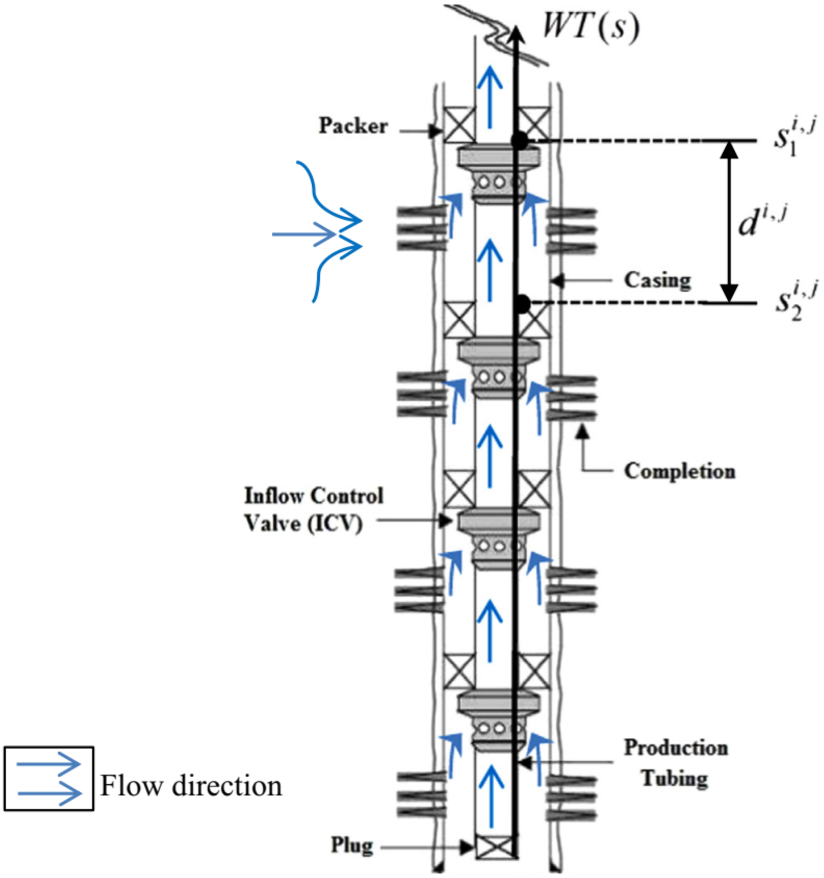
$WT(s)$
Packer
$s_1^{i,j}$
$d^{i,j}$
Casing
$s_2^{i,j}$
Completion
Inflow Control Valve (ICV)
Production Tubing
Flow direction
Plug

Figure 2.8: Intelligent well completion (Barreto & Schiozer 2015).

3 Basic Concepts in Reservoir Simulation

The purpose of this section is to briefly summarize some concepts in modeling porous media flow which includes rock properties, fluid properties, Darcy's law.

3.1 Darcy's law

The basic permeability equation is based on the field experience and observation of Henry Darcy while working on a pressurized water distribution system in the town of Dijon, France. His equation gives the relation between the flow rate and head of water draining through a pile of sand (Ringrose & Bentley 2015).

$$Q_d = K_d A_d \frac{\Delta H_d}{L_d}, \tag{3.1}$$

where

Q_d = volume of flux of water

K_d = constant of hydraulic conductivity or

coefficient of permeability

A_d = cross sectional area

ΔH_d = height of a water column

L_d = length of sand column.

The subscript d in Equation 3.1 indicates Darcy's law.

From Equation 3.1, we can derive a fundamental equation for flow in porous media based on dimensional analysis and the Naiver-Stokes equations for flow in cylinder pores:

$$u_d = -\frac{k_d}{\mu_d} \nabla \left(P_d + \rho g z\right) \tag{3.2}$$

where

u_d = intrinsic fluid velocity

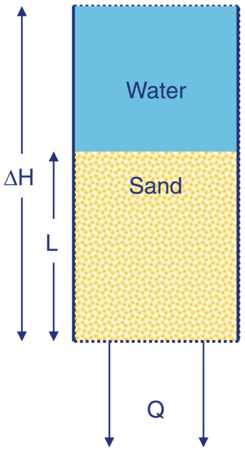

Figure 3.1: Darcy's experiment (Ringrose & Bentley 2015).

k_d = intrinsic permeability

μ_d = fluid permeability

∇P_d = applied pressure gradient

$\rho g \nabla z$ = pressure gradient due to gravity.

For homogeneous medium, permeability k_d has a single value. For the general case of heterogeneous rock medium, k_d is a tensor property.

SI-unit for permeability is m^2 however, it is commonly represented in Darcy (D), or mili-Darcy (mD). A 1 D permeability is defined as the transmission of fluid with viscosity of 1 cp through a homogeneous rock at a speed of 1 cm/s due to pressure gradient of 1 atm/cm.

Mathematically,

$$1\,\mathrm{D} = 1000\,\mathrm{mD} = \frac{(1\,\mathrm{cm}^3/\mathrm{s})\,(1\,\mathrm{cp})}{(1\,\mathrm{cm}^2)\,(1\,\mathrm{atm}/\mathrm{cm})} = 9.869 \times 10^{-13}\,\mathrm{m}^2 \qquad (3.3)$$

3.2 Rock properties

Almost any naturally formed rock contains pores, and the distribution and volume fraction of such pores determine the rock properties. And these are the parameters governing the hydrocarbon flow in the reservoir (Aarnes et al. 2007).

3.2.1 Porosity

The rock porosity is the void volume fraction of the medium which is usually denoted by ϕ. The value of rock porosity ranges from zero to one, i.e., $\phi \in [0,1)$. The porosity usually depends on the pressure; the rock is compressible, and the rock compressibility is defined as

$$C_{\text{rock}} = \frac{1}{\phi}\frac{d\phi}{dP}, \tag{3.4}$$

where P is the overall reservoir pressure. It is customary to neglect the rock compressibility and assume that ϕ only depends on the spatial coordinates (Aarnes et al. 2007).

3.2.2 Absolute permeability

The absolute permeability of a rock which is denoted by K is a measure of the rock's ability to transmit a single fluid at certain conditions. Low permeability means that it takes significant pressure declines to transmit fluids through a rock. While on the other hand, high permeability rock allows fluid passes through the rock with fewer pressure drops. Absolute permeability is normally strongly correlated to ϕ. Rock formations like sandstone tend to have high porosity, and therefore transmit fluids readily. Permeability can vary with the temperature and pressure. When temperature, and pressure are changed, microfractures may open and significantly change the permeability (Aarnes et al. 2007).

In general, K is a tensor property, which means that permeability in different direction depends on the permeability in the other direction. Thus in a 2D plane with r and ℓ coordinates, K can be expressed as

$$K = \begin{bmatrix} K_{rr} & K_{r\ell} \\ K_{\ell r} & K_{\ell\ell} \end{bmatrix} \tag{3.5}$$

Here, $K_{r\ell}$ represents flow along r coordinate due to a pressure gradient along ℓ coordinate and thus K_{rr}, $K_{\ell r}$, and $K_{\ell\ell}$ are also expressed in a similar way. In practice, K is commonly assumed to be a diagonal tensor where off-diagonal terms like $K_{\ell r}$, and $K_{r\ell}$ are neglected. Equation 3.5 thus becomes

$$K = \begin{bmatrix} K_{rr} & 0 \\ 0 & K_{\ell\ell} \end{bmatrix} \tag{3.6}$$

To make the notation simpler, the terms K_{rr} and $K_{\ell\ell}$ are expressed as K_r and K_ℓ, respectively. If K_r and K_ℓ are the same, the medium is called isotropic. Additionally, different fluids will experience different permeability in the same rock sample because the definition of permeability involves certain fluids.

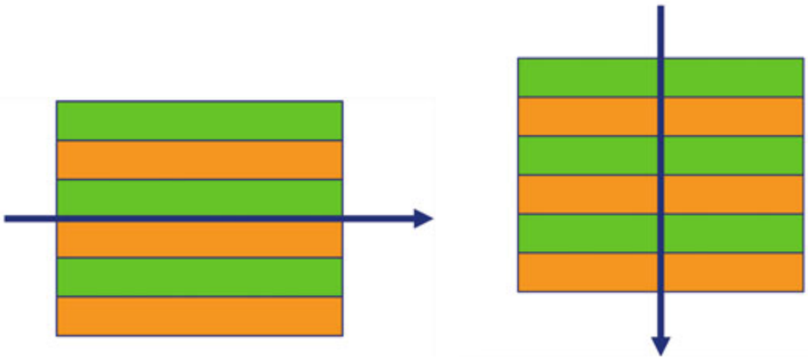

(a) Flow along with continuous parallel layers.
(b) Flow perpendicular to continuous parallel layers.

Figure 3.2: Types of flow (Ringrose & Bentley 2015).

3.2.2.1 Permeability variation and permeability averages

In reality, permeability in the oil reservoir is a highly variable property. Good stones could have permeabilities typically in the range of $1-1000\,\mathrm{mD}$, while the silt and clay-rich units could have permeabilities in the range of $0.001\,\mathrm{mD}$ or lower. Because of this highly variable nature, some form of averaging of permeability is required. The arithmetic average gives the correct permeability for flow along with continuous parallel layers, while the harmonic average gives the correct solution for flow perpendicular to continuous parallel layers (Ringrose & Bentley 2015). These two types of flows are shown in Figure 3.2.

Therefore, for flow along with continuous parallel layers,

$$K_{\text{arithmetic}} = \frac{\sum_1^{n_{\text{layers}}} K_i t_i}{\sum_1^{n_{\text{layers}}} t_i}.$$

Similarly, for flow perpendicular to continuous parallel layers,

$$K_{\text{harmonic}} = \left[\frac{\sum_1^{n_{\text{layers}}} \frac{t_i}{K_i}}{\sum_1^{n_{\text{layers}}} t_i}\right]^{-1}.$$

Here, $K_{\text{arithmetic}}$, and K_{harmonic} are the arithmetic and harmonic means of the permeabilities, respectively. The terms t_i, K_i, and n_{layers} denote thickness of the i^{th} layer, permeability of the i^{th} layer, and number of layers, respectively.

3.2.3 Fluid saturation and constraints

Fluid saturation is defined as the ratio of a fluid phase existing in a reservoir rock sample to the effective pore volume of the sample. It is denoted by S_η where η represents the fluid phase. Therefore, for a two-phase flow containing oil and water, the saturations are defined as follows (Dandekar 2013):

$$S_\mathrm{w} = \frac{\text{volume of water}}{\text{Effective pore volume}} \tag{3.7}$$

$$S_\mathrm{o} = \frac{\text{volume of oil}}{\text{Effective pore volume}}. \tag{3.8}$$

The saturation constraint satisfies

$$S_\mathrm{o} + S_\mathrm{w} = 1. \tag{3.9}$$

Similarly, for three-phase flow containing oil, water, and gas, the saturation constraint satisfies

$$S_\mathrm{o} + S_\mathrm{w} + S_\mathrm{g} = 1. \tag{3.10}$$

3.2.4 Wettability

When two immiscible phases are placed in contact with the solid surface, one of these phases is usually attracted to the surface more strongly than the other phase. This phase is identified as the wetting phase. While the other phase is the non-wetting phase. Wettability is related to rock mineralogy as well as the properties of the fluid pairs. Wettability can be classified to five main states (Dandekar 2013) and are described in Table 3.1.

3.2.5 Capillary pressure

Pores in the reservoir rocks are analogous to the capillary tube in that the diameter is small. When a porous medium is saturated with two or more immiscible fluids, the interface boundary between them is curved due to the interfacial forces between them. This interfacial curvature gives rise to a difference in the pressure across the interface called capillary pressure, P_c. Usually, the pressure of the non-wetting fluid is higher than that of the wetting fluid. Hence, capillary pressure is defined as the difference between

Type	Description
Oil-wet	The oil phase has much more tendency to spread on all pore surfaces of the rock. As a result, water will remain in the center of the pore.
Water-wet	The water phase will attract more towards the pore surface of the rock and as a result, oil and gas will remain in the center of the pore.
Fractional-wet	Some pore-space are strongly oil-wet while others are strongly water-wet.
Intermediate-wet	The pore surfaces have an equal preference for oil and water in this wettability state.
Mixed-wet	The larger pore spaces are oil-wet, and smaller pore spaces are water-wet.

Table 3.1: Classifications of wettability (Dandekar 2013).

the pressure of the non-wetting phase and the pressure of the wetting phase (Dandekar 2013). In a water-wet reservoir, the oil-water capillary pressure, P_{cow}, is calculated as (Dandekar 2013):

$$P_{\text{cow}} = P_{\text{o}} - P_{\text{w}}, \tag{3.11}$$

where P_{o}, and P_{w} are the pressure of oil, and water phases, respectively.

3.2.6 Effective and relative permeability

The general equation of Darcy's law, Equation 3.2, has been developed for a single-phase flow in a porous medium. However, in an oil reservoir, such a single-phase flow system rarely exists. Therefore, further modification in Darcy's law is necessary to cover multiphase flow in a porous medium. In a multiphase flow through porous media, the pore spaces are shared between multiple fluids and the flow of one fluid interferes with the other. To consider this fact, a new parameter called effective permeability, K_{eff}, is used instead of absolute permeability K. Effective permeability is measured by doing some lab experiments. Effective permeability generally depends on wetting characteristics, fluid saturation, and the geometry of pores. Thus, Darcy's equation is valid if the effective permeability of each phase is measured and used instead of using absolute permeability (Moradi 2020).

Furthermore, another parameter called relative permeability, k_{rel}, is used to evaluate the permeability of each phase in a multiphase flow system. Relative permeability is calculated by normalizing values of effective permeability by absolute permeability. Therefore, the relative permeability of phase η can be expressed as (Moradi 2020):

$$k_{\text{rel},\eta} = \frac{K_{\text{eff},\eta}}{K}. \tag{3.12}$$

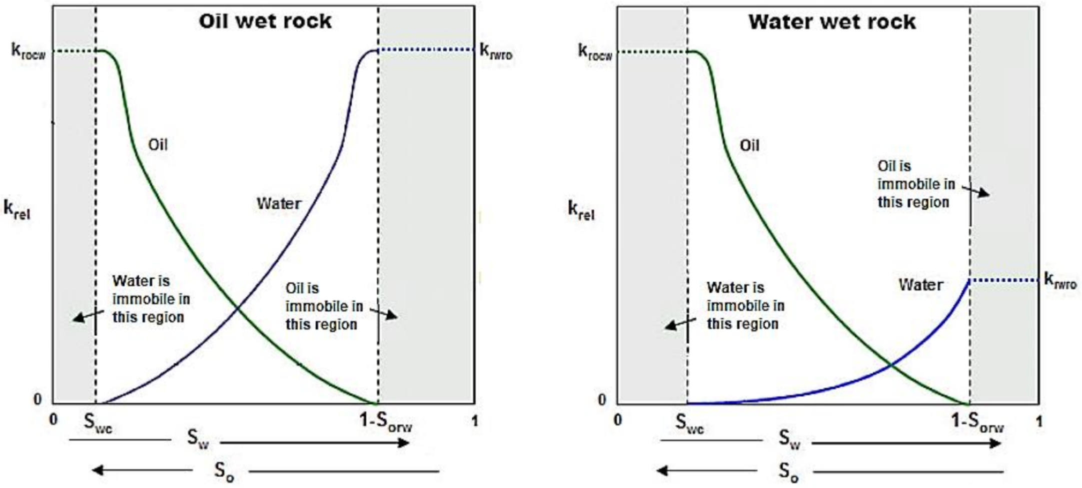

(a) Oil-wet rock relative permeabilities. (b) water-wet relative permeabilities.

Figure 3.3: Water saturation (S_w)versus relative permeability (k_rel) (*Oil and water wet permeabilities* 2014).

Here, $k_{\mathrm{rel},\eta}$, and $K_{\mathrm{eff},\eta}$ represent relative permeability and effective permeability of fluid phase η. Also, $\eta \in \{\mathrm{o},\mathrm{w}\}$, i.e., oil and water.

For two-phase flow, i.e., oil and water (Ringrose & Bentley 2015):

$$k_{\mathrm{rel,w}} + k_{\mathrm{rel,o}} < K. \tag{3.13}$$

Relation between relative permeability and fluid saturation is usually plotted as relative permeability versus fluid saturation curves. In a system with oil and water, the fluid saturation on the x-axis varies from connate water saturation (S_wc) to the residual oil saturation after water flooding (S_orw). Connate water saturation (S_wc) is a water saturation below which the relative permeability of water is zero. Similarly, residual oil saturation (S_orw) is an oil saturation below which the relative permeability of oil is zero. Figure 3.3a, and 3.3b represent relative permeability diagram for oil-wet, and water-wet media, respectively. In Figure 3.3, k_rwro represents maximum relative permeability of water at critical oil saturation, and k_rocw represents maximum relative permeability of oil at critical water saturation.

3.3 Fluid properties

3.3.1 Formation volume factors

Formation volume factor B is defined as the ratio of the volume of oil at reservoir conditions to the volume of oil at standard conditions. It has the unit RB/STB (reservoir barrels per stock tank barrels). The formation volume factor is used to convert the flow rate of oil at standard conditions to reservoir conditions. Formation volume factor is given as (Zhang 2013):

$$B = \frac{V_o}{V_{o_s}}, \tag{3.14}$$

or can be expressed in terms of density as

$$B = \frac{\rho_{o_s}}{\rho_o}. \tag{3.15}$$

Here, V_o, and V_{o_s} denote volume of oil at reservoir conditions and at standard conditions, respectively, ρ_o, and ρ_{o_s}denote density of oil at reservoir conditions and at standard conditions, respectively (Zhang 2013).

The formation volume factor is a function of the pressure and temperature of the oil reservoir. The oil formation volume factor increases with pressure until the bubble point pressure. Then the oil formation volume factor decreases as the pressure increases above the bubble point pressure. This is because, when below the bubble point pressure, more gas goes into the solution as the pressure increases, the dissolved gas causes the oil to swell. When above the bubble point pressure, no more gases available, and the oil is compressed at the same time (Zhang 2013).

3.3.2 Physical classification of crude oils

The specific gravity is one of the most common physical properties used for the classification of crude oils. It is a dimensionless number and is denoted by γ_o. The specific gravity is defined as (Dandekar 2013):

$$\gamma_o = \frac{\rho_{o_s}}{\rho_{w_s}}, \tag{3.16}$$

where ρ_{o_s} and ρ_{w_s} are the density of crude oil and water, respectively at standard conditions i.e., at 60 °F temperature and 14.7 psia.

Classification	API gravity range [°]
Light oil	API $> 31.1°$
Medium oil	$22.3° <$ API $< 31.1°$
Heavy oil	$10° <$ API $< 22.3°$
Extra heavy oil	API $< 10°$

Table 3.2: Classification of crude oils based on API (Wikipedia 2021).

Reservoir fluid	API gravity [°]	Viscosity [cP]	Color	Mol % of C_{7+}
Black oils	$15-40$	$2-300$	Dark black	> 20.0
Volatile oils	$45-55$	$0.25-3$	Brown, orange or green	$12.5-20.0$
Gas condensates	> 50	0.25	water white	< 12.5
Wet gases	> 60	0.25	water white	May be present
Dry gases	No liquid	$0.02-0.05$	-	-

Table 3.3: Basic characteristics of different types of reservoir fluids (Dandekar 2013).

Alternatively, API gravity is also widely used in the petroleum industry. It is defined as (Dandekar 2013):

$$^{\circ}\text{API} = \frac{141.5}{\gamma_o} - 131.5 \tag{3.17}$$

API gravity is the indication of how heavy or light the crude oil is compared to water. Based on this, crude oil can be classified into the four main groups as shown in Table 3.2.

3.3.3 Classification of reservoir fluids

The fluids in the oil reservoir can be classified into five main categories based on their physical properties and phase behavior as black oils, volatile oils, gas condensates or retrograde gases, wet gases, and dry gases (Dandekar 2013). The description of these fluids are shown in Table 3.3.

3.3.4 Important measurement terms in multi-phase fluid flow

Some commonly used multi-phase flow measurement terms are discussed in this part.

3.3.4.1 Water cut

Water cut is defined as the ratio of the volume flow rate of water produced to the volume flow rate of total liquid produced. It is denoted by WC and can be expressed as (Schlumberger 2021*b*):

$$WC = \frac{q_{\mathrm{w,s,tot}}}{q_{\mathrm{mix,tot}}}, \tag{3.18}$$

where $q_{\mathrm{w,s,tot}}$, and $q_{\mathrm{mix,tot}}$ are the volume flow rate of total water produced and the volume flow rate of total liquid produced, respectively.

3.3.4.2 Gas liquid ratio

The gas-liquid ratio is defined as the ratio of the volume flow rate of gas produced to the volume flow rate of total liquid produced. It is denoted by GLR and can be expressed as (Schlumberger 2021*a*):

$$GLR = \frac{q_{\mathrm{g,s,tot}}}{q_{\mathrm{mix,tot}}}, \tag{3.19}$$

where $q_{\mathrm{g,s,tot}}$, and $q_{\mathrm{mix,s,tot}}$ are the volume flow rate of total gas produced and the volume flow rate of the total liquid produced, respectively.

3.3.4.3 Well productivity index

Productivity index, J is defined as the volume of fluids that can be delivered by the reservoir to the wellbore per each unit of the pressure draw-down, the pressure difference between oil reservoir pressure and bottom-hole pressure, during a specific period. The commonly used unit for productivity index is bbl/psi/day (Moradi 2020).

4 Model Uncertainties, Advanced Control Strategies, and State Estimation

4.1 Model uncertainties

In oil and gas production forecasts, subsurface uncertainties play major roles. Therefore, underestimation of these uncertainties can give rise to a high risk to investment decisions for facility designs and exploration targets. Uncertainty comes from several sources such as geological characteristics of oil fields, rock and fluid properties, oil price, capital expenditures, and operating costs, etc., (Zhang 2003). In this work, we only focus on the uncertainty in the oil field that comes from the geological characteristics of oil fields and rock and fluid properties.

Some of the methods developed for uncertainty in the field of the petroleum industry are experimental design, response surface, multiple realization tree, and Monte Carlo simulations. In this work, the uncertainty in the oil reservoir simulation is handled by implementing the Monte Carlo simulation. Monte Carlo is a powerful statistical method that has been used for more than half a century. This method has been used extensively in the petroleum industry for decades. The Monte Carlo method starts with a mathematical model in which a dependent variable is a function of the independent variables. Usually, the dependent variable is the quantity of interest such as cumulative oil production at a future time. The independent variables are reservoir parameters, such as porosity, saturation, and permeability. Different independent variables might have different statistical distributions, such as normal distribution, simple distribution, etc. (Zhang 2003)

4.2 Advanced control strategies

The proper control technology is applied to improve the oil production from the oil field. Advanced controllers are an integral part of a *smart-well* application.

There are a variety of advanced control methods used in the petroleum industry, such as the model predictive controller (MPC), the linear-quadratic optimal control (LQ optimal control), and L1 adaptive control, etc. (Zhang 2013)

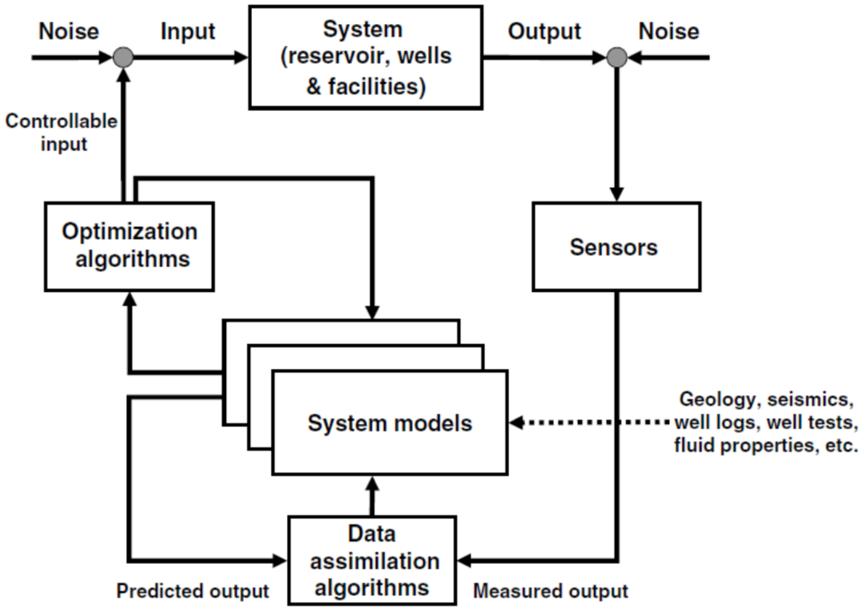
Noise
Input
System (reservoir, wells & facilities)
Output
Noise
Controllable input
Optimization algorithms
Sensors
System models
Geology, seismics, well logs, well tests, fluid properties, etc.
Data assimilation algorithms
Predicted output
Measured output

Figure 4.1: Smart wells expressed as a closed loop model-based control process (Zhang 2013).

Model-based control process in oil production is illustrated in Figure 4.1. The system comprises wells, reservoirs, and production facilities to separate hydrocarbons from water or gas. The model-based control uses the system models to predict the future of a process and adjust the parameters for a system model by data assimilation algorithms through comparison of measured and predicted output. Therefore, it is an effective way to deal with the uncertainties of the reservoir (Zhang 2013).

4.2.1 Model predictive controller

Model predictive controller (MPC) is one of the most commonly used techniques within advanced control. Sometimes MPC is also called a receding horizon control (RHC). According to Mayne et al. (2000), MPC is defined as a form of control in which the current control action is obtained by solving online, at each sampling instant, a finite horizon open-loop optimal control problem.

When the open-loop control sequence is solved repeatedly at each time step, the controller has an inherently closed-loop effect. Stabilizing feedback control can be obtained by calculating the new control sequence from the present state of the system. However, if the system state is not fully measured, the best estimate available is used as the basis for calculation. Initially, the control sequence is calculated for a given time horizon, T_c, and the dynamic behavior of the system is predicted for a horizon T_p. Here, T_p is greater than T_c. The control horizon moves forward in time (Meum 2007).

The model associated with the reservoir model is classified as high-order models. The model contains a high number of static variables in addition to the state variables. Furthermore, the reservoir model is strongly nonlinear because they involve multi-phase flow and variable geological properties (Meum 2007).

There are some model identification techniques to reduce the model order of the complex reservoir model. Model identification methods such as the subspace identification method, and proper orthogonal decomposition (POD) method are found to be promising (Bakke 2009).

In this work subspace identification method is studied to simplify the oil reservoir model. Also, the method of implementation of linear MPC in a simplified model is studied.

4.2.1.1 Subspace identification

A linear system with multiple inputs and multiple outputs (MIMO), may be described in state-space form by

$$\frac{dx}{dt} = Ax + Bu$$

$$y = Cx + Du. \tag{4.1}$$

In discrete form

$$x_{\mathrm{i}+1} = A_\mathrm{d}x_\mathrm{i} + B_\mathrm{d}u_\mathrm{i}$$

$$y_\mathrm{i} = C_\mathrm{d}x_\mathrm{i} + D_\mathrm{d}u_\mathrm{i}, \tag{4.2}$$

where $\boldsymbol{A}$, $\boldsymbol{B}$, $\boldsymbol{C}$, and $\boldsymbol{D}$ are the system matrices, $\boldsymbol{x}$, $\boldsymbol{u}$, and $\boldsymbol{y}$ denote states, inputs, and outputs, respectively. Similarly, the matrices A_d, B_d, C_d, and D_d denote system matrices in a discrete form.

Subspace algorithm seeks to estimate the system matrices A, B, C, and D of the state-space model from input-output data of the system. Subspace identification algorithms are based on concept form system theory, linear algebra, and statistics. Subspace identification methods comprise of three main steps (S.D.M. Borjas 2011):

1. Estimating the predictable subspace for multiple future steps
2. Extract the state variables from the estimated subspace

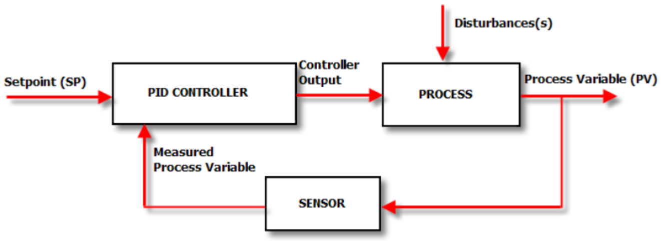

Figure 4.2: Block diagram of PID controller (Zhang 2013).

3. Fitting the estimated states to a state-space model.

In Julia programming language, there is a standard package called *ControlSystemIdentification.jl*. Under this package, there are some methods named *n4sid*, and *pem* to solve subspace identification problem[1].

4.2.2 PI controller

The traditional PID controller is extensively used in the oil industry to control levels, flow rates, pressure and pump rates, etc. In a single loop PID controller, the error between setpoint and measured process output is compared. This gives the control signal to process so that the error of the system is minimized. The block diagram of the PID controller is shown in Figure 4.2. In this paper, a PI controller will be implemented in the oil reservoir model to control the valve opening of ICVs at the production well.

4.2.2.1 Discretization and tuning of a PI controller

The PI controller is often expressed as a continuous-time model in the form of a Laplace transfer function. However, to implement the PI controller in a computer program, it is required to discretize the PI controller in a continuous-time domain to the discrete-time domain.

The equation for the PI controller expressed as a Laplace function domain is given as (Zhang 2013)

---

[1] https://github.com/baggepinnen/ControlSystemIdentification.jl

$$U(s) = K_\mathrm{p} e(s) + \frac{K_\mathrm{p}}{T_\mathrm{i} s} e(s). \tag{4.3}$$

Introducing controller state z as

$$z(s) = \frac{e(s)}{s}. \tag{4.4}$$

Equation 4.3 becomes

$$U(s) = K_\mathrm{p} e(s) + \frac{K_\mathrm{p}}{T_\mathrm{i}} z(s). \tag{4.5}$$

Applying inverse Laplace transformation to Equation 4.4 and Equation 4.5 gives

$$\frac{dz}{dt} = e(t), \tag{4.6}$$

$$U(t) = K_\mathrm{p} e(t) + \frac{K_\mathrm{p}}{T_\mathrm{i}} z(t). \tag{4.7}$$

Finally, applying Euler Backward approximation gives:

$$z_{\mathrm{i}+1} = z_\mathrm{i} + T_\mathrm{s} e_\mathrm{i}, \tag{4.8}$$

$$e_\mathrm{i} = r_\mathrm{i} - y_\mathrm{i}, \tag{4.9}$$

$$U_\mathrm{i} = K_\mathrm{p} e_\mathrm{i} + \frac{K_\mathrm{p}}{T_\mathrm{i}} z_\mathrm{i}, \tag{4.10}$$

where,

T_s = sampling time

e = error

r = setpoint

y = measurement value

U = control input

K_p = controller gain

T_{i} = integral time.

The commonly used methods for PID controller tuning are Skogestad's method, Ziegler-Nichols method, good gain method, etc. However, in the case of, oil reservoir model which has multiple inputs and multiple outputs, the above methods can not be used to tune the PI controller. The PI controller was tuned manually through the trial and error method.

4.3 State estimation

In a real oil reservoir system, it is not possible to measure all the states of the system because of the limited number of sensors available (expensive installation and operational cost of sensors). And sometimes, the measurements from the system are too noisy. In this case, it is very effective and accurate to estimate the states by using the latest available measurements from the real process. The state estimation is usually achieved using estimators and observers. Kalman filter is one of the popular optimal estimators. For linear process models, a standard Kalman filter is used. While for nonlinear process models, extended Kalman filter (EKF), unscented Kalman filter (UKF) etc., are used. Kalman filter is a state estimator which is a type of Bayesian estimator[2].

---

[2] Lecture notes for the course IIA 4117: Model Predictive Control by Roshan Sharma, University of South-Eastern Norway

5 Model Overview

5.1 Two-phase flow in a Porous Media

In this work, we simplify the oil reservoir model by assuming the black oil model. In the black oil model, it is assumed that hydrocarbon components are divided into a gas component and an oil component in a stock tank at standard temperature and pressure and that no mass transfer occurs between the water phase and the other two phases (oil and gas) (Chen et al. 2006).

5.2 Model objective

In this work, we further simplify the black oil model by considering the reservoir as a relatively new heavy oil reservoir that can be approximated by black oil without gas. The model in this work is developed for a slightly slanting wedge-shaped horizontal black oil reservoir with homogeneous dispersion of water and homogeneous in its geological features like permeabilities, porosities, etc. The natural aquifer with constant pressure P_{a} and constant relative permeability k_{wa} is located at the bottom of the reservoir. While a horizontal well is located at the top of the wedge-shaped reservoir. The boundary conditions are zero flux from the left and right sides and top and bottom sides of the wedge-shaped reservoir. The total production rate of the mixture of oil and water from the reservoir $q_{\mathrm{mix,tot}}$ is specified to be constant. 3D schematic view and geometrical characteristics of the reservoir are shown in Figure 5.1. In this work, the 3D problem is simplified to a 2D problem. Finally, a 2D control relevant model is developed. The spatial-temporal variables are represented by (r, ℓ), and t, respectively.

The wedge-shaped reservoir model is combined with the well model. From the combined reservoir and well model, we are interested in finding how the water saturation S_{w}, reservoir pressure P, water and oil production rate ($q_{\mathrm{w,s}}$, and $q_{\mathrm{o,s}}$, respectively), well pressure P_{rw}, well bottom hole pressure P_{bh}, etc., vary with time.

The model objective is illustrated by the functional diagram and is shown in Figure 5.2.

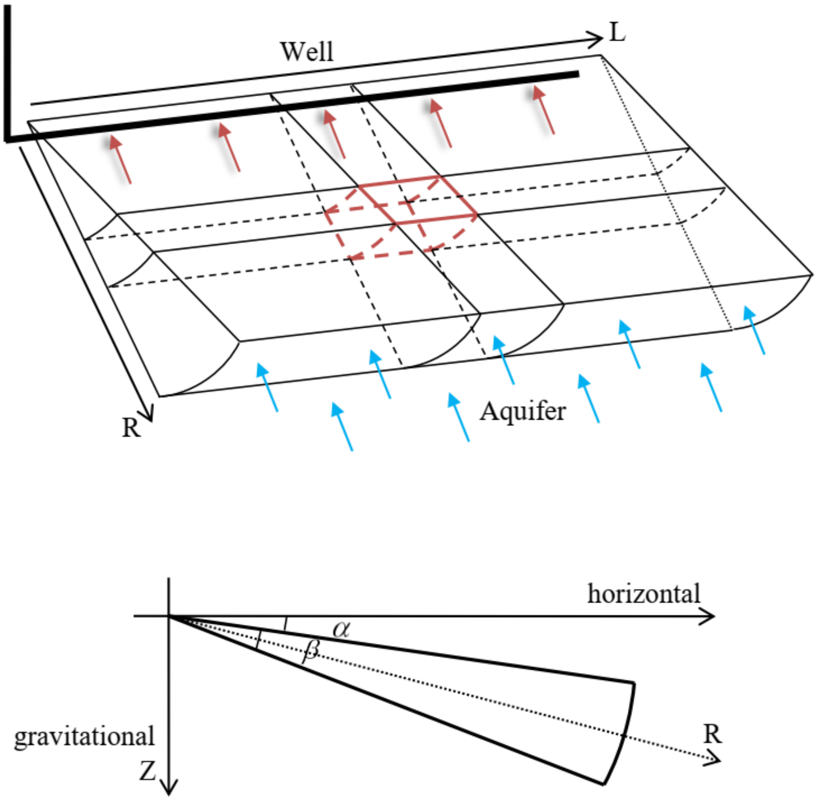
Well
L
R
Aquifer
horizontal
α
β
gravitational
Z
R

Figure 5.1: (a) Schematic view of the reservoir and (b) geometrical characteristics of the reservoir (Zhang 2013).

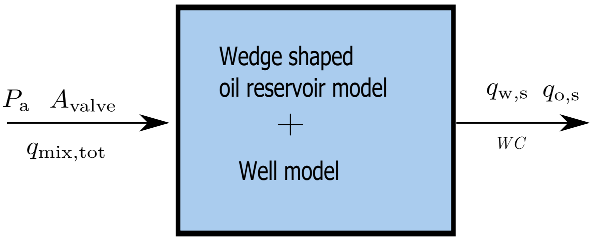
P_a A_valve
$q_\mathrm{mix,tot}$
Wedge shaped
oil reservoir model
+
Well model
$q_\mathrm{w,s}$ $q_\mathrm{o,s}$
WC

Figure 5.2: Model functional diagram.

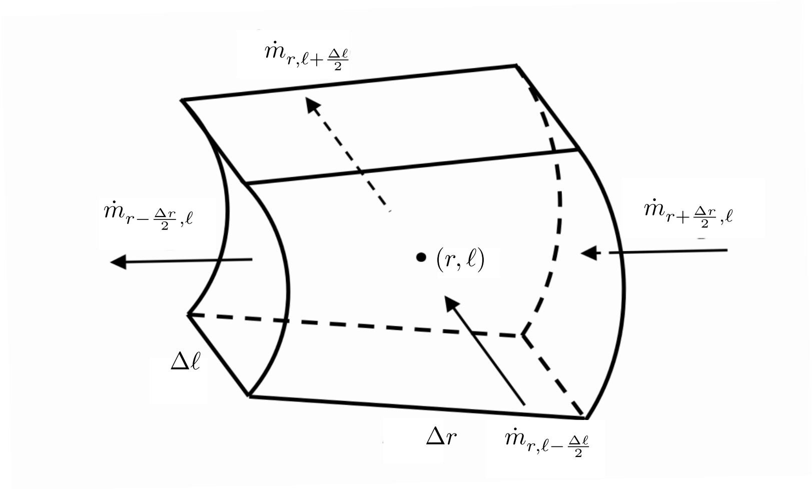
$\dot{m}_{r,\ell+\frac{\Delta\ell}{2}}$
$\dot{m}_{r-\frac{\Delta r}{2},\ell}$
$\dot{m}_{r+\frac{\Delta r}{2},\ell}$
(r,ℓ)
$\Delta\ell$
Δr
$\dot{m}_{r,\ell-\frac{\Delta\ell}{2}}$

Figure 5.3: A single cell of the reservoir (Zhang 2013).

5.3 Model development

The small piece of the cell is taken from the reservoir as shown in Figure 5.3. Let (r,ℓ) be the coordinate of the center of the cell. The model development is divided into two steps.

- Step 1: Introduction to the relevant balance laws.
- Step 2: Relate the quantities in the balance laws to the inputs and outputs.

5.3.1 Step 1: Introduction to the relevant balance laws

The relevant balance laws are described in this step. As the model involves the flow of mass (water and oil), the mass balance is relevant to model development. The total mass balance is can be written as[1]

Mass accumulation = Mass in - Mass out

---

[1] The lecture note for the course FM1015 Modeling of Dynamic Systems at the University of South-Eastern Norway (USN) by Prof. Bernt Lie

$$\frac{dm_{\mathrm{acc}}}{dt} = \dot{m}_{\mathrm{i}} - \dot{m}_{\mathrm{e}}. \tag{5.1}$$

5.3.2 Step 2: Relate the quantities in the balance law to the inputs and outputs

The right and left-hand side terms of the Equation 5.1 is further described in this step.

We divide the reservoir into $n_r \times n_\ell$ number of cells. Here, n_r, and n_ℓ are the number of grids along r and ℓ coordinates, respectively. For each cell, we need mass balance. Let, $(r,\ell) \in [0,R] \times [0,L]$, where R, and L are the radius and length of the reservoir, respectively. Let, Δr and $\Delta\ell$ be the step length along the r, and ℓ coordinates, respectively. Here, $\Delta r = \frac{R}{n_r}$ and $\Delta\ell = \frac{L}{n_\ell}$. There is a constant pressure aquifer at $(r,\ell) \in R \times [0,L]$, and well with constant flow rate at the cells $(r,\ell) \in [0,\Delta r] \times [0,L]$. No mass entering or leaving the reservoir at $(r,\ell) \in [0,R] \times 0$, and $(r,\ell) \in [0,R] \times L$.

The mass m_{acc} of the liquid within the cell is

$$m_{\mathrm{acc}} = \rho \cdot \Delta V = \rho \cdot (\phi \cdot S \cdot \beta r \cdot \Delta r \cdot \Delta\ell), \tag{5.2}$$

where β is an arch angle of a wedge-shaped reservoir, ϕ, S and ρ are the porosity, saturation, and fluid density in the reservoir, respectively.

Now, considering single-phase flow, the mass accumulation per unit time due to compressibility of liquid is

$$\frac{dm_{\mathrm{acc}r,\ell}}{dt} = \frac{d\left(\rho \cdot \phi \cdot S \cdot \beta r \cdot \Delta r \cdot \Delta\ell\right)_{r,\ell}}{dt} = \beta \cdot r \cdot \Delta r \Delta\ell \frac{d\left(\rho \cdot \phi \cdot S\right)_{r,\ell}}{dt}. \tag{5.3}$$

The mass flow per unit time ($\dot{m}$) is given as

$$\begin{aligned} \dot{m} &= \rho \cdot q \\ &= \rho \cdot u \cdot A. \end{aligned} \tag{5.4}$$

Total mass inflow per unit time is

$$\dot{m}_{\mathrm{i}} = \dot{m}_{r+\frac{\Delta r}{2},\ell} + \dot{m}_{r,\ell-\frac{\Delta\ell}{2}}, \tag{5.5}$$

where $\dot{m}_{r+\frac{\Delta r}{2},\ell}$, and $\dot{m}_{r,\ell-\frac{\Delta\ell}{2}}$ are the mass inflow per unit time across the surface at $r+\frac{\Delta r}{2}$ along the r-coordinate, and $\ell-\frac{\Delta\ell}{2}$ along the ℓ-coordinate, respectively, and given as

$$\dot{m}_{r+\frac{\Delta r}{2},\ell} = (\rho\cdot u_r)_{r+\frac{\Delta r}{2},\ell}\cdot A_{r+\frac{\Delta r}{2},\ell}, \tag{5.6}$$

$$\dot{m}_{r,\ell-\frac{\Delta\ell}{2}} = (\rho\cdot u_\ell)_{r,\ell-\frac{\Delta\ell}{2}}\cdot\beta\cdot r\Delta r, \tag{5.7}$$

where

$$A_{r+\frac{\Delta r}{2},\ell} = \beta\left(r+\frac{\Delta r}{2}\right)\Delta\ell, \tag{5.8}$$

leading to

$$\begin{aligned}\dot{m}_{r+\frac{\Delta r}{2},\ell} &= (\rho\cdot u_r)_{r+\frac{\Delta r}{2},\ell}\cdot\beta\left(r+\frac{\Delta r}{2}\right)\Delta\ell\\ &= (\rho\cdot u_r r)_{r+\frac{\Delta r}{2},\ell}\cdot\beta\Delta\ell,\end{aligned} \tag{5.9}$$

where u_r, and u_ℓ are fluid velocities along r, and ℓ-coordinates, respectively.

Similarly, total mass outflow per unit time is

$$\dot{m}_{\mathrm{e}} = \dot{m}_{r-\frac{\Delta r}{2},\ell} + \dot{m}_{r,\ell+\frac{\Delta\ell}{2}} + \dot{m}_{\mathrm{s}_{r,\ell}},$$

where $\dot{m}_{r-\frac{\Delta r}{2},\ell}$, and $\dot{m}_{r,\ell+\frac{\Delta\ell}{2}}$ are the mass outflow per unit time across the surface at $r-\frac{\Delta r}{2}$ along the r-coordinate, and $\ell+\frac{\Delta\ell}{2}$ along the ℓ-coordinate, respectively, and given as

$$\dot{m}_{r-\frac{\Delta r}{2},\ell} = (\rho\cdot u_r r)_{r-\frac{\Delta r}{2},\ell}\cdot\beta\Delta\ell, \tag{5.10}$$

$$\dot{m}_{r,\ell+\frac{\Delta\ell}{2}} = (\rho\cdot u_\ell)_{r,\ell+\frac{\Delta\ell}{2}}\cdot\beta\cdot r\Delta r. \tag{5.11}$$

Also, $\dot{m}_{\mathrm{s}_{r,\ell}}$ is a specified mass flow rate at the cells $(r,\ell)\in[0,\Delta r]\times[0,L_{\mathrm{well}}]$ where L_{well} is the length of the well,

$$\dot{m}_{\mathrm{s}_{r,\ell}} = (\rho\cdot q_{\mathrm{s}})_{r,\ell}, \tag{5.12}$$

where $q_{\mathrm{s}_{r,\ell}}$ denotes specified volumetric flow rate of the well.

Now, substituting Equation 5.3 to 5.12 into Equation 5.1 yields mass balance equation for a single cell

$$\begin{aligned}\beta r \Delta r \Delta \ell \frac{d\left(\rho\cdot\phi\cdot S\right)_{r,\ell}}{dt} &= \left(\left(\rho\cdot u_r r\right)_{r+\frac{\Delta r}{2},\ell}\cdot\beta\Delta\ell+\left(\rho\cdot u_\ell\right)_{r,\ell-\frac{\Delta\ell}{2}}\cdot\beta r\Delta r\right)\\ &-\left(\left(\rho\cdot u_r r\right)_{r-\frac{\Delta r}{2},\ell}\cdot\beta\Delta\ell+\left(\rho\cdot u_\ell\right)_{r,\ell+\frac{\Delta\ell}{2}}\cdot\beta r\Delta r+\left(\rho\cdot q_{\mathrm{s}}\right)_{r,\ell}\right). \qquad (5.13)\end{aligned}$$

Dividing Equation 5.13 by $\beta r \Delta r \Delta \ell$

$$\begin{aligned}\frac{d\left(\rho\cdot\phi\cdot S\right)_{r,\ell}}{dt} &= \frac{\left(\rho\cdot u_r r\right)_{r+\frac{\Delta r}{2},\ell}-\left(\rho\cdot u_r r\right)_{r-\frac{\Delta r}{2},\ell}}{r_{r,\ell}\cdot\Delta r}\\ &-\frac{\left(\rho\cdot u_\ell\right)_{r,\ell+\frac{\Delta\ell}{2}}-\left(\rho\cdot u_\ell\right)_{r,\ell-\frac{\Delta\ell}{2}}}{\Delta\ell}-\frac{\left(\rho\cdot q_{\mathrm{s}}\right)_{r,\ell}}{\beta r_{r,\ell}\Delta r\Delta\ell}. \qquad (5.14)\end{aligned}$$

Introducing formation volume factor $B = \frac{\rho_{\mathrm{s}}}{\rho}$ where ρ_{s} is the fluid density at standard condition. Equation 5.14 now becomes

$$\begin{aligned}\frac{d}{dt}\left(\frac{\rho_{\mathrm{s}}}{B}\cdot\phi\cdot S\right)_{r,\ell} &= \frac{\left(\frac{\rho_{\mathrm{s}}}{B}\cdot u_r r\right)_{r+\frac{\Delta r}{2},\ell}-\left(\frac{\rho_{\mathrm{s}}}{B}\cdot u_r r\right)_{r-\frac{\Delta r}{2},\ell}}{r_{r,\ell}\cdot\Delta r}\\ &-\frac{\left(\frac{\rho_{\mathrm{s}}}{B}\cdot u_\ell\right)_{r,\ell+\frac{\Delta\ell}{2}}-\left(\frac{\rho_{\mathrm{s}}}{B}\cdot u_\ell\right)_{r,\ell-\frac{\Delta\ell}{2}}}{\Delta\ell}-\frac{\left(\frac{\rho_{\mathrm{s}}}{B}\cdot q_{\mathrm{s}}\right)_{r,\ell}}{\beta r_{r,\ell}\Delta r\Delta\ell}. \qquad (5.15)\end{aligned}$$

For two-phase flow model, the Equation 5.15 becomes

$$\begin{aligned}\frac{d}{dt}\left(\frac{\rho_{\eta_{\mathrm{s}}}}{B_\eta}\cdot\phi\cdot S_\eta\right)_{r,\ell} &= \frac{\left(\frac{\rho_{\eta_{\mathrm{s}}}}{B_\eta}\cdot u_{\eta,r} r\right)_{r+\frac{\Delta r}{2},\ell}-\left(\frac{\rho_{\eta_{\mathrm{s}}}}{B_\eta}\cdot u_{\eta,r} r\right)_{r-\frac{\Delta r}{2},\ell}}{r_{r,\ell}\cdot\Delta r}\\ &-\frac{\left(\frac{\rho_{\eta_{\mathrm{s}}}}{B_\eta}\cdot u_{\eta,\ell}\right)_{r,\ell+\frac{\Delta\ell}{2}}-\left(\frac{\rho_{\eta_{\mathrm{s}}}}{B_\eta}\cdot u_{\eta,\ell}\right)_{r,\ell-\frac{\Delta\ell}{2}}}{\Delta\ell}-\frac{\left(\frac{\rho_{\eta_{\mathrm{s}}}}{B_\eta}\cdot q_{\eta,\mathrm{s}}\right)_{r,\ell}}{\beta r_{r,\ell}\Delta r\Delta\ell}. \qquad (5.16)\end{aligned}$$

Fluid velocity u can be written in terms of pressure head gradient using Darcy's law. For a two-phase, and two-dimensional flow model

$$u_\eta = -\frac{k_{\mathrm{rel},\eta}}{\mu_\eta}K\left(\nabla P_\eta-\rho_\eta\cdot g\cdot\nabla z\right), \qquad (5.17)$$

where K is the absolute permeability, $k_{\mathrm{rel},\eta}$ is a relative permeability for phase η, μ_η is a viscosity of phase η, P_η is the fluid pressure, and g is the acceleration of gravity.

The z-term has to be projected to the r-coordinate according to Figure 5.1 (b).

$$z = r\sin\left(\alpha + \frac{\beta}{2}\right). \tag{5.18}$$

Substituting Equation 5.18 into Equation 5.17

$$u_\eta = -\frac{k_{\mathrm{rel},\eta}}{\mu_\eta} K \left(\nabla P_\eta - \rho_\eta \cdot g \cdot \sin\left(\alpha + \frac{\beta}{2}\right) \nabla r\right). \tag{5.19}$$

For simplification, defining the following coefficient and constant

$$\lambda_\eta = \frac{k_{\mathrm{rel},\eta}}{\mu_\eta} K, \tag{5.20}$$

$$h_\eta = \rho_\eta \cdot g \cdot \sin\left(\alpha + \frac{\beta}{2}\right). \tag{5.21}$$

The term λ_η denotes mobility of the fluid phase η. For the directions along r and ℓ coordinates, λ_η becomes

$$\begin{aligned} \lambda_{\eta,r} &= \frac{k_{\mathrm{rel},\eta}}{\mu_\eta} K_r \\ \lambda_{\eta,\ell} &= \frac{k_{\mathrm{rel},\eta}}{\mu_\eta} K_\ell, \end{aligned} \tag{5.22}$$

where

P_η= liquid pressure of phase η

$\lambda_{\eta,r}$ = mobility of liquid of phase η along r-coordinate

$\lambda_{\eta,\ell}$ = mobility of liquid of phase η along ℓ-coordinate

$k_{\mathrm{rel},\eta}$=relative permeability of liquid of phase η

$k_{\mathrm{rel},\eta}$= relative permeability of liquid of phase η

K_r=absolute permeability of reservoir rock along r-coordinate

K_ℓ = absolute permeability of reservoir rock along ℓ-coordinate

Fluid velocity in the direction along r-coordinate becomes

$$u_{\eta,r} = -\lambda_{\eta,r}\left(\nabla P_{\eta,r} - h_\eta \nabla r_r\right), \tag{5.23}$$

where $\nabla r_r = \frac{\partial r}{\partial r} = 1$, $\nabla P_{\eta,r} = \frac{\partial P_\eta}{\partial r}$

$$u_{\eta,r} = -\lambda_{\eta,r}\left(\frac{\partial P_\eta}{\partial r} - h_\eta\right). \tag{5.24}$$

Fluid velocity in the direction along ℓ-coordinate becomes

$$u_{\eta,\ell} = -\lambda_{\eta,\ell}\left(\nabla P_{\eta,\ell} - h_\eta \nabla r_\ell\right), \tag{5.25}$$

where $\nabla r_\ell = \frac{\partial r}{\partial \ell} = 0$, $\nabla P_{\eta,\ell} = \frac{\partial P_\eta}{\partial \ell}$

$$u_{\eta,\ell} = -\lambda_{\eta,\ell}\left(\frac{\partial P_\eta}{\partial \ell}\right). \tag{5.26}$$

Now, substituting Equation 5.24 and Equation 5.26 into Equation 5.16

$$\begin{aligned}
\frac{d}{dt}\left(\frac{\rho_{\eta_\mathrm{s}}}{B_\eta}\cdot\phi\cdot S_\eta\right)_{r,\ell} = {} & \frac{-\left(\frac{\rho_{\eta_\mathrm{s}}}{B_\eta}\cdot\lambda_{\eta,r}\left(\frac{\partial P_\eta}{\partial r} - h_\eta\right)r\right)_{r+\frac{\Delta r}{2},\ell} + \left(\frac{\rho_{\eta_\mathrm{s}}}{B_\eta}\cdot\lambda_{\eta,r}\left(\frac{\partial P_\eta}{\partial r} - h_\eta\right)r\right)_{r-\frac{\Delta r}{2},\ell}}{r_{r,\ell}\cdot\Delta r} \\
& - \frac{-\left(\frac{\rho_{\eta_\mathrm{s}}}{B_\eta}\cdot\lambda_{\eta,\ell}\left(\frac{\partial P_\eta}{\partial \ell}\right)\right)_{r,\ell+\frac{\Delta \ell}{2}} + \left(\frac{\rho_{\eta_\mathrm{s}}}{B_\eta}\cdot\lambda_{\eta,\ell}\left(\frac{\partial P_\eta}{\partial \ell}\right)\right)_{r,\ell-\frac{\Delta \ell}{2}}}{\Delta \ell} \\
& - \frac{\left(\frac{\rho_{\eta_\mathrm{s}}}{B_\eta}\cdot q_{\eta,\mathrm{s}}\right)_{r,\ell}}{\beta r_{r,\ell}\Delta r\Delta \ell}.
\end{aligned} \tag{5.27}$$

5.3.2.1 Representation of the Well:

According to Chen & Zhang (2009), the pressure close to the well declines much faster than near the aquifer. Therefore, a small step size Δr near the well is required for accurate pressure calculation in the reservoir cell at the neighborhood of the well. This can be handled by using local grids refinement in the neighborhood of the well. However, this can lead to restrictions on time steps in the numerical simulation (Chen et al. 2006). The alternative solution is to derive an analytical solution for the steady-state flow model that yields the Peaceman equation (Peaceman 1993). Let us assume only radial flow in grids near the well. Considering single-phase flow,

$$\frac{\partial\left(\frac{\rho_s}{B}\cdot\phi\cdot S\right)_{r,\ell}}{\partial t}=\frac{1}{r}\cdot\frac{\partial\left(\frac{\rho_s}{B}\cdot u_r r\right)}{\partial r}. \tag{5.28}$$

At steady-state condition, the well produces liquids at a constant rate q_s, hence, there is no mass accumulation in the reservoir cell at the neighborhood of the well.

$$\frac{\partial\left(\frac{\rho_s}{B}\cdot\phi\cdot S\right)}{\partial t}=0 \tag{5.29}$$

$$\frac{1}{r}\cdot\frac{\partial\left(\frac{\rho_s}{B}\cdot u_r r\right)}{\partial r}=0 \tag{5.30}$$

$$\frac{\rho_s}{B}\cdot u_r r=\text{constant.}$$

The mass flow rate is thus constant

$$\dot{m}_{\text{s},r,\ell}=\left(\frac{\rho_s}{B}\cdot u_r A_\text{c}\right)_{r,\ell}, \tag{5.31}$$

here, circumferential flow area, $(A_\text{c})=2\pi r\Delta\ell$.

$$\dot{m}_{\text{s},r,\ell}=\left(\frac{\rho_s}{B}\cdot u_r 2\pi r\Delta\ell\right)_{r,\ell}. \tag{5.32}$$

Substituting Darcy's law into Equation 5.32

$$\begin{aligned}\dot{m}_{\text{s},r,\ell}&=-\left(\frac{\rho_s}{B}\cdot\lambda_r\left(\nabla P_r-h\nabla r_r\right)\cdot 2\pi r\Delta\ell\right)_{r,\ell}\\ \left(\frac{\dot{m}_\text{s}B}{\rho_\text{s}}\cdot\frac{1}{r}\right)_{r,\ell}&=-\left(2\pi\Delta\ell\cdot\lambda_r\left(\frac{\partial P}{\partial r}-h\frac{\partial r}{\partial r}\right)\right)_{r,\ell}\\ \left(q_\text{s}\cdot\frac{\partial r}{r}\right)_{r,\ell}&=-\left(2\pi\Delta\ell\cdot\lambda_r\left(\partial P-h\partial r\right)\right)_{r,\ell}.\end{aligned} \tag{5.33}$$

Now, integrating both sides for $r\in[r_\text{e},r_\text{well}]$, and $P\in[P_\text{re},P_\text{rw}]$ as shown in Figure 5.4. Here, r_e is an equivalent radius at which the pressure P_re is equivalent to the average pressure $P_{r,\ell}$ at the cell neighborhood of the well, r_well is a well bore radius, and P_rw is a pressure at well.

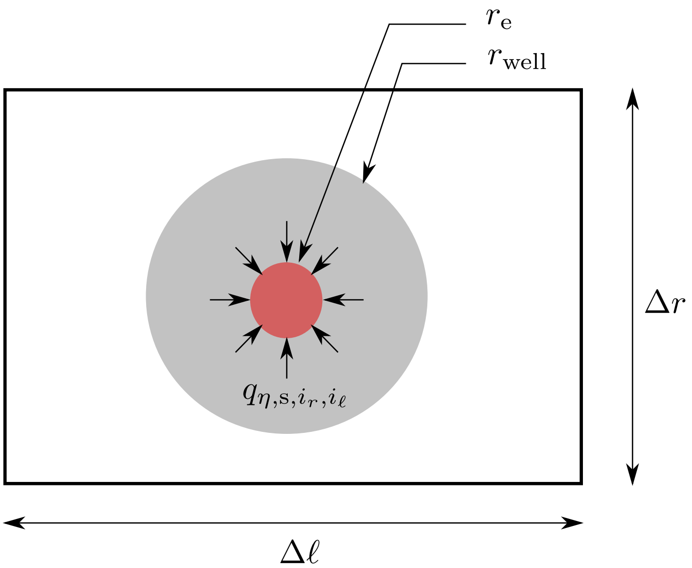

Figure 5.4: 2D diagram of horizontal well in a single cell.

$$\begin{aligned}\left(q_{\mathrm{s}}\cdot\int_{r_{\mathrm{e}}}^{r_{\mathrm{well}}}\frac{\partial r}{r}\right)_{r,\ell}&=-\left(2\pi\Delta\ell\cdot\lambda_r\left(\int_{P_{\mathrm{re}}}^{P_{\mathrm{rw}}}\partial P-h\int_{r_{\mathrm{e}}}^{r_{\mathrm{well}}}\partial r\right)\right)_{r,\ell}\\ \left(q_{\mathrm{s}}\cdot\ln\left(\frac{r_{\mathrm{well}}}{r_{\mathrm{e}}}\right)\right)_{r,\ell}&=-\left(2\pi\Delta\ell\cdot\lambda_r\left(P_{\mathrm{rw}}-P_{\mathrm{re}}-h\left(r_{\mathrm{well}}-r_{\mathrm{e}}\right)\right)\right)_{r,\ell}\\ q_{\mathrm{s,r},\ell}&=-\left(\frac{2\pi\Delta\ell}{\ln\left(\frac{r_{\mathrm{well}}}{r_{\mathrm{e}}}\right)}\cdot\lambda_r\left(P_{\mathrm{rw}}-P_{\mathrm{re}}-h\left(r_{\mathrm{well}}-r_{\mathrm{e}}\right)\right)\right)_{r,\ell},\end{aligned}\tag{5.34}$$

For two-phase flow, Equation 5.34 can be written as

$$q_{\eta,\mathrm{s},r,\ell}=-\left(\frac{2\pi\Delta\ell}{\ln\left(\frac{r_{\mathrm{well}}}{r_{\mathrm{e}}}\right)}\cdot\lambda_{\eta,r}\left(P_{\mathrm{rw},\eta}-P_{\mathrm{re},\eta}-h_\eta\left(r_{\mathrm{well}}-r_{\mathrm{e}}\right)\right)\right)_{r,\ell}\tag{5.35}$$

Total specified flow rate $q_{\eta,\mathrm{s,tot}}$ is the sum of the flow rates from all perforated zones

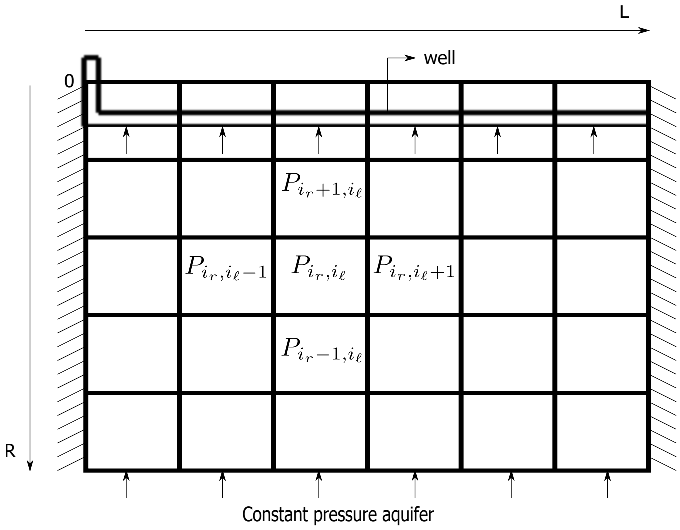

Figure 5.5: The block-centered grid system and a five-point stencil scheme (Zhang 2013).

$$q_{\eta,\mathrm{s,tot}} = -\sum_{n=1}^{N_\mathrm{v}} \left(\frac{2\pi\Delta\ell}{\ln\left(\frac{r_\mathrm{well}}{r_\mathrm{e}}\right)} \cdot \lambda_{\eta,r} \left(P_{\mathrm{rw},\eta} - P_{\mathrm{re},\eta} - h_\eta \left(r_\mathrm{well} - r_\mathrm{e}\right)\right) \right)_{r,\ell}, \tag{5.36}$$

here, N_v is the total number of perforated zones of the well, and $(r,\ell) \in [0,\Delta r] \times [0, L_\mathrm{well}]$.

Specified total oil and water mixture production rate $q_\mathrm{mix,tot}$ can be written as

$$q_\mathrm{mix,tot} = q_\mathrm{w,s,tot} + q_\mathrm{o,s,tot}, \tag{5.37}$$

here, $q_\mathrm{w,s,tot}$ and $q_\mathrm{o,s,tot}$ are the total production rate of water, and oil, respectively.

Total oil, and water mixture production rate for each cell near the well $q_{\mathrm{mix},r,\ell}$ can be written as

$$q_{\mathrm{mix},r,\ell} = q_{\mathrm{w,s},r,\ell} + q_{\mathrm{o,s},r,\ell}. \tag{5.38}$$

5.3.2.2 Assumptions and Model Simplification

To simplify the implementation of the model, it is convenient to number the grids by i_r and i_ℓ . By numbering the grids for $(i_r, i_\ell) \in \{1,\ldots,n_r\} \times \{1,\ldots,n_\ell\}$ as shown in Figure 5.5. From Equation 5.27, the model for the cell centered at (i_r, i_ℓ), as shown in Figure 5.6, can now be written as

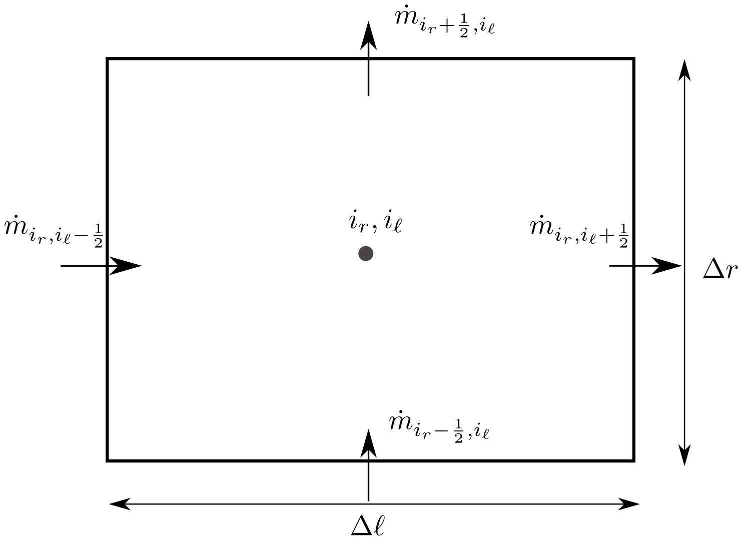
$\dot{m}_{i_r+\frac{1}{2},i_\ell}$
$\dot{m}_{i_r,i_\ell-\frac{1}{2}}$
i_r, i_ℓ
$\dot{m}_{i_r,i_\ell+\frac{1}{2}}$
Δr
$\dot{m}_{i_r-\frac{1}{2},i_\ell}$
$\Delta\ell$

Figure 5.6: Single cell of the reservoir in (i_r, i_ℓ) coordinate (Zhang 2013).

$$\begin{aligned}\frac{d\left(\frac{1}{B_\eta}\cdot\phi\cdot S_\eta\right)_{i_r,i_\ell}}{dt} &= \frac{-\left(\frac{1}{B_\eta}\cdot\lambda_{\eta,r}\left(\frac{\partial P_\eta}{\partial r}-h_\eta\right)r\right)_{i_r-\frac{1}{2},i_\ell}+\left(\frac{1}{B_\eta}\cdot\lambda_{\eta,r}\left(\frac{\partial P_\eta}{\partial r}-h_\eta\right)r\right)_{i_r+\frac{1}{2},i_\ell}}{r_{i_r,i_\ell}\cdot\Delta r}\\ &-\frac{-\left(\frac{1}{B_\eta}\cdot\lambda_{\eta,\ell}\left(\frac{\partial P_\eta}{\partial\ell}\right)\right)_{i_r,i_\ell+\frac{1}{2}}+\left(\frac{1}{B_\eta}\cdot\lambda_{\eta,\ell}\left(\frac{\partial P_\eta}{\partial\ell}\right)\right)_{i_r,i_\ell-\frac{1}{2}}}{\Delta\ell}\\ &-\frac{\left(\frac{1}{B_\eta}\cdot q_{\eta,\mathrm{s}}\right)_{i_r,i_\ell}}{\beta r_{r,\ell}\Delta r\Delta\ell},\end{aligned} \tag{5.39}$$

here, $(i_r, i_\ell) \in \{1,\ldots,n_r\}\times\{1,\ldots,n_{\text{well}}\}$ where n_ℓ, and n_r represent number of grids along the length, and the radius of a reservoir, respectively.

Let n_{well} be the number of grids along the well length. Let us assume that $\Delta\ell_{\text{well}} = \Delta\ell$ which leads to

$$\frac{L_{\text{well}}}{\Delta\ell_{\text{well}}} = \frac{L_{\text{well}}}{\Delta\ell} = n_{\text{well}}, \tag{5.40}$$

here, $\Delta\ell_{\text{well}}$, and L_{well} represent step length of a well, and the total length of a well, respectively.

Horizontal well lies next to the grids at $(i_r, i_\ell) \in n_r \times \{1,\ldots,n_{\text{well}}\}$. Oil and water produced from the oil reservoir will flow into the well through perforated zones.

Let us consider, each grid along the well contains one perforated zone i.e., the number of grids along the well n_{well} equal the number of perforated zones N_{v}.

The fluid production terms $\frac{\left(\frac{\rho_{\eta\text{s}}}{B_\eta}\cdot q_{\eta,\text{s}}\right)_{i_r,i_\ell}}{\beta r_{r,\ell}\Delta r\Delta\ell}$ are nonzero at grids $(i_r,i_\ell)\in n_r\times\{1,\ldots,n_{\text{well}}\}$ i.e.,

$$q_{\eta,\text{s},i_r,i_\ell}=\begin{cases}0, & (i_r,i_\ell)\in\{1,\ldots,n_r-1\}\times\{1,\ldots,n_{\text{well}}\}\\ q_{\eta,\text{s},i_r,i_\ell}, & (i_r,i_\ell)\in n_r\times\{1,\ldots,n_{\text{well}}\}\end{cases} \tag{5.41}$$

In Equation 5.39, $\left(\frac{1}{B_\eta}\cdot\phi\cdot S_\eta\right)_{i_r,i_\ell}$ is the average value of $\left(\frac{1}{B_\eta}\cdot\phi\cdot S_\eta\right)$ in intervals $(r,l)\in[(R-(i_r-1))\cdot\Delta r,R-i_r\cdot\Delta r]\times[(i_\ell-1)\cdot\Delta\ell,i_\ell\cdot\Delta\ell]$ while,

$$\left(\frac{1}{B_\eta}\cdot\lambda_{\eta,r}\left(\frac{\partial P_\eta}{\partial r}-h_\eta\right)r\right)_{i_r-\frac{1}{2},i_\ell}=\left(\frac{1}{B_\eta}\cdot\lambda_{\eta,r}\left(\frac{\partial P_\eta}{\partial r}-h_\eta\right)r\right)(t,r,\ell),$$
$$\text{where: } (r,l)\in(R-(i_r-1)\cdot\Delta r)\times[(i_\ell-1)\cdot\Delta\ell,i_\ell\cdot\Delta\ell] \tag{5.42}$$

$$\left(\frac{1}{B_\eta}\cdot\lambda_{\eta,r}\left(\frac{\partial P_\eta}{\partial r}-h_\eta\right)r\right)_{i_r+\frac{1}{2},i_\ell}=\left(\frac{1}{B_\eta}\cdot\lambda_{\eta,r}\left(\frac{\partial P_\eta}{\partial r}-h_\eta\right)r\right)(t,r,\ell),$$
$$\text{where: } (r,l)\in(R-i_r\cdot\Delta r)\times[(i_\ell-1)\cdot\Delta\ell,i_\ell\cdot\Delta\ell] \tag{5.43}$$

$$\left(\frac{1}{B_\eta}\cdot\lambda_{\eta,\ell}\left(\frac{\partial P_\eta}{\partial\ell}\right)\right)_{i_r,i_\ell+\frac{1}{2}}=\left(\frac{1}{B_\eta}\cdot\lambda_{\eta,\ell}\left(\frac{\partial P_\eta}{\partial\ell}\right)\right)(t,r,\ell),$$
$$\text{where: } (r,l)\in[(R-(i_r-1)\cdot\Delta r),(R-i_r\cdot\Delta r)]\times i_\ell\cdot\Delta\ell \tag{5.44}$$

$$\left(\frac{1}{B_\eta}\cdot\lambda_{\eta,\ell}\left(\frac{\partial P_\eta}{\partial\ell}\right)\right)_{i_r,i_\ell-\frac{1}{2}}=\left(\frac{1}{B_\eta}\cdot\lambda_{\eta,\ell}\left(\frac{\partial P_\eta}{\partial\ell}\right)\right)(t,r,\ell),$$
$$\text{where: } (r,l)\in[(R-(i_r-1)\cdot\Delta r),(R-i_r\cdot\Delta r)]\times(i_\ell-1)\cdot\Delta\ell \tag{5.45}$$

For cells neighborhood of the well i.e., $(i_r,i_\ell)\in n_r\times\{1,\ldots,n_{\text{well}}\}$

$$q_{\eta,\text{s},i_r,i_\ell}=-\left(\frac{2\pi\Delta\ell}{\ln\left(\frac{r_{\text{well}}}{r_{\text{e}}}\right)}\cdot\lambda_{\eta,r}\left(P_{\text{rw},\eta}-P_{\text{re},\eta}-h_\eta\left(r_{\text{well}}-r_{\text{e}}\right)\right)\right)_{i_r,i_\ell}, \tag{5.46}$$

where $P_{\text{re},\eta,i_r,i_\ell}=P_{\eta,i_r,i_\ell}$.

Furthermore, left hand side of Equation 5.39 can be evaluated as

$$\begin{aligned}\frac{d\left(\frac{1}{B_\eta}\cdot\phi\cdot S_\eta\right)}{dt} &= \phi\cdot S_\eta\frac{d\left(\frac{1}{B_\eta}\right)}{dt}+\frac{S_\eta}{B_\eta}\frac{d\phi}{dt}+\frac{\phi}{B_\eta}\frac{dS_\eta}{dt}\\ &= \left[\frac{B_\eta}{B_\eta}\phi\cdot S_\eta\frac{d\left(\frac{1}{B_\eta}\right)}{dP_\eta}+\frac{\phi\cdot S_\eta}{\phi\cdot B_\eta}\frac{d\phi}{dP_\eta}\right]\frac{dP_\eta}{dt}+\frac{\phi}{B_\eta}\frac{dS_\eta}{dt}. \end{aligned} \tag{5.47}$$

Introducing, $C_\eta = B_\eta\frac{d\left(\frac{1}{B_\eta}\right)}{dP_\eta}$ and $C_{\text{rock}} = \frac{1}{\phi}\frac{d\phi}{dP_\eta}$, where C_η, and C_{rock} are the compressibility of fluid and rock, respectively.

The Equation 5.47 now becomes

$$\frac{d\left(\frac{1}{B_\eta}\cdot\phi\cdot S_\eta\right)}{dt} = \left(\frac{\phi S_\eta}{B_\eta}C_\eta+\frac{\phi S_\eta}{B_\eta}C_{\text{rock}}\right)\frac{dP_\eta}{dt}+\frac{\phi}{B_\eta}\frac{dS_\eta}{dt}.$$

Introducing the definition

$$\begin{aligned}\Delta z_{\Delta i_r,i_\ell} &\triangleq z_{i_r+\frac{1}{2},i_\ell}-z_{i_r-\frac{1}{2},i_\ell}\\ \Delta z_{i_r,\Delta i_\ell} &\triangleq z_{i_r,i_\ell+\frac{1}{2}}-z_{i_r,i_\ell-\frac{1}{2}},\end{aligned}$$

Equation 5.39 now becomes

$$\begin{aligned}\left[\left(\frac{\phi S_\eta}{B_\eta}C_\eta+\frac{\phi S_\eta}{B_\eta}C_{\text{rock}}\right)\frac{dP_\eta}{dt}+\frac{\phi}{B_\eta}\frac{dS_\eta}{dt}\right]_{i_r,i_\ell} &= \frac{\Delta\left(\frac{1}{B_\eta}\cdot\lambda_{\eta,r}\left(\frac{\partial P_\eta}{\partial r}-h_\eta\right)r\right)_{\Delta i_r,i_\ell}}{r_{i_r,i_\ell}\cdot\Delta r}\\ &+\frac{\Delta\left(\frac{1}{B_\eta}\cdot\lambda_{\eta,\ell}\left(\frac{\partial P_\eta}{\partial\ell}\right)\right)_{i_r,\Delta i_\ell}}{\Delta\ell}\\ &-\frac{\left(\frac{1}{B_\eta}\cdot q_{\eta,\text{s}}\right)_{i_r,i_\ell}}{\beta r_{r,\ell}\Delta r\Delta\ell}.\end{aligned} \tag{5.48}$$

For the simplification, the following assumptions can be made:

1. Both rock and fluid are incompressible, i.e., $C_\eta = 0$, and $C_{\text{rock}} = 0$.
2. Constant density and formation volume factor.
3. Immiscible two-phase flow.

4. Capillary pressure is assumed to be equal to zero, i.e., $P_{\text{cow}} = P_{\text{o}} - P_{\text{w}} = 0$. Here, P_{o} and P_{w} are pressure exerted by oil and water, respectively.

5. Effect of temperature is neglected.

6. Uniform rock porosity, i.e., $\phi_{i_r,i_\ell} = \phi$.

7. Isotropic medium $K_r = K_\ell$

With these assumptions, Equation 5.48 can be simplified to

$$\begin{aligned}\phi\left(\frac{dS_\eta}{dt}\right)_{i_r,i_\ell} &= \frac{\Delta\left(\lambda_{\eta,r}\left(\frac{\partial P_\eta}{\partial r} - h_\eta\right)r\right)_{\Delta i_r,i_\ell}}{r_{i_r,i_\ell}\cdot\Delta r} \\ &\quad + \frac{\Delta\left(\lambda_{\eta,\ell}\left(\frac{\partial P_\eta}{\partial \ell}\right)\right)_{i_r,\Delta i_\ell}}{\Delta\ell} - \frac{q_{\eta,\text{s}_{i_r,i_\ell}}}{\beta r_{r,\ell}\Delta r\Delta\ell}. \end{aligned} \tag{5.49}$$

For $P_{\text{w}} = P_{\text{o}} = P$, and $\lambda_{\eta,r} = \lambda_{\eta,\ell}$

$$\begin{aligned}\frac{\partial P_\eta}{\partial \ell} &= \frac{\partial P}{\partial \ell}, \\ \frac{\partial P_\eta}{\partial r} &= \frac{\partial P}{\partial r},\end{aligned} \tag{5.50}$$

which leads to

$$\phi\left(\frac{dS_\eta}{dt}\right)_{i_r,i_\ell} = \frac{\Delta\left(\lambda_\eta\left(\frac{\partial P}{\partial r} - h_\eta\right)r\right)_{\Delta i_r,i_\ell}}{r_{i_r,i_\ell}\cdot\Delta r} + \frac{\Delta\left(\lambda_\eta\left(\frac{\partial P}{\partial \ell}\right)\right)_{i_r,\Delta i_\ell}}{\Delta\ell} - \frac{q_{\eta,\text{s}_{i_r,i_\ell}}}{\beta r_{r,\ell}\Delta r\Delta\ell}. \tag{5.51}$$

Also, $P_{\text{rw},\eta} = P_{\text{rw}}$ and $P_{\text{re},\eta} = P_{\text{re}}$. This leads to

$$q_{\eta,\text{s}_{i_r,i_\ell}} = -\left(\frac{2\pi\Delta\ell}{\ln\left(\frac{r_{\text{well}}}{r_{\text{e}}}\right)}\cdot\lambda_\eta\left(P_{\text{rw}} - P_{\text{re}} - h_\eta\left(r_{\text{well}} - r_{\text{e}}\right)\right)\right)_{i_r,i_\ell} \tag{5.52}$$

5.3.2.3 Mobility determination at the integration points

Most of the works in the literature use an upstream scheme to evaluate the mobilities (Cordazzo et al. 2002). The upstream scheme can be summarized in the form

$$\lambda_{\eta,i_r-\frac{1}{2},i_\ell} = \begin{cases} \lambda_{\eta,i_r,i_\ell}, & \lambda_{\eta,i_r,i_\ell} > \lambda_{\eta,i_r-1,i_\ell} \\ \lambda_{\eta,i_r-\frac{1}{2},i_\ell}, & \lambda_{\eta,i_r,i_\ell} < \lambda_{\eta,i_r-1,i_\ell} \end{cases}$$

$$\lambda_{\eta,i_r+\frac{1}{2},i_\ell} = \begin{cases} \lambda_{\eta,i_r,i_\ell}, & \lambda_{\eta,i_r,i_\ell} > \lambda_{\eta,i_r+1,i_\ell} \\ \lambda_{\eta,i_r+1,i_\ell}, & \lambda_{\eta,i_r,i_\ell} < \lambda_{\eta,i_r+1,i_\ell} \end{cases}$$

Similarly,

$$\lambda_{\eta,i_r,i_\ell+\frac{1}{2}} = \begin{cases} \lambda_{\eta,i_r,i_\ell}, & \lambda_{\eta,i_r,i_\ell} > \lambda_{\eta,i_r,i_\ell+1} \\ \lambda_{\eta,i_r,i_\ell+1}, & \lambda_{\eta,i_r,i_\ell} < \lambda_{\eta,i_r,i_\ell+1} \end{cases}$$

$$\lambda_{\eta,i_r,i_\ell-\frac{1}{2}} = \begin{cases} \lambda_{\eta,i_r,i_\ell}, & \lambda_{\eta,i_r,i_\ell} > \lambda_{\eta,i_r,i_\ell-1} \\ \lambda_{\eta,i_r,i_\ell-1}, & \lambda_{\eta,i_r,i_\ell} < \lambda_{\eta,i_r,i_\ell-1} \end{cases}$$

5.3.2.4 Representation of valve and pipe

The valves are represented by a homogeneous flow model of sub-critical flow through a pipe containing restriction as

$$\Delta P_{\text{valve}} = 2C_{\text{u}} \frac{\rho_{\text{mix}}}{2C_{\text{v}}^2 A_{\text{valve}}^2} q_{\text{mix}}^2,$$

where

$$\rho_{\text{mix}} = \frac{q_{\text{w,s}}\rho_{\text{w}} + q_{\text{s,o}}\rho_{\text{o}}}{q_{\text{mix}}},$$

and

$$\Delta P_{\text{valve}} = P_{\text{rw}} - P_{\text{bh}},$$

here, C_{u} is a unit conversion constant, C_{v} is a dimensionless flow coefficient of the valve, A_{valve} is the constriction effective area, ρ_{mix} is the density of the fluid mixture, q_{mix} is the volumetric flow rate of the mixture, P_{rw} is the well pressure, and P_{bh} is the bottom hole pressure.

Let us assume that each grid block along the well contains one ICV with maximum effective constriction area A_{valve}. Effective constriction area of inflow control valves can be manipulated with the help of actuators.

$$(\Delta P_{\text{valve}})_{i_r,i_\ell} = 2C_{\text{u}} \frac{(q_{\text{w,s},i_r,i_\ell}\rho_{\text{w}} + q_{\text{o,s},i_r,i_\ell}\rho_{\text{o}})}{2C_{\text{v}}^2 A_{\text{valve},i_r,i_\ell}^2} q_{\text{mix},i_r,i_\ell}, \tag{5.53}$$

here,

$$(\Delta P_{\text{valve}})_{i_r,i_\ell} = P_{\text{rw},i_r,i_\ell} - P_{\text{bh},i_r,i_\ell},$$

where $(i_r, i_\ell) \in n_r \times \{1, \ldots, n_{\text{well}}\}$.

The pipes are modeled as a hydraulic network using the following equation:

$$\left(\Delta P_{\text{pipe}}\right)_{i_r,i_\ell} = f \cdot (q_{\text{w,s},i_r,i_\ell}\rho_{\text{w}} + q_{\text{o,s},i_r,i_\ell}\rho_{\text{o}}) \frac{8\Delta L_{\text{pipe}}}{\pi^2 \left(2r_{\text{p}}\right)^5}, \tag{5.54}$$

where

$$\left(\Delta P_{\text{pipe}}\right)_{i_r,i_\ell} = P_{\text{bh},i_r,i_\ell} - P_{\text{bh},i_r,i_\ell-1},$$

where $(i_r, i_\ell) \in n_r \times \{1, \ldots, n_{\text{well}}\}$, f is the fanning friction factor, ΔL_{pipe} is the pipe step length which assumed to be equal to well step length $\Delta\ell_{\text{well}}$ and reservoir step length $\Delta\ell$, r_{p} is the radius of a production pipe.

5.3.3 Numerical Solution

In the numerical simulation, the finite difference method uses finite differences to approximate derivatives of ordinary differential equations. The forward difference method is used in this work.

Forward difference scheme can be expressed as

$$\Delta f(x) = f(x+h) - f(x). \tag{5.55}$$

Equation 5.49 can be further discretized by applying forward difference approximation to the gradient of pressure as

$$
\begin{aligned}
\left(\frac{\partial P}{\partial r}\right)_{i_r-\frac{1}{2},i_\ell} &= \frac{P_{i_r,i_\ell} - P_{i_r-1,i_\ell}}{\Delta r},\\
\left(\frac{\partial P}{\partial r}\right)_{i_r+\frac{1}{2},i_\ell} &= \frac{P_{i_r+1,i_\ell} - P_{i_r,i_\ell}}{\Delta r}.
\end{aligned}
\tag{5.56}
$$

Similarly,

$$
\begin{aligned}
\left(\frac{\partial P}{\partial \ell}\right)_{i_r,i_\ell-\frac{1}{2}} &= \frac{P_{i_r,i_\ell} - P_{i_r,i_\ell-1}}{\Delta \ell},\\
\left(\frac{\partial P}{\partial \ell}\right)_{i_r,i_\ell+\frac{1}{2}} &= \frac{P_{i_r,i_\ell+1} - P_{i_r,i_\ell}}{\Delta \ell}.
\end{aligned}
\tag{5.57}
$$

Now,

$$
\begin{aligned}
\phi\left(\frac{dS_\eta}{dt}\right)_{i_r,i_\ell} = {} & \left[\frac{(\lambda_\eta r)_{i_r+\frac{1}{2},i_\ell}}{r_{i_r,i_\ell}\cdot\Delta r^2}\right] P_{i_r+1,i_\ell} + \left[\frac{\lambda_{\eta,i_r,i_\ell-\frac{1}{2}}}{\Delta\ell^2}\right] P_{i_r,i_\ell-1}\\
& + \left[-\frac{(\lambda_\eta r)_{i_r-\frac{1}{2},i_\ell}}{r_{i_r,i_\ell}\cdot\Delta r^2} - \frac{(\lambda_\eta r)_{i_r+\frac{1}{2},i_\ell}}{r_{i_r,i_\ell}\cdot\Delta r^2} - \frac{\lambda_{\eta,i_r,i_\ell-\frac{1}{2}}}{\Delta\ell^2} - \frac{\lambda_{\eta,i_r,i_\ell+\frac{1}{2}}}{\Delta\ell^2}\right] P_{i_r,i_\ell}\\
& + \left[\frac{\lambda_{\eta,i_r,i_\ell+\frac{1}{2}}}{\Delta\ell^2}\right] P_{i_r,i_\ell+1} + \left[\frac{(\lambda_\eta r)_{i_r-\frac{1}{2},i_\ell}}{r_{i_r,i_\ell}\cdot\Delta r^2}\right] P_{i_r-1,i_\ell}\\
& - \left[\left(\frac{(\lambda_\eta r)_{i_r-\frac{1}{2},i_\ell}}{r_{i_r,i_\ell}\cdot\Delta r} - \frac{(\lambda_\eta r)_{i_r+\frac{1}{2},i_\ell}}{r_{i_r,i_\ell}\cdot\Delta r}\right) h_\eta + \frac{q_{\eta,\mathrm{s},i_r,i_\ell}}{\beta r_{r,\ell}\Delta r\Delta\ell}\right].
\end{aligned}
\tag{5.58}
$$

For simplification, defining the following coefficients

$$
\begin{aligned}
a_{\eta,1,i_r,i_\ell} &= \frac{(\lambda_\eta r)_{i_r+\frac{1}{2},i_\ell}}{r_{i_r,i_\ell}\cdot\Delta r^2}\\
a_{\eta,2,i_r,i_\ell} &= \frac{\lambda_{\eta,i_r,i_\ell-\frac{1}{2}}}{\Delta\ell^2}\\
a_{\eta,3,i_r,i_\ell} &= -\frac{(\lambda_\eta r)_{i_r-\frac{1}{2},i_\ell}}{r_{i_r,i_\ell}\cdot\Delta r^2}-\frac{(\lambda_\eta r)_{i_r+\frac{1}{2},i_\ell}}{r_{i_r,i_\ell}\cdot\Delta r^2}-\frac{\lambda_{\eta,i_r,i_\ell-\frac{1}{2}}}{\Delta\ell^2}-\frac{\lambda_{\eta,i_r,i_\ell+\frac{1}{2}}}{\Delta\ell^2}\\
a_{\eta,4,i_r,i_\ell} &= \frac{\lambda_{\eta,i_r,i_\ell+\frac{1}{2}}}{\Delta\ell^2}\\
a_{\eta,5,i_r,i_\ell} &= \frac{(\lambda_\eta r)_{i_r-\frac{1}{2},i_\ell}}{r_{i_r,i_\ell}\cdot\Delta r^2}\\
a_{\eta,6,i_r,i_\ell} &= \left(\frac{(\lambda_\eta r)_{i_r-\frac{1}{2},i_\ell}}{r_{i_r,i_\ell}\cdot\Delta r}-\frac{(\lambda_\eta r)_{i_r+\frac{1}{2},i_\ell}}{r_{i_r,i_\ell}\cdot\Delta r}\right)h_\eta+\frac{q_{\eta,\mathrm{s},i_r,i_\ell}}{\beta r_{r,\ell}\Delta r\Delta\ell}.
\end{aligned}
\tag{5.59}
$$

Substituting Equation 5.59 into Equation 5.58 yields:

$$
\begin{aligned}
\phi\left(\frac{dS_\eta}{dt}\right)_{i_r,i_\ell} &= a_{\eta,1,i_r,i_\ell}P_{i_r+1,i_\ell}+a_{\eta,2,i_r,i_\ell}P_{i_r,i_\ell-1}+a_{\eta,3,i_r,i_\ell}P_{i_r,i_\ell}\\
&\quad+a_{\eta,4,i_r,i_\ell}P_{i_r,i_\ell+1}+a_{\eta,5,i_r,i_\ell}P_{i_r-1,i_\ell}-a_{\eta,6,i_r,i_\ell}.
\end{aligned}
\tag{5.60}
$$

5.3.3.1 Boundary conditions

The reservoir boundary conditions are no flux from the left and right sides and roof and bottom of the wedge-shaped reservoir, and constant pressure from the aquifer on the bottom side. The well boundary is expressed as a specified liquid flow rate.

For $(i_r,i_\ell)\in\{1,\ldots,n_r\}\times 1$, no flux from the left side of the boundary

$$\left(\frac{\partial P}{\partial\ell}\right)_{i_r,i_\ell-\frac{1}{2}}=0. \tag{5.61}$$

For $(i_r,i_\ell)\in\{1,\ldots,n_r\}\times n_\ell$, no flux from the right side of the boundary

$$\left(\frac{\partial P}{\partial\ell}\right)_{i_r,i_\ell+\frac{1}{2}}=0. \tag{5.62}$$

For $(i_r,i_\ell)\in 1\times\{1,\ldots,n_\ell\}$, cells next to constant pressure aquifer:

Using forward difference method to discretize $\left(\frac{\partial P}{\partial r}\right)_{i_r-\frac{1}{2},i_\ell}$

$$\left(\frac{\partial P}{\partial r}\right)_{i_r-\frac{1}{2},i_\ell}=\frac{P_{i_r,i_\ell}-P_{i_r-1,i_\ell}}{\Delta r} \tag{5.63}$$

When $i_r=1$, P_{i_r-1,i_ℓ} lies beyond the reservoir boundary i.e., aquifer region, thus $P_{0,i_\ell}=P_\mathrm{a}$ where P_a is a constant aquifer pressure

$$\left(\frac{\partial P}{\partial r}\right)_{i_r-\frac{1}{2},i_\ell}=\frac{P_{1,i_\ell}-P_\mathrm{a}}{\Delta r}. \tag{5.64}$$

Specified liquid flow rate

$$q_\mathrm{mix,tot}=q_\mathrm{w,s,tot}+q_\mathrm{o,s,tot}, \tag{5.65}$$

where

$$q_\mathrm{w,s,tot}=-\sum_{i_\ell=1}^{n_\mathrm{well}}\left(\frac{2\pi\Delta\ell}{\ln\left(\frac{r_\mathrm{well}}{r_\mathrm{e}}\right)}\cdot\lambda_\mathrm{w}\left(P_\mathrm{rw}-P_\mathrm{re}-h_\mathrm{w}\left(r_\mathrm{well}-r_\mathrm{e}\right)\right)\right)_{n_r,i_\ell} \tag{5.66}$$

$$q_\mathrm{o,s,tot}=-\sum_{i_\ell=1}^{n_\mathrm{well}}\left(\frac{2\pi\Delta\ell}{\ln\left(\frac{r_\mathrm{well}}{r_\mathrm{e}}\right)}\cdot\lambda_\mathrm{o}\left(P_\mathrm{rw}-P_\mathrm{re}-h_\mathrm{o}\left(r_\mathrm{well}-r_\mathrm{e}\right)\right)\right)_{n_r,i_\ell} \tag{5.67}$$

5.3.3.2 Pressure Equation For Incompressible Immiscible flow

To derive the pressure equation, we sum Equation 5.60 for the oil and water phases, and using the fact that $S_\mathrm{w}+S_\mathrm{o}=1$, we deduce

$$\begin{aligned}\phi\left(\frac{dS_\mathrm{w}}{dt}+\frac{dS_\mathrm{o}}{dt}\right)_{i_r,i_\ell}&=\left(a_\mathrm{w,1}+a_\mathrm{o,1}\right)_{i_r,i_\ell}P_{i_r+1,i_\ell}+\left(a_\mathrm{w,2}+a_\mathrm{o,2}\right)_{i_r,i_\ell}P_{i_r,i_\ell-1} && (5.68)\\&+\left(a_\mathrm{w,3}+a_\mathrm{o,3}\right)_{i_r,i_\ell}P_{i_r,i_\ell}+\left(a_\mathrm{w,4}+a_\mathrm{o,4}\right)_{i_r,i_\ell}P_{i_r,i_\ell+1} && (5.69)\\&+\left(a_\mathrm{w,5}+a_\mathrm{o,5}\right)_{i_r,i_\ell}P_{i_r-1,i_\ell}-\left(a_\mathrm{w,6}+a_\mathrm{o,6}\right)_{i_r,i_\ell},\end{aligned}$$

here,

$$\phi\left(\frac{dS_\mathrm{w}}{dt}+\frac{dS_\mathrm{o}}{dt}\right)_{i_r,i_\ell}=\phi\left(\frac{dS_\mathrm{w}}{dt}+\frac{d\left(1-S_\mathrm{w}\right)}{dt}\right)_{i_r,i_\ell}=0,$$

and

$$\begin{aligned}
a_{\mathrm{w},1} + a_{\mathrm{o},1} &= a_1 \\
a_{\mathrm{w},2} + a_{\mathrm{o},2} &= a_2 \\
a_{\mathrm{w},3} + a_{\mathrm{o},3} &= a_3 \\
a_{\mathrm{w},4} + a_{\mathrm{o},4} &= a_4 \\
a_{\mathrm{w},5} + a_{\mathrm{o},5} &= a_5 \\
a_{\mathrm{w},6} + a_{\mathrm{o},6} &= a_6,
\end{aligned}$$

which leads Equation 5.68 to

$$a_{1,i_r,i_\ell} P_{i_r+1,i_\ell} + a_{2,i_r,i_\ell} P_{i_r,i_\ell-1} + a_{3,i_r,i_\ell} P_{i_r,i_\ell} + a_{4,i_r,i_\ell} P_{i_r,i_\ell+1} + a_{5,i_r,i_\ell} P_{i_r-1,i_\ell} = a_{6,i_r,i_\ell}. \tag{5.70}$$

The pressure Equation 5.70 can be written in matrix form

$$AP = B,$$

where A is a five-diagonal sparse matrix, and P is a vector of pressure.

$$A = \begin{bmatrix}
\times & \times & & & \times & & & & \\
\times & \times & \times & & & \times & & & \\
& \times & \times & \times & & & \times & & \\
& & & \cdot & & & & \times & \\
\times & & & & \cdot & & & & \times \\
& \times & & & & \cdot & & & \\
& & \times & & & \times & \times & \times & \\
& & & \times & & & \times & \times & \times \\
& & & & \times & & & \times & \times
\end{bmatrix}, P = \begin{bmatrix} P_{1,1} \\ P_{1,2} \\ \vdots \\ P_{1,n_\ell} \\ P_{2,1} \\ \vdots \\ P_{i_r,i_\ell} \\ \vdots \\ P_{n_r,n_\ell} \end{bmatrix}, B = \begin{bmatrix} B_{1,1} \\ B_{1,2} \\ \vdots \\ B_{1,n_\ell} \\ B_{2,1} \\ \vdots \\ B_{i_r,i_\ell} \\ \vdots \\ B_{n_r,n_\ell} \end{bmatrix}$$

The pressure is solved implicitly.

5.4 Model summary

For $(i_r, i_\ell) \in 1 \times 1$,

$$\phi \frac{dS_{\eta,i_r,i_\ell}}{dt} = \frac{u_{\mathrm{wa},i_r,i_\ell} R - (u_{\eta,r} r)_{i_r+\frac{1}{2},i_\ell}}{r_{i_r,i_\ell} \cdot \Delta r} - \frac{u_{\eta,\ell,i_r,i_\ell+\frac{1}{2}}}{\Delta \ell}$$

For $(i_r, i_\ell) \in 1 \times n_\ell$,

$$\phi \frac{dS_{\eta,i_r,i_\ell}}{dt} = \frac{u_{\mathrm{wa},i_r,i_\ell} R - (u_{\eta,r} r)_{i_r+\frac{1}{2},i_\ell}}{r_{i_r,i_\ell} \cdot \Delta r} + \frac{u_{\eta,\ell,i_r,i_\ell-\frac{1}{2}}}{\Delta \ell}$$

For $(i_r, i_\ell) \in n_r \times 1$,

$$\phi \frac{dS_{\eta,i_r,i_\ell}}{dt} = \frac{(u_{\eta,r} r)_{i_r-\frac{1}{2},i_\ell}}{r_{i_r,i_\ell} \cdot \Delta r} - \frac{u_{\eta,\ell,i_r,i_\ell+\frac{1}{2}}}{\Delta \ell} - \frac{q_{\eta,\mathrm{s},i_r,i_\ell}}{\beta r_{i_r,i_\ell} \Delta r \Delta \ell}$$

For $(i_r, i_\ell) \in n_r \times n_\ell$,

$$\phi \frac{dS_{\eta,i_r,i_\ell}}{dt} = \frac{(u_{\eta,r} r)_{i_r-\frac{1}{2},i_\ell}}{r_{i_r,i_\ell} \cdot \Delta r} + \frac{u_{\eta,\ell,i_r,i_\ell-\frac{1}{2}}}{\Delta \ell} - \frac{q_{\eta,\mathrm{s},i_r,i_\ell}}{\beta r_{i_r,i_\ell} \Delta r \Delta \ell}$$

For $(i_r, i_\ell) \in \{2, \ldots, n_r - 1\} \times \{2, \ldots, n_\ell - 1\}$,

$$\phi \frac{dS_{\eta,i_r,i_\ell}}{dt} = \frac{(u_{\eta,r} r)_{i_r-\frac{1}{2},i_\ell} - (u_{\eta,r} r)_{i_r+\frac{1}{2},i_\ell}}{r_{i_r,i_\ell} \cdot \Delta r} - \frac{u_{\eta,\ell,i_r,i_\ell+\frac{1}{2}} - u_{\eta,\ell,i_r,i_\ell-\frac{1}{2}}}{\Delta \ell}$$

For $(i_r, i_\ell) \in \{2, \dots, n_r - 1\} \times 1$,

$$\begin{aligned}\phi \frac{dS_{\eta,i_r,i_\ell}}{dt} = & \frac{(u_{\eta,r} r)_{i_r-\frac{1}{2},i_\ell} - (u_{\eta,r} r)_{i_r+\frac{1}{2},i_\ell}}{r_{i_r,i_\ell} \cdot \Delta r} \\ & - \frac{u_{\eta,\ell,i_r,i_\ell+\frac{1}{2}}}{\Delta \ell}\end{aligned}$$

For $(i_r, i_\ell) \in \{2, \dots, n_r - 1\} \times n_\ell$,

$$\begin{aligned}\phi \frac{dS_{\eta,i_r,i_\ell}}{dt} = & \frac{(u_{\eta,r} r)_{i_r-\frac{1}{2},i_\ell} - (u_{\eta,r} r)_{i_r+\frac{1}{2},i_\ell}}{r_{i_r,i_\ell} \cdot \Delta r} \\ & + \frac{u_{\eta,\ell,i_r,i_\ell-\frac{1}{2}}}{\Delta \ell}\end{aligned}$$

For $(i_r, i_\ell) \in 1 \times \{2, \dots, n_\ell - 1\}$,

$$\begin{aligned}\phi \frac{dS_{\eta,i_r,i_\ell}}{dt} = & \frac{u_{\mathrm{wa},i_r,i_\ell} - (u_{\eta,r} r)_{i_r+\frac{1}{2},i_\ell}}{r_{i_r,i_\ell} \cdot \Delta r} \\ & - \frac{u_{\eta,\ell,i_r,i_\ell+\frac{1}{2}} - u_{\eta,\ell,i_r,i_\ell-\frac{1}{2}}}{\Delta \ell}\end{aligned}$$

For $(i_r, i_\ell) \in n_r \times \{2, \dots, n_\ell - 1\}$,

$$\begin{aligned}\phi \frac{dS_{\eta,i_r,i_\ell}}{dt} = & \frac{(u_{\eta,r} r)_{i_r-\frac{1}{2},i_\ell}}{r_{i_r,i_\ell} \cdot \Delta r} \\ & - \frac{u_{\eta,\ell,i_r,i_\ell+\frac{1}{2}} - u_{\eta,\ell,i_r,i_\ell-\frac{1}{2}}}{\Delta \ell} - \frac{q_{\eta,\mathrm{s},i_r,i_\ell}}{\beta r_{i_r,i_\ell} \Delta r \Delta \ell}\end{aligned}$$

$u_{\eta,r} = -\lambda_\eta \left(\nabla P_{\eta,r} - h_\eta \nabla r_r\right)$

$u_{\eta,\ell} = -\lambda_\eta \left(\nabla P_{\eta,\ell} - h_\eta \nabla r_\ell\right)$

$q_{\eta,\mathrm{s}} = -\frac{2\pi\Delta\ell}{\ln\left(\frac{r_{\mathrm{well}}}{r_{\mathrm{e}}}\right)} \cdot \lambda_\eta \left(P_{\mathrm{rw},\eta} - P_{\mathrm{re},\eta} - h_\eta \left(r_{\mathrm{well}} - r_{\mathrm{e}}\right)\right)$

$\lambda_\eta = \frac{k_{\mathrm{rel},\eta}}{\mu_\eta} K$

$$h_\eta = \rho_\eta \cdot g \cdot \sin\left(\alpha + \frac{\beta}{2}\right)$$

$$P_{\mathrm{re},\eta} = P_\eta$$

$$\nabla P_{\eta,r} = \frac{\partial P_\eta}{\partial r}$$

$$\nabla P_{\eta,\ell} = \frac{\partial P_\eta}{\partial \ell}$$

$$\nabla r_r = \frac{\partial r}{\partial r}$$

$$\nabla r_\ell = \frac{\partial r}{\partial \ell}$$

$$u_{\mathrm{wa}} = -\lambda_{\mathrm{wa}}\left(\frac{P_{1,i_\ell} - P_{\mathrm{a}}}{\Delta r} - h_{\mathrm{w}}\right)$$

$$\lambda_{\mathrm{wa}} = \frac{k_{\mathrm{wa}}}{\mu_{\mathrm{w}}} K$$

For simplified model, $P_{\mathrm{re},\eta} = P_{\mathrm{re}}$, and $P_{\mathrm{rw},\eta} = P_{\mathrm{rw}}$

For simplified model, $P_\eta = P_{\mathrm{w}} = P_{\mathrm{o}} = P$

For calculation of pressure:

$$a_{1,i_r,i_\ell} P_{i_r+1,i_\ell} + a_{2,i_r,i_\ell} P_{i_r,i_\ell-1} + a_{3,i_r,i_\ell} P_{i_r,i_\ell} + a_{4,i_r,i_\ell} P_{i_r,i_\ell+1} + a_{5,i_r,i_\ell} P_{i_r-1,i_\ell} = a_{6,i_r,i_\ell}$$

$$a_{1,i_r,i_\ell} = a_{\mathrm{w},1,i_r,i_\ell} + a_{\mathrm{o},1,i_r,i_\ell}$$

$$a_{2,i_r,i_\ell} = a_{\mathrm{w},2,i_r,i_\ell} + a_{\mathrm{o},2,i_r,i_\ell}$$

$$a_{3,i_r,i_\ell} = a_{\mathrm{w},3,i_r,i_\ell} + a_{\mathrm{o},3,i_r,i_\ell}$$

$$a_{4,i_r,i_\ell} = a_{\mathrm{w},4,i_r,i_\ell} + a_{\mathrm{o},4,i_r,i_\ell}$$

$$a_{5_{i_r,i_\ell}} = a_{\mathrm{w},5_{i_r,i_\ell}} + a_{\mathrm{o},5_{i_r,i_\ell}}$$

$$a_{6,i_r,i_\ell} = a_{\mathrm{w},6,i_r,i_\ell} + a_{\mathrm{o},6,i_r,i_\ell}$$

$$a_{\eta,1,i_r,i_\ell} = \frac{\left(\lambda_\eta r\right)_{i_r+\frac{1}{2},i_\ell}}{r_{i_r,i_\ell} \cdot \Delta r^2}$$

$$a_{\eta,2,i_r,i_\ell} = \frac{\lambda_{\eta,i_r,i_\ell-\frac{1}{2}}}{\Delta \ell^2}$$

$$a_{\eta,3,i_r,i_\ell} = -\frac{\left(\lambda_\eta r\right)_{i_r-\frac{1}{2},i_\ell}}{r_{i_r,i_\ell} \cdot \Delta r^2} - \frac{\left(\lambda_\eta r\right)_{i_r+\frac{1}{2},i_\ell}}{r_{i_r,i_\ell} \cdot \Delta r^2} - \frac{\lambda_{\eta,i_r,i_\ell-\frac{1}{2}}}{\Delta \ell^2} - \frac{\lambda_{\eta,i_r,i_\ell+\frac{1}{2}}}{\Delta \ell^2}$$

$$a_{\eta,4,i_r,i_\ell} = \frac{\lambda_{\eta,i_r,i_\ell+\frac{1}{2}}}{\Delta \ell^2}$$

$$a_{\eta,5,i_r,i_\ell} = \frac{\left(\lambda_\eta r\right)_{i_r-\frac{1}{2},i_\ell}}{r_{i_r,i_\ell} \cdot \Delta r^2}$$

$$a_{\eta,6,i_r,i_\ell} = \left(\frac{(\lambda_\eta r)_{i_r-\frac{1}{2},i_\ell}}{r_{i_r,i_\ell} \cdot \Delta r} - \frac{(\lambda_\eta r)_{i_r+\frac{1}{2},i_\ell}}{r_{i_r,i_\ell} \cdot \Delta r} \right) h_\eta + \frac{q_{\eta,\mathrm{s},i_r,i_\ell}}{\beta r_{r,\ell} \Delta r \Delta \ell}$$

$$\lambda_{\eta,i_r-\frac{1}{2},i_\ell} = \begin{cases} \lambda_{\eta,i_r,i_\ell}, & \lambda_{\eta,i_r,i_\ell} > \lambda_{\eta,i_r-1,i_\ell} \\ \lambda_{\eta,i_r-\frac{1}{2},i_\ell}, & \lambda_{\eta,i_r,i_\ell} < \lambda_{\eta,i_r-1,i_\ell} \end{cases}$$

$$\lambda_{\eta,i_r+\frac{1}{2},i_\ell} = \begin{cases} \lambda_{\eta,i_r,i_\ell}, & \lambda_{\eta,i_r,i_\ell} > \lambda_{\eta,i_r+1,i_\ell} \\ \lambda_{\eta,i_r+1,i_\ell}, & \lambda_{\eta,i_r,i_\ell} < \lambda_{\eta,i_r+1,i_\ell} \end{cases}$$

$$\lambda_{\eta,i_r,i_\ell+\frac{1}{2}} = \begin{cases} \lambda_{\eta,i_r,i_\ell}, & \lambda_{\eta,i_r,i_\ell} > \lambda_{\eta,i_r,i_\ell+1} \\ \lambda_{\eta,i_r,i_\ell+1}, & \lambda_{\eta,i_r,i_\ell} < \lambda_{\eta,i_r,i_\ell+1} \end{cases}$$

$$\lambda_{\eta,i_r,i_\ell-\frac{1}{2}} = \begin{cases} \lambda_{\eta,i_r,i_\ell}, & \lambda_{\eta,i_r,i_\ell} > \lambda_{\eta,i_r,i_\ell-1} \\ \lambda_{\eta,i_r,i_\ell-1}, & \lambda_{\eta,i_r,i_\ell} < \lambda_{\eta,i_r,i_\ell-1} \end{cases}$$

$$AP = B$$

$$A = \begin{bmatrix} \times & \times & & & \times & & & & \\ \times & \times & \times & & & \times & & & \\ & \times & \times & \times & & & \times & & \\ & & & \cdot & & & & \times & \\ \times & & & & \cdot & & & & \times \\ & \times & & & & \cdot & & & \\ & & \times & & & \times & \times & \times & \\ & & & \times & & & \times & \times & \times \\ & & & & \times & & & \times & \times \end{bmatrix}, P = \begin{bmatrix} P_{1,1} \\ P_{1,2} \\ \vdots \\ P_{1,n_\ell} \\ P_{2,1} \\ \vdots \\ P_{i_r,i_\ell} \\ \vdots \\ P_{n_r,n_\ell} \end{bmatrix}, B = \begin{bmatrix} B_{1,1} \\ B_{1,2} \\ \vdots \\ B_{1,n_\ell} \\ B_{2,1} \\ \vdots \\ B_{i_r,i_\ell} \\ \vdots \\ B_{n_r,n_\ell} \end{bmatrix}$$

Pipe and valve model:

$$q_{\mathrm{mix},i_r,i_\ell} = \frac{2(\Delta P_{\mathrm{valve}})_{i_r,i_\ell} C_{\mathrm{v}}^2 A_{\mathrm{valve},i_r,i_\ell}^2}{2C_{\mathrm{u}} (q_{\mathrm{w,s}}\rho_{\mathrm{w}} + q_{\mathrm{o,s}}\rho_{\mathrm{o}})_{i_r,i_\ell}}$$

$$WC = \frac{q_{\mathrm{w,s}}}{q_{\mathrm{w,s}} + q_{\mathrm{o,s}}}$$

$$(\Delta P_{\mathrm{valve}})_{i_r,i_\ell} = P_{\mathrm{rw},i_r,i_\ell} - P_{\mathrm{bh},i_r,i_\ell}$$

$$P_{\mathrm{bh},i_r,i_\ell} = \left(\Delta P_{\mathrm{pipe}}\right)_{i_r,i_\ell} + P_{\mathrm{bh},i_r,i_\ell-1}$$

$$\left(\Delta P_{\mathrm{pipe}}\right)_{i_r,i_\ell} = f \cdot (q_{\mathrm{w,s}}\rho_{\mathrm{w}} + q_{\mathrm{o,s}}\rho_{\mathrm{o}})_{i_r,i_\ell} \frac{8\Delta L_{\mathrm{pipe}}}{\pi^2 \left(2r_{\mathrm{p}}\right)^5}$$

Symbol	Description	Unit
	Inputs $\boldsymbol{u}$	
A_{valve}	Maximum constriction effective area of a valve	m^2
P_{a}	Aquifer pressure	Pa
$q_{\text{mix,tot}}$	Total specified fluid production rate	m^3/s
	Outputs y	
$q_{\text{w,s},n_r,1:n_\ell}$	Water production rate	m^3/day
$q_{\text{o,s},n_r,1:n_\ell}$	Oil production rate	m^3/day
$\boldsymbol{WC}$	Water cut	-

Table 5.1: Descriptions of the inputs and outputs of the oil reservoir model.

The model can be expressed in standard DAE form as

$$\frac{dx}{dt} = f(x, z, u; \theta) \tag{5.71}$$

$$0 = g(x, z, u; \theta) \tag{5.72}$$

$$y = h(x, z, u; \theta) \tag{5.73}$$

The description of inputs $\boldsymbol{u}$, outputs y, differential variables x, algebraic variables z, and parameters $\boldsymbol{\theta}$ are given in Table 5.1, and Table 5.2.

Symbol	Description	Unit
Differential variables x		
$S_{\mathrm{w},1:n_r,1:n_\ell}$	Water saturation	-
$S_{\mathrm{o},1:n_r,1:n_\ell}$	Oil saturation	-
Algebraic variables z		
$u_{\mathrm{wa},1,1:n_\ell}$	Water velocity from aquifer	m/s
$u_{\mathrm{w},r,2:n_r-1,1:n_\ell}$	Water velocity along reservoir radius	m/s
$u_{\mathrm{o},r,2:n_r-1,1:n_\ell}$	Oil velocity along reservoir radius	m/s
$q_{\mathrm{mix},n_r,1:n_\ell}$	Fluid production rate	m^3/s
$u_{\mathrm{w},\ell,1:n_r,2:n_\ell-1}$	Water velocity along reservoir length	m/s
$u_{\mathrm{o},\ell,1:n_r,2:n_\ell-1}$	Oil velocity along reservoir length	m/s
$\lambda_{\mathrm{w},1:n_r,1:n_\ell}$	Mobility of water	$\mathrm{m}^3\mathrm{s}/\mathrm{kg}$
$\lambda_{\mathrm{o},1:n_r,1:n_\ell}$	Mobility of oil	$\mathrm{m}^3\mathrm{s}/\mathrm{kg}$
$k_{\mathrm{rel,w},1:n_r,1:n_\ell}$	Relative permeability of water	$\mathrm{m}^3\mathrm{s}/\mathrm{kg}$
$k_{\mathrm{rel,o},1:n_r,1:n_\ell}$	Relative permeability of oil	-
$P_{1:n_r,1:n_\ell}$	Reservoir pressure	-
$P_{\mathrm{rw},n_r,1:n_\ell}$	Well pressure	Pa
$P_{\mathrm{re},n_r,1:n_\ell}$	Equivalent reservoir pressure	Pa
$P_{\mathrm{bh},n_r,1:n_\ell+1}$	Bottom hole pressure	Pa
Parameters θ		
ϕ	Porosity	-
R	Reservoir radius	m
L	Reservoir length	m
K	Absolute permeability of a reservoir	mD
k_{wa}	Relative permeability of an aquifer	-
λ_{wa}	Mobility of aquifer water	$\mathrm{m}^3\mathrm{s}/\mathrm{kg}$
ρ_{w}	Water density	kg/m^3
ρ_{o}	Oil density	kg/m^3
μ_{o}	Oil viscosity	Pa.s
μ_{w}	Water viscosity	Pa.s
α	Inclination angle of a reservoir	degree
β	Arch angle of a wedge shaped reservoir	degree
r_{well}	Well radius	m
h_{o}	Oil pressure head	$\mathrm{kg}/\mathrm{m}^2/\mathrm{s}^2$
h_{w}	Water pressure head	$\mathrm{kg}/\mathrm{m}^2/\mathrm{s}^2$
r_{e}	Equivalent radius	m
d_{valve}	Maximum orifice diameter of a valve	m
L_{well}	Horizontal well length	m

Table 5.2: Description of parameters, the algebraic variables, and the differential variables used in oil reservoir model.

6 Implementation of model

6.1 Implementation of oil reservoir and well model in Julia

In this section, the black oil model with fully opened ICVs is implemented in Julia. Simulation setup, and simulation results are discussed in this section.

6.1.1 Simulation setup

To perform the oil reservoir simulation, the oil reservoir is discretized into 20 grids along the reservoir radius and 20 grids along the reservoir length. Parameter values and initial values of the states are shown in Table 6.1.

6.1.2 Curve fitting for the relationship between saturation and relative permeability

The data for the water saturation $S_{\mathrm{w}}$and corresponding relative permeabilities, provided by the contact in Equinor ASA, is used to establish the relationship between water saturation and relative permeabilities. This is achieved through least-square fit using a standard package in Julia called *LsqFit*[1]. Comparison of water saturation and permeability relation for actual data and least-square function is shown in Figure 6.1. The Julia code used to fit the data is given in Appendix B.6.

6.1.3 Simulation results and discussion

The ordinary differential Equation 5.60 is solved using *Tsit5()* solver in Julia. A *Tsit5()* is an ODE solver algorithm in the *DifferentialEquations.jl*[2] package in Julia and is based on Tsitouras 5/4 Runge-Kutta method. The pressure equations, given by Equation 5.70, involves a large number of linear algebraic equations. These equations are solved implicitly

---

[1] https://julianlsolvers.github.io/LsqFit.jl/latest/tutorial/

[2] *Documentation link for DifferentialEquations.jl package*

Symbol	Description	Value	Unit
Initial conditions			
S_{w_0}	Initial water saturation	0.15	-
S_{o_0}	Initial oil saturation	0.85	-
Inputs u			
A_{valve}	Constriction effective area of a valve	$\frac{\pi d_{\mathrm{valve}}^2}{4}$	m^2
P_a	Aquifer pressure	11500000	Pa
$q_{\mathrm{mix,tot}}$	Total specified fluid production rate	800	m^3/day
Parameters θ			
ϕ	Porosity	0.27	-
R	Reservoir radius	200	m
L	Reservoir length	1200	m
K	Absolute permeability of a reservoir	1500	mD
k_{wa}	Relative permeability of an aquifer	1	-
λ_{wa}	Mobility of aquifer water	$\frac{k_{\mathrm{wa}}}{\mu_w}K$	$m^3 s/kg$
ρ_w	Water density	1050	kg/m^3
ρ_o	Oil density	950	kg/m^3
μ_o	Oil viscosity	$100 \cdot 10^{-3}$	Pa.s
μ_w	Water viscosity	10^{-3}	Pa.s
α	Inclination angle of a reservoir	20	degree
β	Arch angle of a wedge shaped reservoir	25	degree
r_{well}	Well radius	0.124	m
h_o	Oil pressure head	$\rho_o \cdot g \cdot \sin\left(\alpha + \frac{\beta}{2}\right)$	$kg/m^2/s^2$
h_w	Water pressure head	$\rho_w \cdot g \cdot \sin\left(\alpha + \frac{\beta}{2}\right)$	$kg/m^2/s^2$
r_e	Equivalent radius	$0.5 \cdot \Delta r$	m
d_{valve}	Maximum orifice diameter of a valve	$3.217 \cdot 10^{-3}$	m
L_{well}	Horizontal well length	1200	m
n_r	Number of grids along reservoir radius	20	-
n_ℓ	Number of grids along reservoir length	20	-
n_{well}	Number of grids along well length	20	-
Δr	Step length along reservoir radius	$\frac{L}{n_r}$	m
$\Delta \ell$	Step length along reservoir length	$\frac{L}{n_\ell}$	m
$\Delta \ell_{\mathrm{well}}$	Step length along well length	$\frac{L_{\mathrm{well}}}{n_{\mathrm{well}}}$	m

Table 6.1: Operating conditions for black oil model.

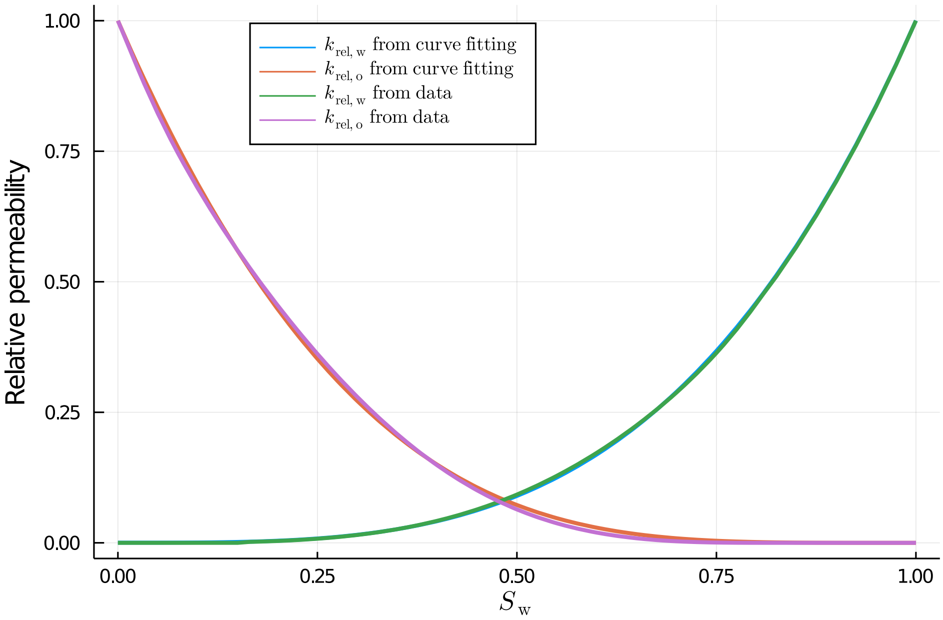

Figure 6.1: Relation between water saturation S_{w} and relative permeabilities.

using the *backslash* operator in Julia. The function in Julia called *sparse*[3] is used to convert these large matrices into sparse matrices which helps to reduce the computational time significantly. The model was simulated up to 1000 days. The ODE solver *Tsit5()* selects variable time steps while solving the model, thus reduces computational time. Some of the important measurements in the oil reservoir model such as water cut, flow rates of water, and oil at the well, pressure profiles, saturation profiles, bottom hole pressure at the well, etc., are given and analyzed in this section. The codes used for these simulations are given and in Appendix B.1.

6.1.3.1 Fluid flow rates at the well and water cut

In Figure 6.2, we can see that the water cut starts to increase after 390 days. It means that the water breakthrough occurs after 390 days,i.e., $t_{\mathrm{bt}} = 390\,\mathrm{days}$. Water breakthrough refers to the moment when the water from the aquifer first reaches the wellbore. We can see that the water cut ratio is in the range of 0.24 even before the water breakthrough. This is because we assumed that the initial water saturation in the reservoir to be 0.15. This indicates that the water is permeable in the initial state. In Figure 6.2, we can see that the water cut is almost the same for the different grid locations along the well length. This is because the volumetric flow rate of fluids in the well is assumed to be evenly distributed. In other words, the heel-toe effect in the well is assumed to be insignificant.

---

[3] *Sparse matrix_link*

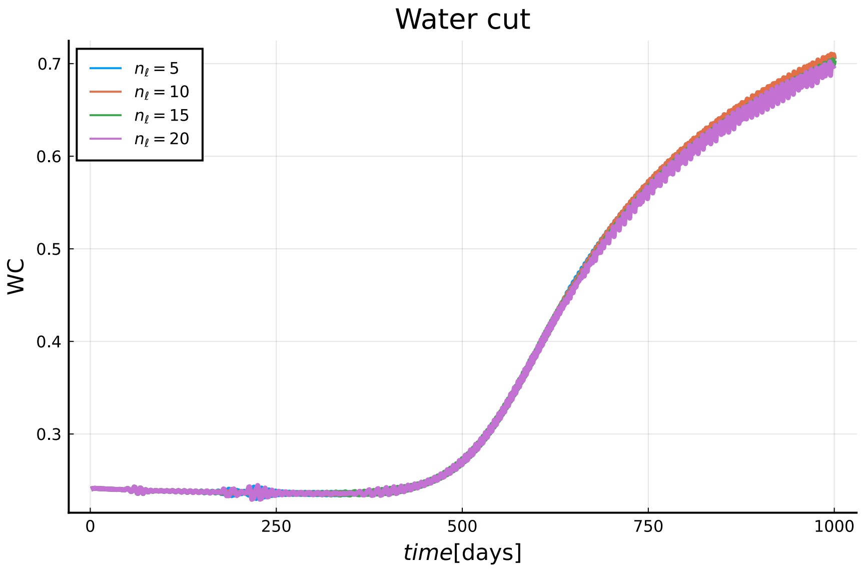

Figure 6.2: Water cut at the well at different positions along the well length.

Symbol	Description	Time [days]	Value	Unit
WC	Water cut	390	0.2342	-
		1000	0.6981	-
$q_{\mathrm{w,s,tot}}$	Water volumetric flow rate	390	189.6532	$\mathrm{m}^3/\mathrm{day}$
		1000	562.0173	$\mathrm{m}^3/\mathrm{day}$
$q_{\mathrm{o,s,tot}}$	Oil volumetric flow rate	390	610.3468	$\mathrm{m}^3/\mathrm{day}$
		1000	237.9827	$\mathrm{m}^3/\mathrm{day}$

Table 6.2: Water cut and volumetric flow rate of oil, and water.

The volumetric flow rate of oil and water is shown in Figure 6.3. In this figure, the volumetric flow rate for oil is indicated by the dark red line, while the volumetric flow rate of water is indicated by the blue line. The water breakthrough time t_{bt} can also be identified from Figure 6.3. Initially, the volumetric flow rate of water is in the range of $191.808\,\mathrm{m}^3/\mathrm{day}$, while the volumetric flow rate of oil is in the range of $607.392\,\mathrm{m}^3/\mathrm{day}$. The volumetric flow rate of water starts to increase after the water breakthrough time which is $390\,\mathrm{days}$. The details of the total fluid flow rates, and water cut (at fully open ICVs condition) are given in Table 6.2.

6.1.3.2 Bottom hole pressure

Corresponding bottom hole pressure has to be manipulated to maintain the total liquid volumetric flow rate at well to be constant i.e., $q_{\mathrm{mix,tot}} = 800\,\mathrm{m}^3/\mathrm{day}$ at standard temperature and pressure. In Figure 6.4, we can see that the bottom hole pressure starts to

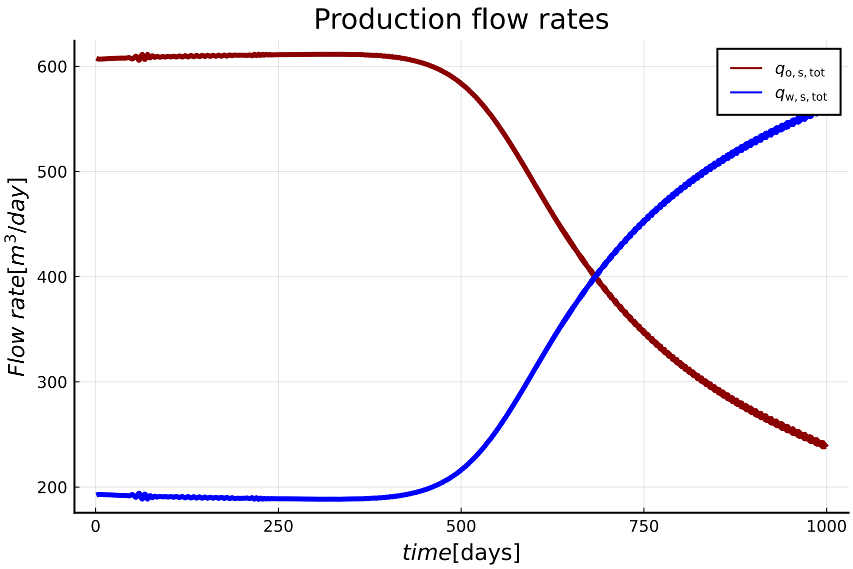

Figure 6.3: Total flow rates of oil and water, respectively at the well.

increase significantly after the water breakthrough.

The Equation 5.52 for the mixture of oil and water can be modified and written as follows:

$$P_{\mathrm{rw},i_r,i_\ell} = \left(-q_{\mathrm{mix}} \frac{\ln\left(\frac{r_{\mathrm{well}}}{r_{\mathrm{e}}}\right)}{2\pi\Delta\ell\left(\lambda_{\mathrm{w}}+\lambda_{\mathrm{o}}\right)} + P_{\mathrm{re}} + \frac{\left(\lambda_{\mathrm{w}}h_{\mathrm{w}}+\lambda_{\mathrm{o}}h_{\mathrm{o}}\right)\left(r_{\mathrm{well}}-r_{\mathrm{e}}\right)}{\left(\lambda_{\mathrm{w}}+\lambda_{\mathrm{o}}\right)} \right)_{i_r,i_\ell}, \tag{6.1}$$

where

$$\left(\lambda_{\mathrm{w}}+\lambda_{\mathrm{o}}\right) = K\left(\frac{k_{\mathrm{rel,w}}}{\mu_{\mathrm{w}}} + \frac{k_{\mathrm{rel,o}}}{\mu_{\mathrm{o}}}\right) \tag{6.2}$$

In our simulation parameter, we have assumed that the viscosity of the oil is 100 times higher than that of water. The relative permeability of water increases significantly after water breakthrough causing the term $\left(\frac{k_{\mathrm{rel,w}}}{\mu_{\mathrm{w}}} + \frac{k_{\mathrm{rel,o}}}{\mu_{\mathrm{o}}}\right)$ to increase significantly. Thus, well pressure and bottom hole pressure also increase.

6.1.3.3 Pressure profile

The reservoir pressure at different radius and length after 400 days is shown in Figure 6.5. At $r = R$, the grids near the aquifer, the pressure is higher. The pressure decreases with a decrease in reservoir radius r. In the region near the well, the pressure begins to decrease rapidly. In Figure 6.5, we can see that the pressure profiles at different reservoir lengths

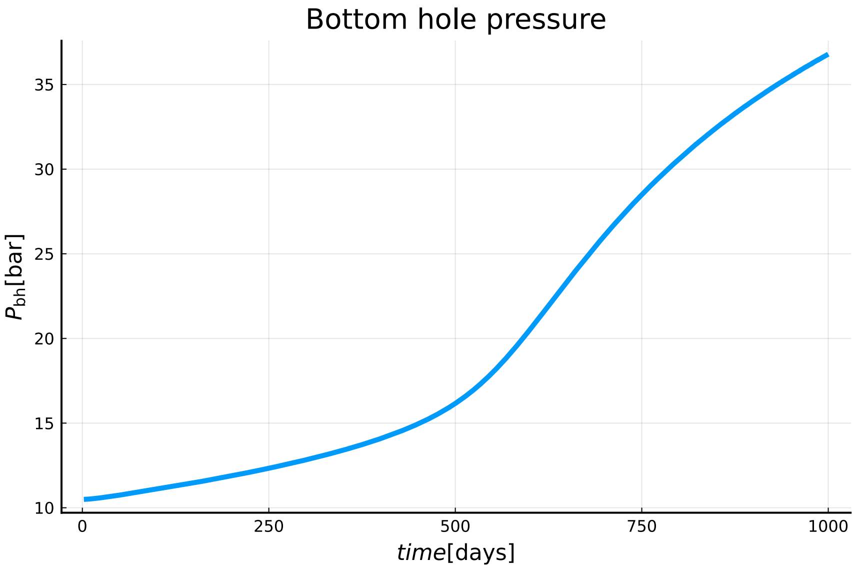

Figure 6.4: Bottom hole pressure at the well heel.

are almost identical. This is because of the evenly distributed flow at the well when the ICVs are fully open. The Julia code for calculation of fluid flow through each ICV, and corresponding bottom hole pressure is given in Appendix B.5.

The Figure 6.6, shows 3D pressure profiles after 50, 100, 300, 500, 800, and 1000 days of production, respectively. It can be observed that the pressure profile after 50, 100, and 300 days of production are almost identical. However, a significant increase in pressure can be seen after 500 days of production and so on. This is because water breakthrough occurs after 390 days of production.

Variations of average reservoir pressure over time at different reservoir radius are shown in Figure 6.7. In this figure, it can be observed that the variation of pressure over time at grids near the aquifer i.e., $n_r = 1$ is small. However, as we move from $n_r = 1$ to $n_r = 20$ or $r = R$ to $r = 0$, the pressure variation over time becomes significant and is highest at grids near the production well i.e., $n_r = 20$. An increase in reservoir pressure after water breakthrough can be seen in this figure as well.

6.1.3.4 Saturation profile

The Figure 6.8, shows 3D water saturation profiles after 50, 100, 300, 500, 800, and 1000 days of production, respectively. Water from the aquifer slowly advances towards the production well. When water flooding front reaches the wellbore at $r = 0$, water breakthrough occurs. In Figure 6.8, it can be observed that the water saturation slowly starts to increase along the reservoir radius with the increase in production time. In these

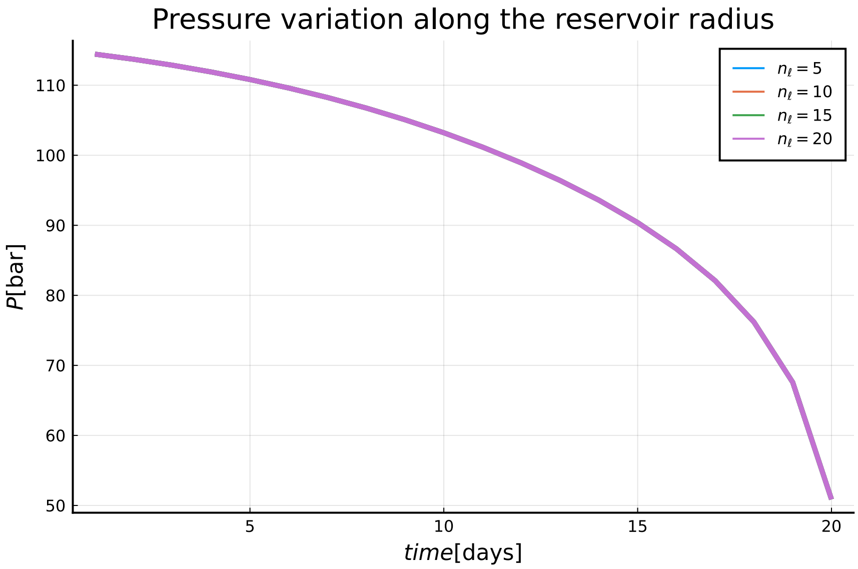

Figure 6.5: Pressure profiles at different radius and different length after 400 days.

Description	Time [days]	Value	Unit
Total oil production	1000	$490.8337 \cdot 10^3$	m^3
Total water production	1000	$308.3627 \cdot 10^3$	m^3

Table 6.3: Total oil and water production in 1000 days.

water saturation profiles, the water coning effect is not visible because the volumetric flow rate of fluids in the well is assumed to be evenly distributed.

In the water saturation profile after 300 days of production, the water saturation at grids $n_r = 10$ to $n_r = 20$ are the same as the initial water saturation of the reservoir i.e., 0.15. However, after 500 days of production, we can observe that the water saturation at grids $n_r = 20$ is higher than 0.15. This is because the water breakthrough already occurred after 390 days of production. After 1000 days of water production, the average water saturation at $n_r = 20$ is observed to be 0.24893.

Figure 6.9 shows the 2D profile of average water saturation at different reservoir radius.

6.1.3.5 Total oil and water production

Figure 6.10, and Figure 6.11 shows the total production of oil and water in 1000 days, respectively. The detailed values of the total production of oil and water from the reservoir are shown in Table 6.3.

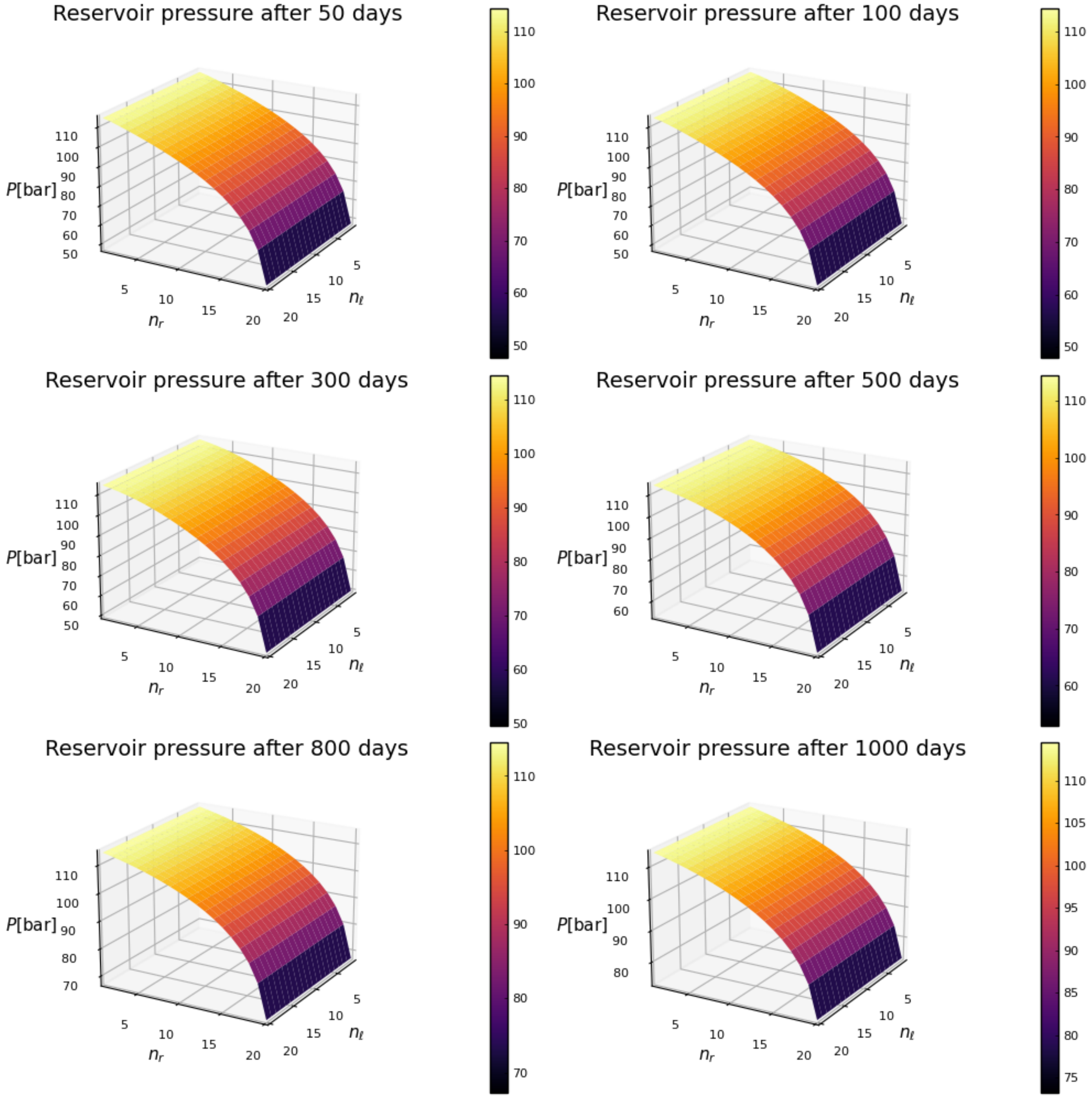

Figure 6.6: Pressure profiles after different days of production.

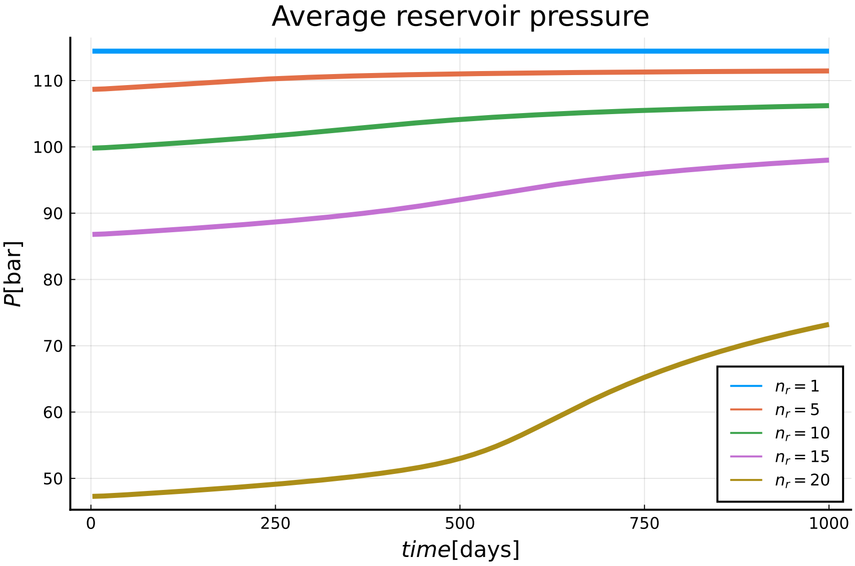

Figure 6.7: Average pressure profile at different radius.

Symbol	Description	Range	Value	Unit
ϕ	Porosity	Lower limit Upper limit	$0.27 \times 80\%$ $0.27 \times 120\%$	-
S_{w_0}	Initial water saturation	Lower limit Upper limit	$0.15 \times 80\%$ $0.15 \times 120\%$	-
K	Absolute permeability of a reservoir	Lower limit Upper limit	$1500 \times 80\%$ $1500 \times 120\%$	mD
n_{sim}	Number of Monte Carlo simulations	-	100	-

Table 6.4: Monte Carlo simulation setup.

6.1.4 Implementation of Monte Carlo Simulation

In this work, we assume the statistical distribution of parameters such as porosity, permeability, and initial water saturation as a simple distribution. Also, the upper limit and lower limit of these parameters are varied by $\pm 20\%$. Monte Carlo simulation is performed using *EnsembleProblem* in Julia which interfaces well with the standard differential equation solving package *DifferentialEquations.jl*. The simulation setup for Monte Carlo simulation is shown in Table 6.4. The random value between the upper and lower limit for the parameters are generated using *rand*, and *Uniform* functions in Julia. The codes are given in Appendix B.3.

Figure 6.12 demonstrates the uncertainties in the total oil production volume in $1000\,\mathrm{days}$. The maximum and minimum total oil production volumes are $657.235 \cdot 10^3\,\mathrm{m}^3$ and $326.486 \cdot 10^3\,\mathrm{m}^3$, respectively. Similarly, Figure 6.13 demonstrates the uncertainties in the total wa-

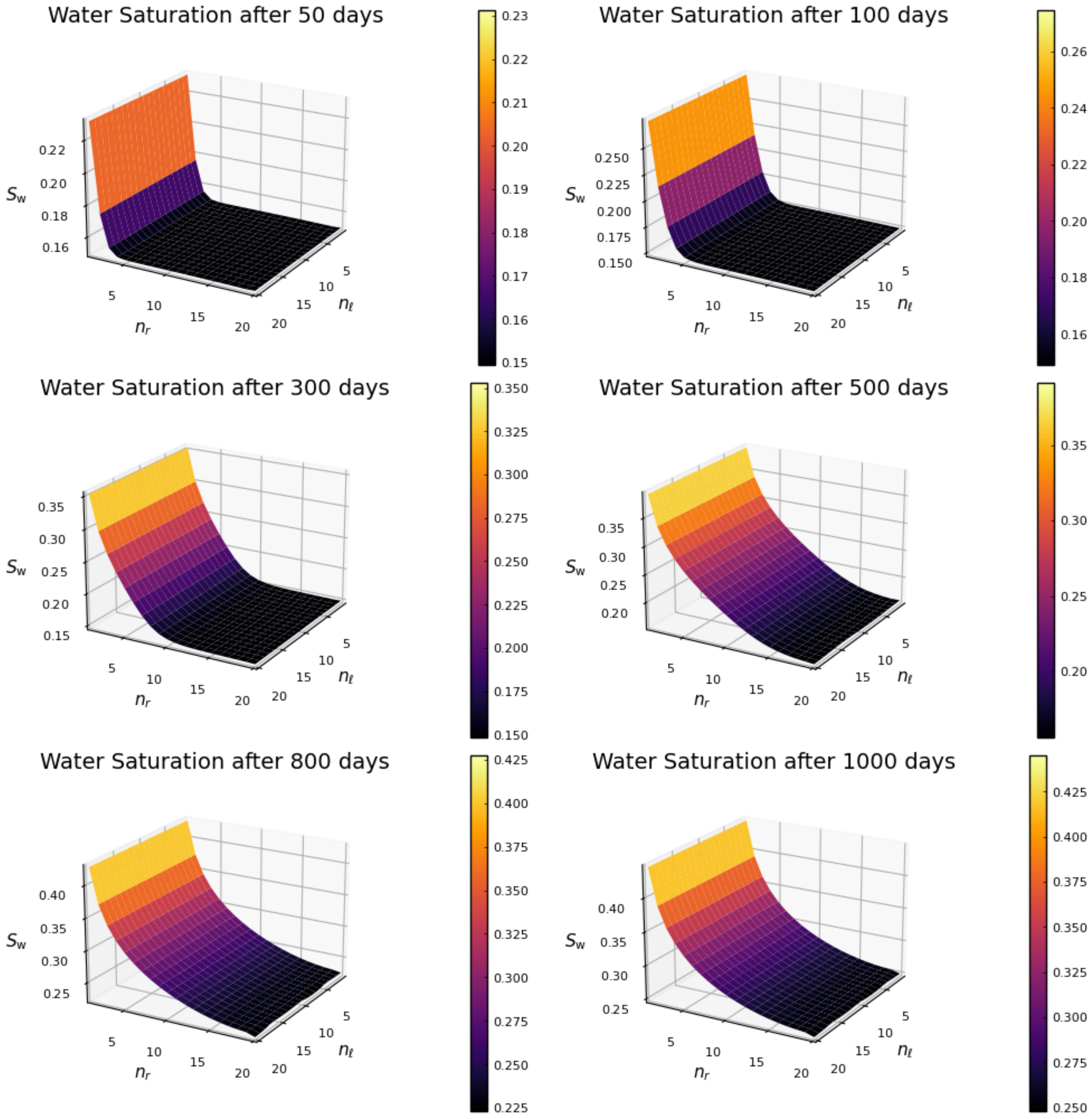

Figure 6.8: Water saturation profiles after different days of production.

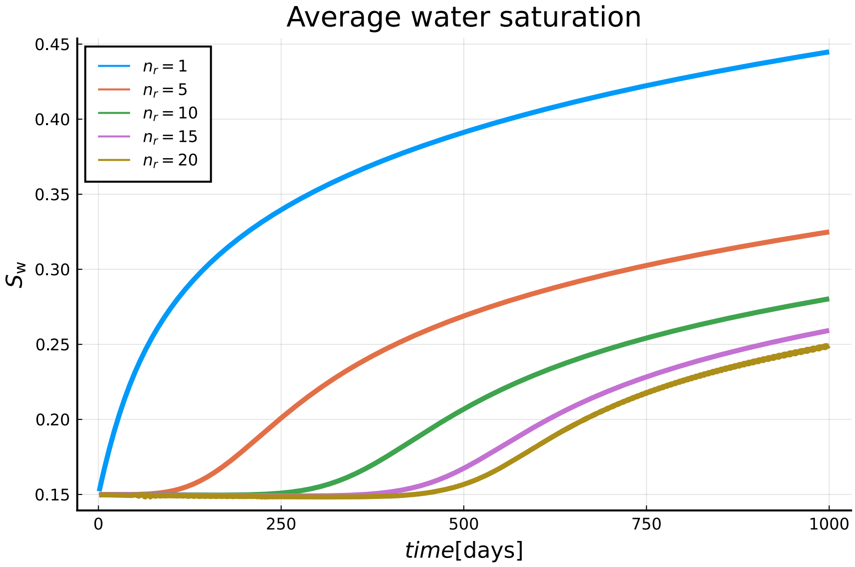

Figure 6.9: Average water saturation profile at different radius.

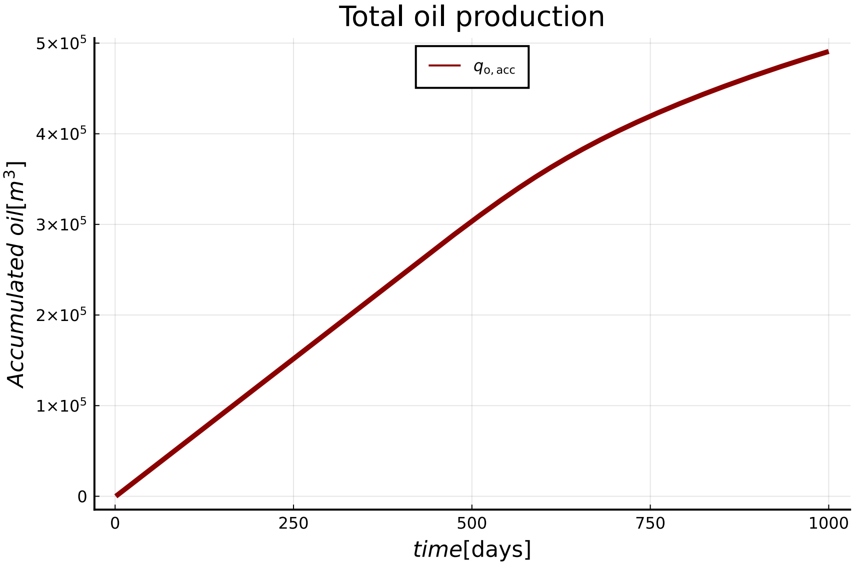

Figure 6.10: Total production of oil in 1000 days.

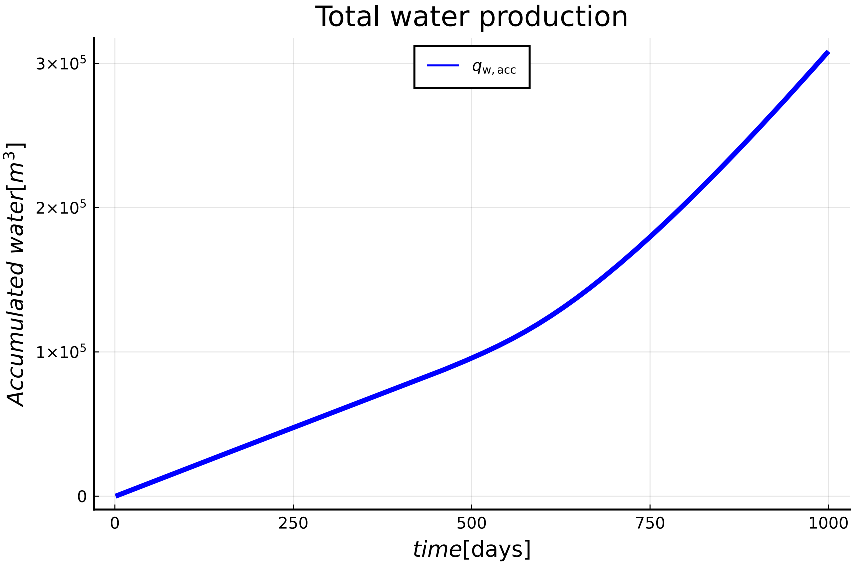

Figure 6.11: Total production of water in 1000 days .

Description	Time [days]	Range	Value	Unit
Total oil production	1000	Maximum	$657.235 \cdot 10^3$	m^3
		Minimum	$326.486 \cdot 10^3$	
Total water production	1000	Maximum	$473.510 \cdot 10^3$	m^3
		Minimum	$142.761 \cdot 10^3$	
Water cut	1000	Maximum	0.8938	-
		Minimum	0.4866	-
Approximate water breakthrough time	-	Maximum	700	days
		Minimum	250	

Table 6.5: Simulation results based on model with uncertainties.

ter production volume in 1000 days. The maximum and minimum total water production volumes in 1000 days are $473.510 \cdot 10^3\,\mathrm{m}^3$ and $142.761 \cdot 10^3\,\mathrm{m}^3$, respectively.

Moreover, Figure 6.14, and Figure 6.15 demonstrates the uncertainties in the measurement of water cut at the length of $\ell = 0.5L$, and flow rate of the oil. From these figures, we can conclude that the total oil production volume, water cut, volumetric flow rates, water breakthrough time, etc., are dependent upon the parameters of rock such as porosity, initial water saturation in the reservoir, and rock permeabilities. The description of the uncertainties in the measurements for the case of fully open ICVs are given in Table 6.5.

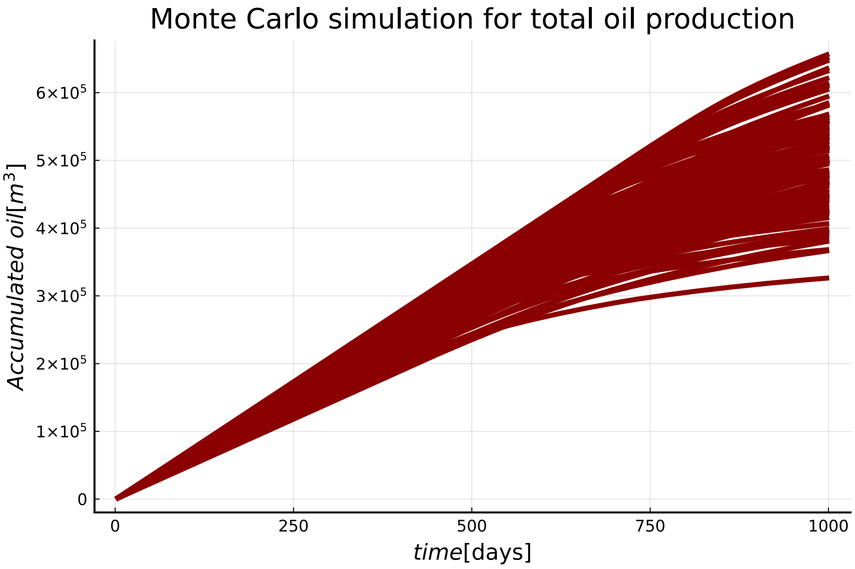

Figure 6.12: Monte Carlo simulation for production of oil in 1000 days.

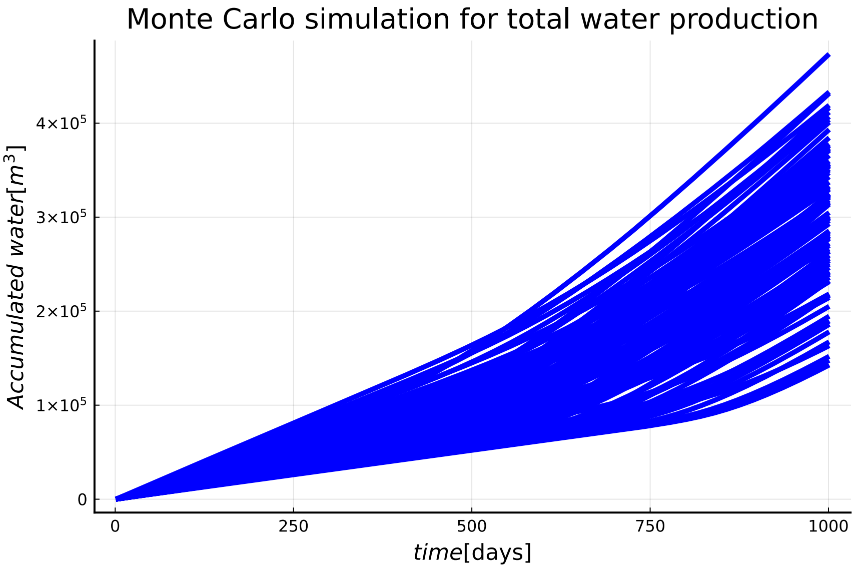

Figure 6.13: Monte Carlo simulation for production of water in 1000 days.

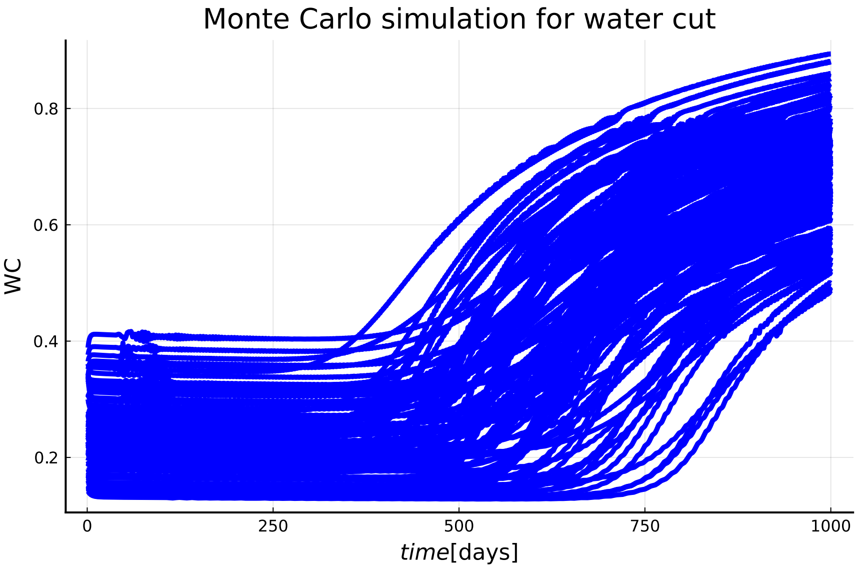

Figure 6.14: Monte Carlo simulation for water cut at $\ell = 0.5L$.

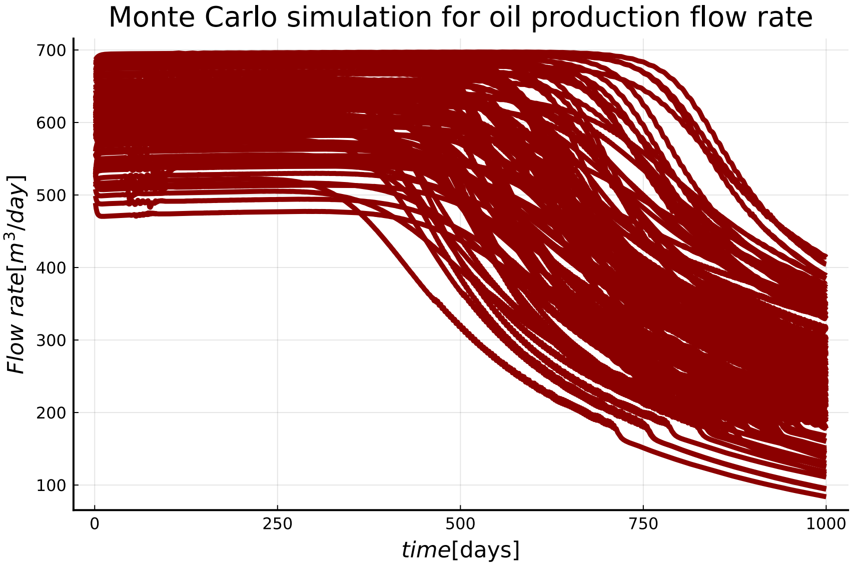

Figure 6.15: Monte Carlo simulation for flow rate of oil.

6.2 Implementation of PI controller

The main objective of the PI controller is to reduce the water cut while increasing the oil production rate. The valve areas of ICVs are fully or partially closed at areas where the water cut is higher than the others and open the valves at areas where the water cut is lower than the others. The minimum value of water cut is taken as the setpoint for the controller. In previous work by Zhang (2013), the minimum water saturation $S_{\mathrm{w}}$was taken as a setpoint for the controller. However, in reality, the sensors can not measure water saturation in the reservoir. Thus, considering minimum water cut as a setpoint is more realistic and achievable.

There is a number of ICDs with the flow that is contained in an *inner pocket* in the production pipe. The ICVs give a controlled flow out of this *inner pocket* and into the production pipe. To deal with these ICVs, and ICDs configuration, it is assumed that the ICVs are installed at every $60\,\mathrm{m}$ length along the oil production pipe i.e., at each segment of the pipe length. The group of ICVs receives the same control signals. In other words, there are 20 ICVs installed at the production pipe in which the group of valves at $n_{\mathrm{well}} = \{1,\ldots,5\}$, $n_{\mathrm{well}} = \{6,\ldots,10\}$, $n_{\mathrm{well}} = \{11,\ldots,15\}$, and $n_{\mathrm{well}} = \{16,\ldots,20\}$ receive the same control signals, respectively. The control signals for these four groups of ICVs are shown in Figure 6.16. The implementation of a PI controller is given in Appendix B.2.

Figure 6.17 and Figure 6.18 demonstrate the effect of PI controller in total production of oil and water in $1000\,\mathrm{days}$, respectively. In these figures, we can see that the total oil production, after implementing the PI controller, is increased by 1.7873% while the total water production is decreased by 2.5942%. In Zhang (2013) work, the increase in total oil production and decrease in total water production, after implementing PI controller, was 3.1%, and 4.9%, respectively. The reason behind the decrease in performance of PI controller, in this work, could be because the group of ICVs is controlled with a single control signal instead of controlling individual ICVs with an independent control signal. Also, in this work, we used minimum water cut as a reference for the controller while in Zhang (2013) work, the minimum water saturation was used as a reference for the controller. Furthermore, as the performance of the PI controller is highly dependent upon the selection of the values of K_{p} and T_{i}, perfect selection of these values could result in better controller performance. The values of K_{p} and T_{i} are taken as $7.506 \cdot 10^{-6}$, and $2.9376 \cdot 10^{9}$, respectively.

Figure 6.19 demonstrates the total volumetric flow rate of oil and water after implementing the PI controller. The average oil volumetric flow rate per day is increased by 1.738%, while the average water volumetric flow rate per day is decreased by 2.7715%. Similarly, Figure 6.20, shows the effect of PI controller on water cut at $\ell = 0.5L$ or $n_{\ell} = 10$. The average water cut is decreased by 2.755% after implementing the PI controller. Finally, in Figure 6.21, we can observe that the bottom hole pressure tends to decrease after the use

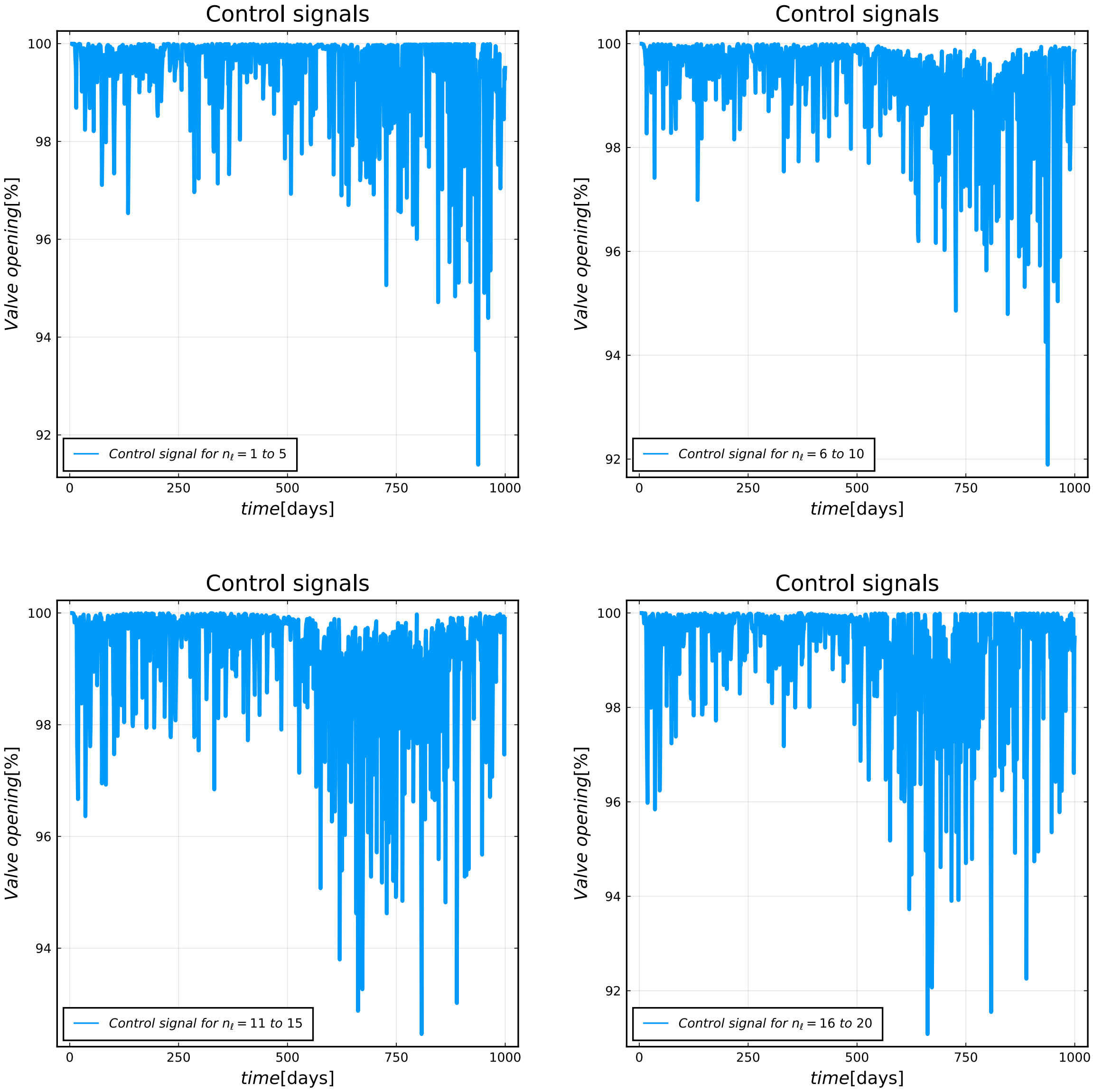

Figure 6.16: ICVs control signals.

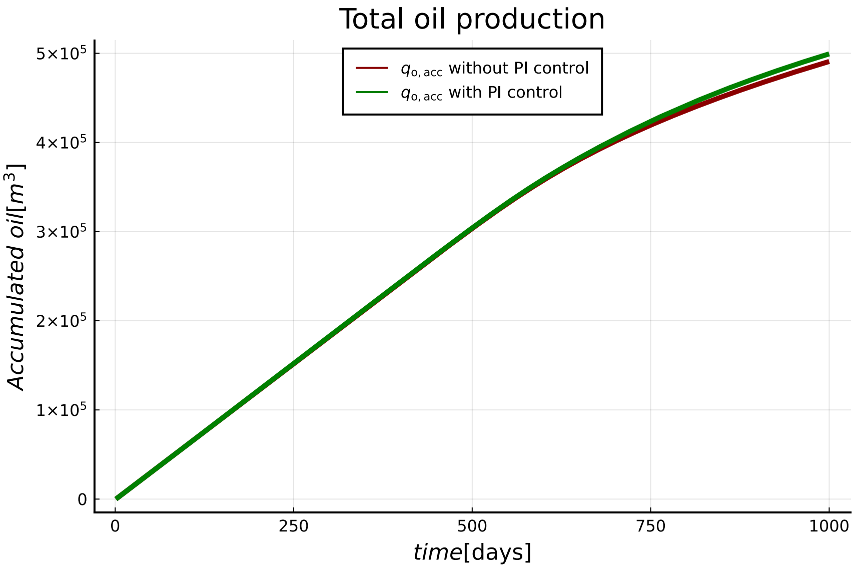

Figure 6.17: Comparison of total production of oil in 1000 days with and without PI controller.

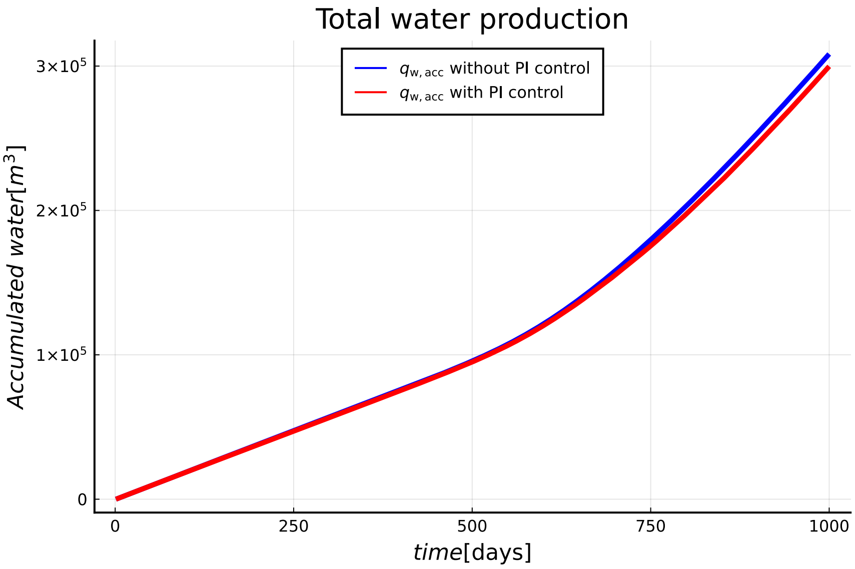

Figure 6.18: Comparison of total production of water in 1000 days with and without PI controller.

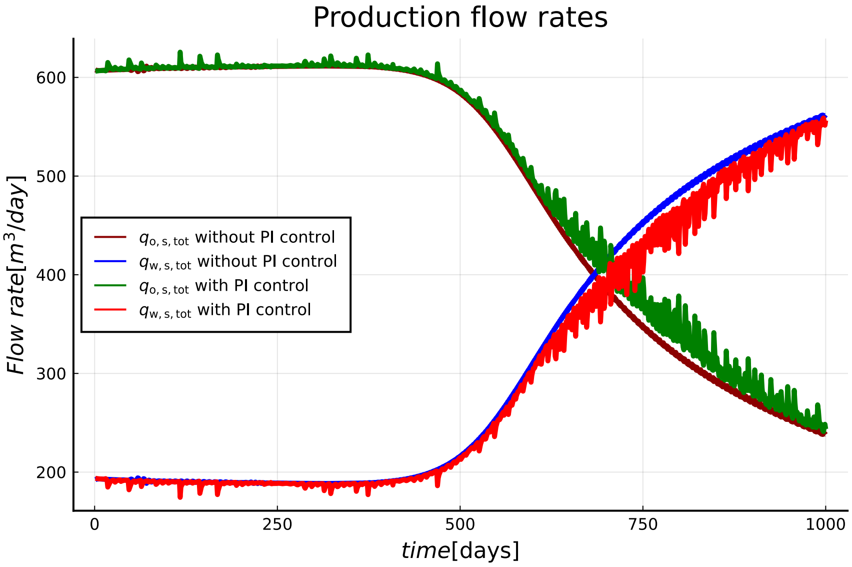

Figure 6.19: Comparison of total volumetric flow rates of oil and water with and without PI controller.

of the PI controller. The summary of the effect of the PI controller in an oil production system is given in Table 6.6.

6.2.1 Implementation of PI controller based on model with uncertainties

The PI controller is implemented in a model with uncertainties. The comparison for the total oil and water production volume after implementing PI controller is shown in Figure 6.22, and 6.23, respectively. In Figure 6.22, the solid lines with maroon color represent uncertainties in total oil production volume without PI controller, while the green dot lines represent uncertainties in total oil production with PI controller. In this figure, we can observe that the minimum total oil production volume in $1000\,\mathrm{days}$ after implementing the PI controller is $359.0391 \cdot 10^3\,\mathrm{m}^3$which is higher than that of the model without PI controller i.e., $326.4863 \cdot 10^3\,\mathrm{m}^3$. However, the maximum total oil production volume in $1000\,\mathrm{days}$ after implementing the PI controller is $614.6868 \cdot 10^3\,\mathrm{m}^3$ which is lower than that of the model with PI controller i.e., $657.2351 \cdot 10^3\,\mathrm{m}^3$. The implementation of a PI controller is given in Appendix B.4.

Similarly, In Figure 6.23, blue solid lines represent uncertainties in total water production volume without PI controller, while the red dot lines represent uncertainties in total water production with PI controller. In this figure, the maximum total water production volume in $1000\,\mathrm{days}$ after implementing the PI controller is $440.9470 \cdot 10^3\,\mathrm{m}^3$ which is lower than that of the model without PI controller i.e., $473.5101 \cdot 10^3\,\mathrm{m}^3$. However, the minimum total water production volume in $1000\,\mathrm{days}$ after implementing the PI controller is $185.3096 \cdot 10^3\,\mathrm{m}^3$which is higher than that of the model without PI controller i.e., $142.7613 \cdot 10^3\,\mathrm{m}^3$.

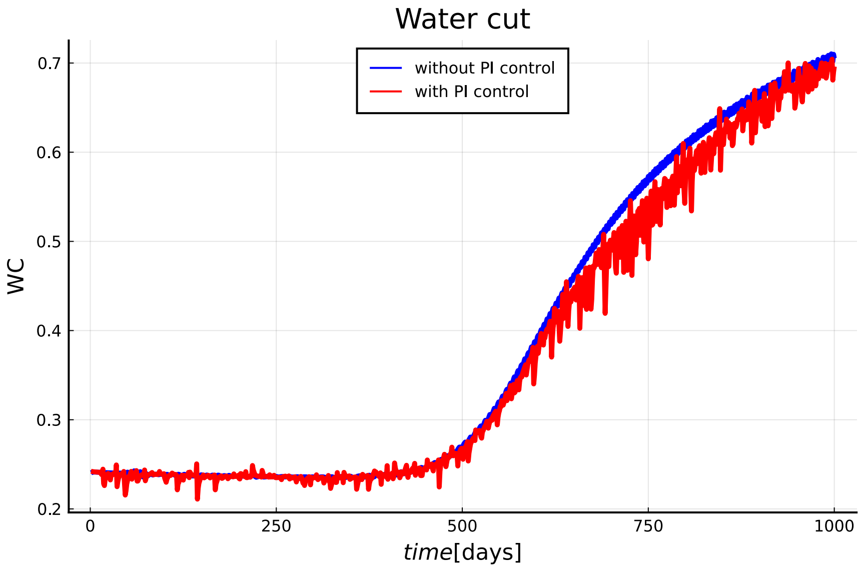

Figure 6.20: Comparison of water cut at the well at $\ell = 0.5L$ with and without PI controller.

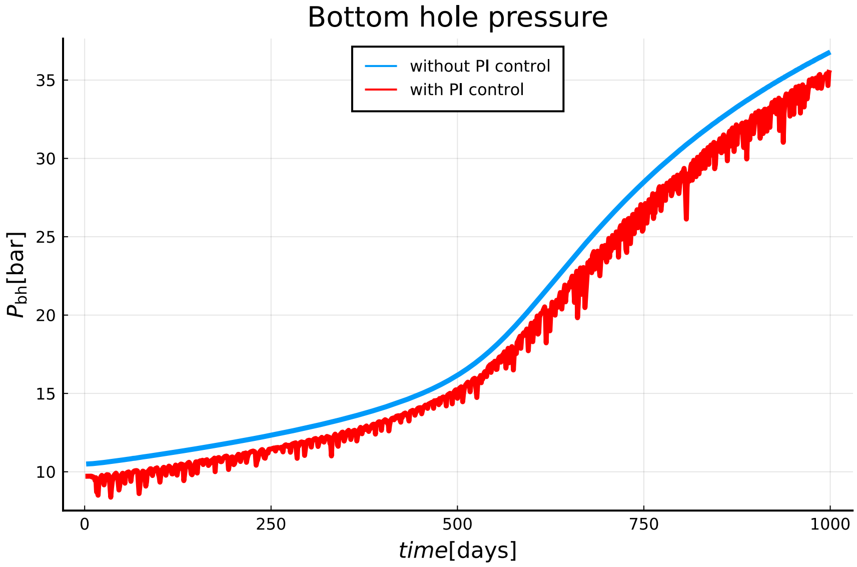

Figure 6.21: Comparison of bottom hole pressure at the well heel with and without PI controller.

Description	Configuration	Value	Change[%]	Unit
Total oil production	Without PI	$490.8337 \cdot 10^3$	+1.7873	m^3
	With PI	$499.6065 \cdot 10^3$		
Total water production	Without PI	$308.3627 \cdot 10^3$	−2.5942	m^3
	With PI	$300.3629 \cdot 10^3$		
Average water cut	Without PI	0.3862	−2.755	-
	With PI	0.3755		-
Average oil volumetric flow rate	Without PI	491.0716	+1.738	m^3/day
	With PI	499.6065		m^3/day
Average water volumetric flow rate	Without PI	308.9247	−2.7715	m^3/day
	With PI	300.3628		m^3/day

Table 6.6: Total oil and water production and average water cut in 1000 days after implementing PI controller.

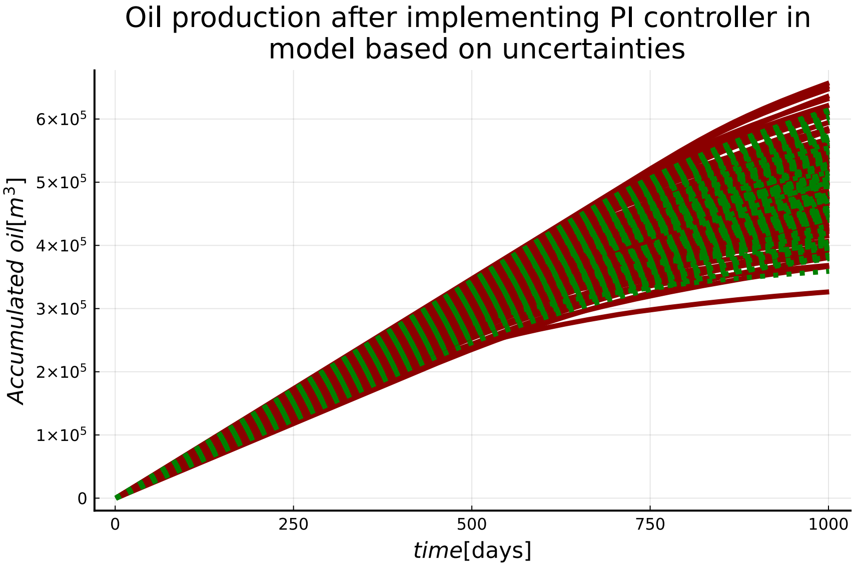

Figure 6.22: Comparison of Monte Carlo simulation for production of oil in 1000 days with PI controller (green dot lines) and without PI controller (maroon solid lines).

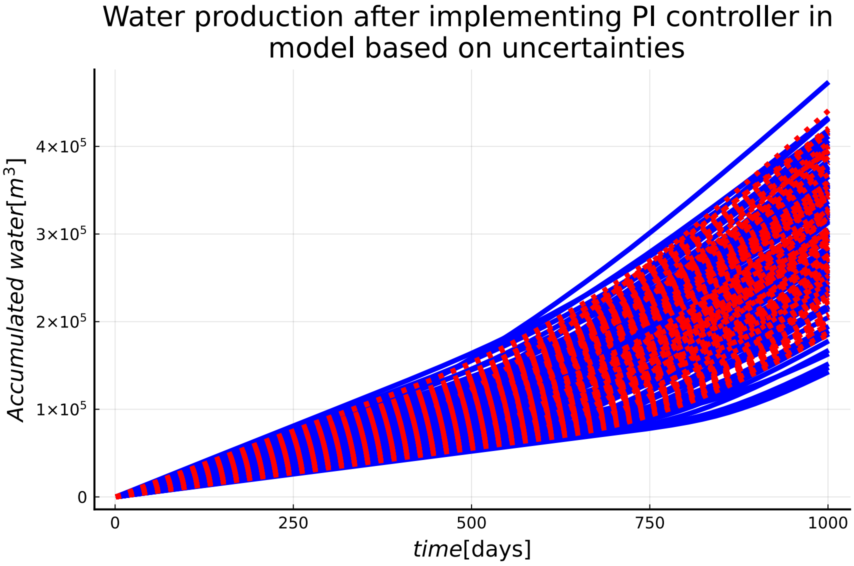

Figure 6.23: Comparison of Monte Carlo simulation for production of water in 1000 dayswith PI controller (red dot lines) and without PI controller (blue solid lines).

7 Conclusion

In this thesis, an overview of an oil well holding black oil, with a reservoir, and pipes is given. A simplified $\mathbf{2D}$ control-relevant model is developed and implemented in Julia programming language. The model is solved using a standard ODE solver in Julia called *Tsit5()*. This solver solves the ODE problems with variable time steps which reduce the computational time and improve the performance.

The results such as total production volume of oil and water, water cut, volumetric flow rates of oil and water, bottom hole pressure etc., are obtained and verified based on Zhang (2013) work. The values of parameters, such as specified fluid flow rate, maximum bottom hole pressure, constant aquifer pressure, absolute permeability of the rock, etc., used in this work are different from that used in Zhang (2013) work. However, the nature of results such as volumetric flow rate of oil and water, and bottom hole pressure, etc., are similar to that of Zhang (2013) work. Furthermore, the uncertainties in the model are discussed and the Monte Carlo simulation is implemented to predict the model uncertainties. Finally, a PI controller is implemented in the model based on uncertainties to enhance the oil production, while minimizing the water production. The PI controller helps to increase the oil production by manipulating the ICVs at the production well. Implementation of PI controller improved the total oil production in $1000\,\mathrm{days}$ by 1.7873%. However, the effect is not very significant due to the limited capability of a PI controller. In this case, a more effective controller is required, such as MPC.

Initially, it was planned to implement MPC instead of a PI controller. However, because of the time constraint, this task could not be performed. Some background studies related to simplifying the model into a subspace model using the system identification tool were done, but this task could not be implemented in Julia because of the limited time.

8 Future work

Some of the tasks recommended for future work are:

1. Building subspace model using suitable system identification tool.
2. Implementing MPC into a data-driven model obtained from the previous task.

Bibliography

Aakre, H. (2017), 'The impact of autonomous inflow control valve on increased oil production and recovery', *University College of Southeast Norway, Faculty of Technology, Natural Sciences and Maritime Sciences* .

Aarnes, J. E., Gimse, T. & Lie, K.-A. (2007), *Geometric Modelling, Numerical Simulation, and Optimization: Applied Mathematics at Sintef*, Springer, Springer, Berlin, Heidelberg, chapter An introduction to the numerics of flow in porous media using Matlab, pp. 265–306.

Bakke, M. (2009), Subspace Identification Using Closed Lopp Data, mathesis, Norwegian University of Science and Technology.
URL: *https://folk.ntnu.no/skoge/diplom/diplom09/bakke/master_morten_levert.pdf*

Barreto, C. E. A. G. & Schiozer, D. J. (2015), 'Optimal placement design of inflow control valve using a dynamic optimization process based on technical and economic indicators', *Journal of petroleum science and engineering* **125**, 117–127.

Chammout, O. J., Ghosh, B. & Alklih, M. Y. (2017), 'Downhole flow controllers in mitigating challenges of long reach horizontal wells: A practical outlook with case studies', *Journal of Petroleum and Gas Engineering* **8**(10), 97–110.

Chen, Z., Huan, G. & Ma, Y. (2006), *Computational Methods for Multiphase Flows in Porous Media*, Society for Industrial and Applied Mathematics.
URL: *https://epubs.siam.org/doi/abs/10.1137/1.9780898718942*

Chen, Z. & Zhang, Y. (2009), 'Well flow models for various numerical methods', *International Journal of Numerical Analysis and Modeling* **6**, 375–388. No. 3.

Cordazzo, J., Maliska, C. R. & Silva, A. (2002), Interblock transmissibility calculation analysis for petroleum reservoir simulation, *in* 'Proceedings from the 2nd Meeting on Reservoir Simulation', Vol. 5, Department of Mechanical Engineering, Federal University of Santa Catarina ñ UFSC, Buenos Aires. No. 6.

Crotogino, F. (2016), *Storing Energy*, first edn, Elsevier, chapter Traditional Bulk Energy Storage—Coal and Underground Natural Gas and Oil Storage, pp. 391–409.

Dandekar, A. Y. (2013), *Petroleum reservoir rock and fluid properties*, second edn, CRC Press Taylor Francis Group.

D.G. Hatzignatiou, F. M. (1994), Water and gas coning in horizontal and vertical wells, *in* 'Annual technical meeting', Petroleum Society of Canada.

Editor, O. (28th jun 2016), 'Contract let for third Peregrino Platform', *Oil and Gas Journal* .
URL: *https://www.ogj.com/drilling-production/article/17250312/contract-let-for-third-peregrino-platform?cmpid=utm_source=enlutm_medium=emailutm_campaign=ogj_exploratio 07-12*

Hasan, A. (2015), Infinite-dimensional observer for process monitoring in managed pressure drilling, Vol. 48, Elsevier, pp. 82–87.

Jahn, F., Cook, M. & Grahm, M. (2008), Chapter 4 Drilling Engineering, *in* F. Jahn, M. Cook & M. Graham, eds, 'Hydrocarbon Exploration Production', Vol. 55 of *Developments in Petroleum Science*, Elsevier, pp. 47–81.
URL: *https://www.sciencedirect.com/science/article/pii/S0376736107000040*

Li, G. (2011), *World atlas of oil and gas basins*, John Wiley & Sons.
URL: *https://www.wiley.com/en-ar/WorldAtlasofOilandGasBasins-p-9780470656617*

Mayne, D., Rawlings, J., Rao, C. & Scokaert, P. (2000), 'Constrained Model Predictive Control: Stability and Optimality', *Automatica* **36**, 789–814.

Meum, P. (2007), Optimal reservoir control usingnonlinear MPC and ECLIPSE, Master's thesis, Norwegian University of Science and Technology.

Moradi, A. (2020), Cost effective and safe oil production from existing and near-future oil fields, Master's thesis, University of South-eastern Norway, Porsgrunn, Norway.

Nævdal, G., Brouwer, D. & Jansen, J. (2006), 'Waterflooding using closed-loop control', *Computational Geosciences* **10**(1), 37–60.

Oil and water wet permeabilities (2014).
URL: *http://www.epgeology.com/gallery/image.php?album_id=12image_id=269*

Ouyang, L.-B. et al. (2009), Practical consideration of an inflow-control device application for reducing water production, *in* 'SPE Annual Technical Conference and Exhibition', Society of Petroleum Engineers.

Peaceman, D. (1993), 'Representation of a horizontal well in numerical reservoir simulation', *SPE Advanced Technology Series* **1**(01), 7–16.

PetroWiki (2018), 'Horizontal wells'. [Online; accessed 10-March-2021].
URL: *https://petrowiki.spe.org/Horizontal_wells*

Ringrose, P. & Bentley, M. (2015), The Property Model, *in* 'Reservoir Model Design', first edn, Springer Netherlands, pp. 61–113.

Salamander (2021), 'BoostWell-Viscosity Improvement'. [Online; accessed 16-March-2021].
URL: *https://salamandersolutions.com/applications/boostwell-viscosity-improvement/*

Schlumberger (2021*a*), 'Oilfield glossary/GLR'. [Online; accessed 05-April-2021].
URL: *https://glossary.oilfield.slb.com/en/Terms/g/glr.aspx*

Schlumberger (2021*b*), 'Oilfield glossary/water cut'. [Online; accessed 10-April-2021].
URL: *https://glossary.oilfield.slb.com/en/Terms/w/water_cut.aspx*

S.D.M. Borjas, C. G. (2011), 'Subspace identification for industrial processes', *TEMA (São Carlos)* **12**(3), 183–194.

Tzimas, E., Georgakaki, A., Cortes, C. & Peteves, S. (2005), 'Enhanced oil recovery using carbon dioxide in the European energy system', *Report EUR* **21895**(6).

Völcker, C., Jørgensen, J. B. & Stenby, E. H. (2011), Oil reservoir production optimization using optimal control, *in* '2011 50th IEEE Conference on Decision and Control and European Control Conference', IEEE, pp. 7937–7943.

Wikipedia (2020), 'Extraction of petroleum — Wikipedia, The Free Encyclopedia'. [Online; accessed 24-January-2021].
URL: *https://en.wikipedia.org/wiki/Extraction_of_petroleum*

Wikipedia (2021), 'API gravity'. [Online; accessed 27-April-2021].
URL: *https://en.wikipedia.org/wiki/API_gravity*

Zhang, G. (2003), Estimating uncertainties in integrated reservoir studies, PhD thesis, Texas AM University.

Zhang, J. (2013), Improved oil recovery through advanced control, Master's thesis, University of South-Eastern Norway, Porsgrunn, Norway.

Appendix A

Master’s Thesis Task Description

University of
South-Eastern Norway

Faculty of Technology, Natural Sciences and Maritime Sciences, Campus Porsgrunn

FMH606 Master's Thesis

Title: Improved Oil Recovery through Advanced Control

USN supervisor: Bernt Lie

External partner: Equinor ASA, Juan Videla

Task background:

A new research project at University of South-Eastern Norway is *Digital wells for optimal production and drainage («DigiWell»)*, funded by the Norwegian Research Council, project no. 308817, as well as energy company Equinor ASA, and USN.

As part of this project, it is of interest to study the dynamics of a simplified oil field with the goal of using the model for control design.

Oil reservoirs consist of oil contained in porous rock, next to aquifers. In oil production, it is important to maximize the transport of oil to the surface while minimizing the water fraction in the oil. Based on seismic investigations, geological data, and physical laws (Darcy's law, two phase flow, etc.), a computer model can be built for studying an oil field. Equinor ASA builds detailed 3D models in the simulation tool Eclipse or using the MATLAB Reservoir Simulation Toolbox (MRST, SINTEF Digital). All such models contain uncertainties: the exact boundaries of the reservoir are not known, the exact content of oil is not known, the porosity etc. is not known.

To produce oil, a well is drilled and contain numerous horizontal single- or multi-branch, multizone pipes. Oil is then transported into this pipe system, and then to the production platform. Initial investigation indicates that depending on the production operation, the recovery of oil may vary with as much as 50%. With an uncertain description of the system, it is thus believed that advanced control is important in maximizing the oil recovery.

To simplify the description, it may be useful to consider the *black oil* model. The black oil model represents hydrocarbon components (arbitrary number) in (lumped) oil phase, (lumped) gas phase, and water phase. A two-phase oil-water model can be used to represent a heavy oil field, e.g., such as in the Peregrino Field in Brazil.

Previous work:

Zhang, Jianghui (2013). *Improved Oil Recovery through Advanced Control*. M.Sc. thesis at Telemark University College.

Task description:

The following describes the thesis:

1. An overview should be given of an oil well holding black oil, with reservoir, pipes/completion, etc.

2. A simplified 2D control-relevant model of the reservoir with pipes should be developed, and verified, based on the work of Zhang (2013). The model should be implemented in Julia.
3. Model uncertainty should be discussed, and a strategy for providing prediction uncertainty via Monte Carlo simulation should be investigated.
4. Based on the model with uncertainty, some control strategies should be investigated. These could be based on basic PID control, nonlinear control, or model predictive control. The need for state estimation should be studied.
5. If there is time, the developed control strategy for oil recovery should be tested against a detailed model in Eclipse, MRST, or the Julia ModelingToolkit.
6. The work should be documented in a written report (the thesis). It would be advantageous to produce a conference paper, e.g., for SIMS EUROSIM 2021.

Student category: The thesis is suitable for EET, IIA, or PT students with interest in control theory and modeling of dynamic systems.

The task is suitable for online students (not present at the campus): Yes

Practical arrangements:
A working place for the candidate will be offered at University of South-Eastern Norway, Campus Porsgrunn; candidates can choose to sit elsewhere. The candidate will receive information from Equinor ASA.

Supervision:
One-hour weekly supervision meetings are offered (on campus or via MS Teams), as well as feedback on partial reports every 3 weeks, and help with formulating a scientific paper. The last month of the work, the candidate is expected to work independently. In total, this surpasses the 15-20 hours of supervision that the candidate is entitled to.

Signatures:

Supervisor (date and signature): Bernt Lie Feb 2, 2021

Student (write clearly in all capitalized letters): ASHISH BHATTARAI

Student (date and signature): Ashish

Appendix B

List of Codes and Additional Results

All the codes implemented in Julia using Jupyter graphical notebook are available in the following GitHub repository.

`https://github.com/asis643/MS_Thesis_2021.git`

B.1 Implementation of model with fully open ICVs

Jupyter Notebook_1

B.2 Implementation of PI controller in the model

Jupyter Notebook_2

B.3 Implementation of Monte Carlo simulation in model with fully open ICVs

Jupyter Notebook_3

B.4 Implementation of Monte Carlo simulation in model with PI controller

Jupyter Notebook_4

B.5 Calculation of fluid flow distribution at the production well

The bottom hole pressure is manipulated in such a way that the volumetric flow rates through each valve are almost equal. The approximation of bottom hole pressure is done by using the pipe and valve models. After calculating the initial approximated value of bottom hole pressure at the heel of the well, we calculate the pressure drop using a pipe model for the first valve. Then we get the pressure drop and upstream pressure for the first valve. We now calculate the flow contribution given by this valve to the total flow using the valve model. We repeat the same process for the other valves as well.

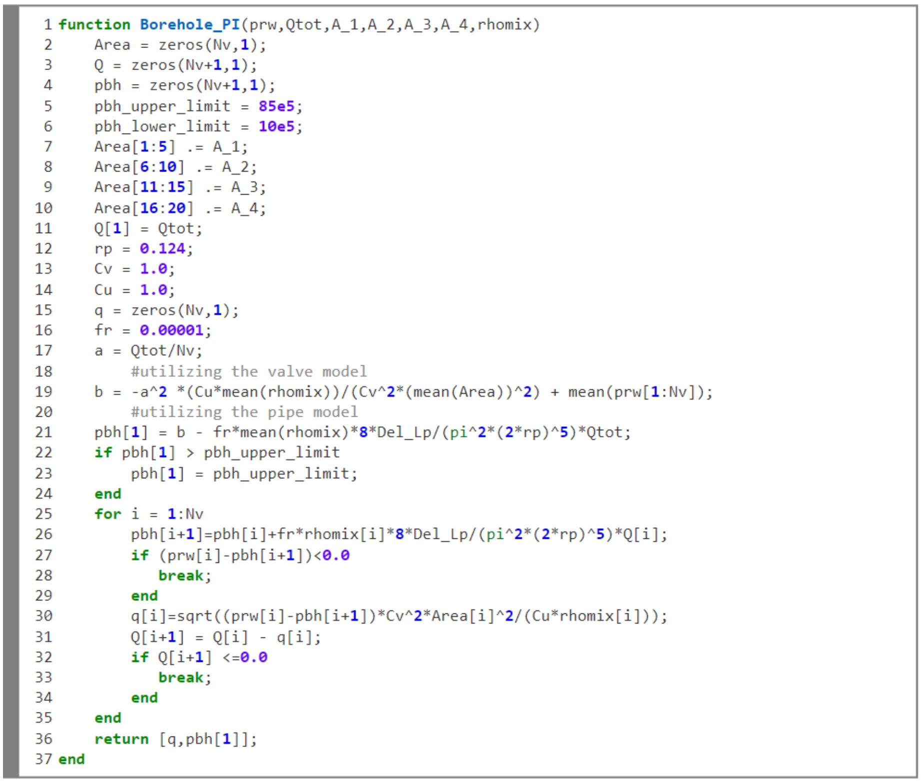

```
function Borehole_PI(prw,Qtot,A_1,A_2,A_3,A_4,rhomix)
    Area = zeros(Nv,1);
    Q = zeros(Nv+1,1);
    pbh = zeros(Nv+1,1);
    pbh_upper_limit = 85e5;
    pbh_lower_limit = 10e5;
    Area[1:5] .= A_1;
    Area[6:10] .= A_2;
    Area[11:15] .= A_3;
    Area[16:20] .= A_4;
    Q[1] = Qtot;
    rp = 0.124;
    Cv = 1.0;
    Cu = 1.0;
    q = zeros(Nv,1);
    fr = 0.00001;
    a = Qtot/Nv;
        #utilizing the valve model
    b = -a^2 *(Cu*mean(rhomix))/(Cv^2*(mean(Area))^2) + mean(prw[1:Nv]);
        #utilizing the pipe model
    pbh[1] = b - fr*mean(rhomix)*8*Del_Lp/(pi^2*(2*rp)^5)*Qtot;
    if pbh[1] > pbh_upper_limit
        pbh[1] = pbh_upper_limit;
    end
    for i = 1:Nv
        pbh[i+1]=pbh[i]+fr*rhomix[i]*8*Del_Lp/(pi^2*(2*rp)^5)*Q[i];
        if (prw[i]-pbh[i+1])<0.0
           break;
        end
        q[i]=sqrt((prw[i]-pbh[i+1])*Cv^2*Area[i]^2/(Cu*rhomix[i]));
        Q[i+1] = Q[i] - q[i];
        if Q[i+1] <=0.0
           break;
        end
    end
    return [q,pbh[1]];
end
```

B.6 Curve fitting for the water saturation and relative permeability data

Jupyter Notebook_5

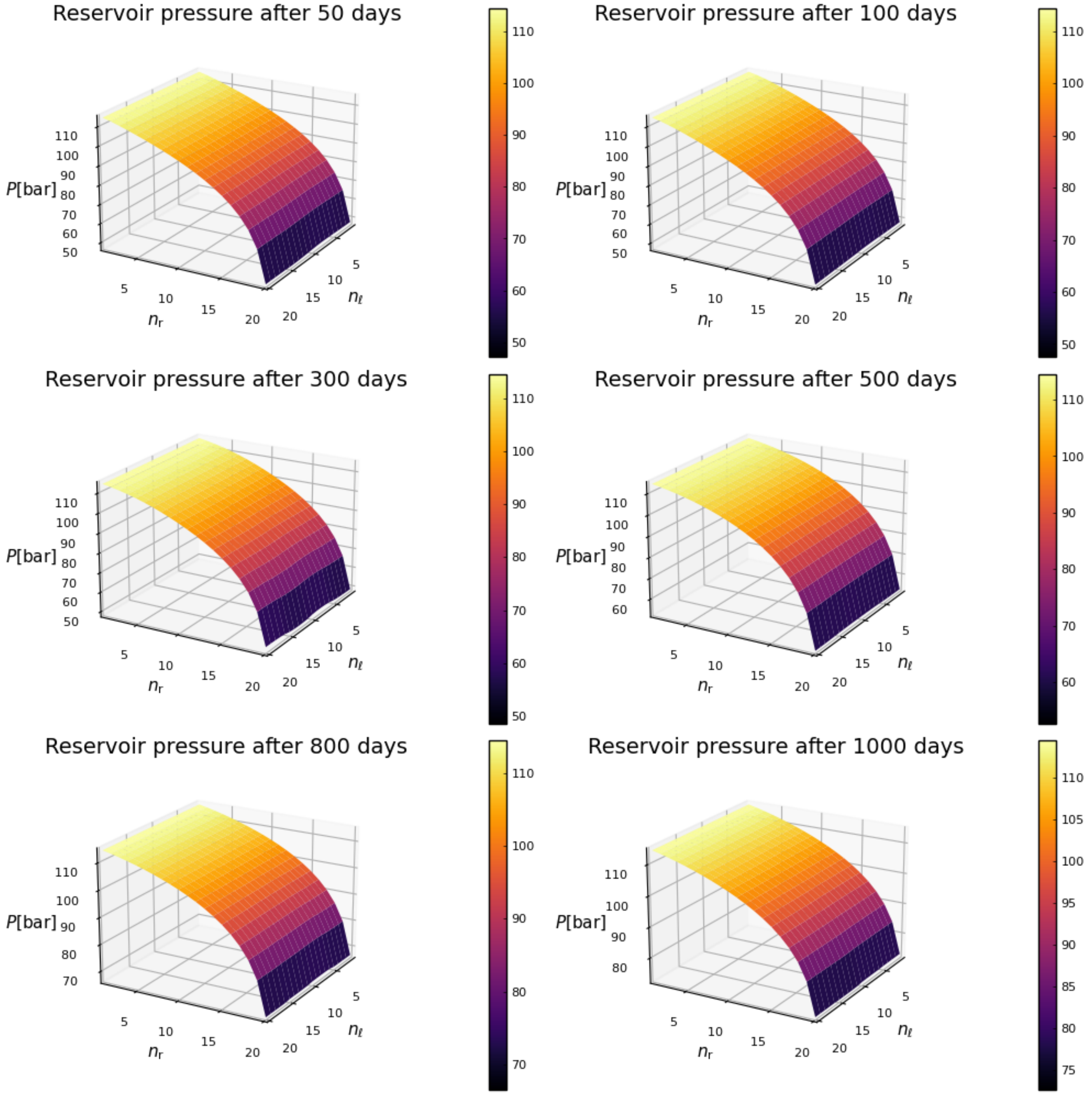

Figure B.1: Pressure profile for model with PI controller.

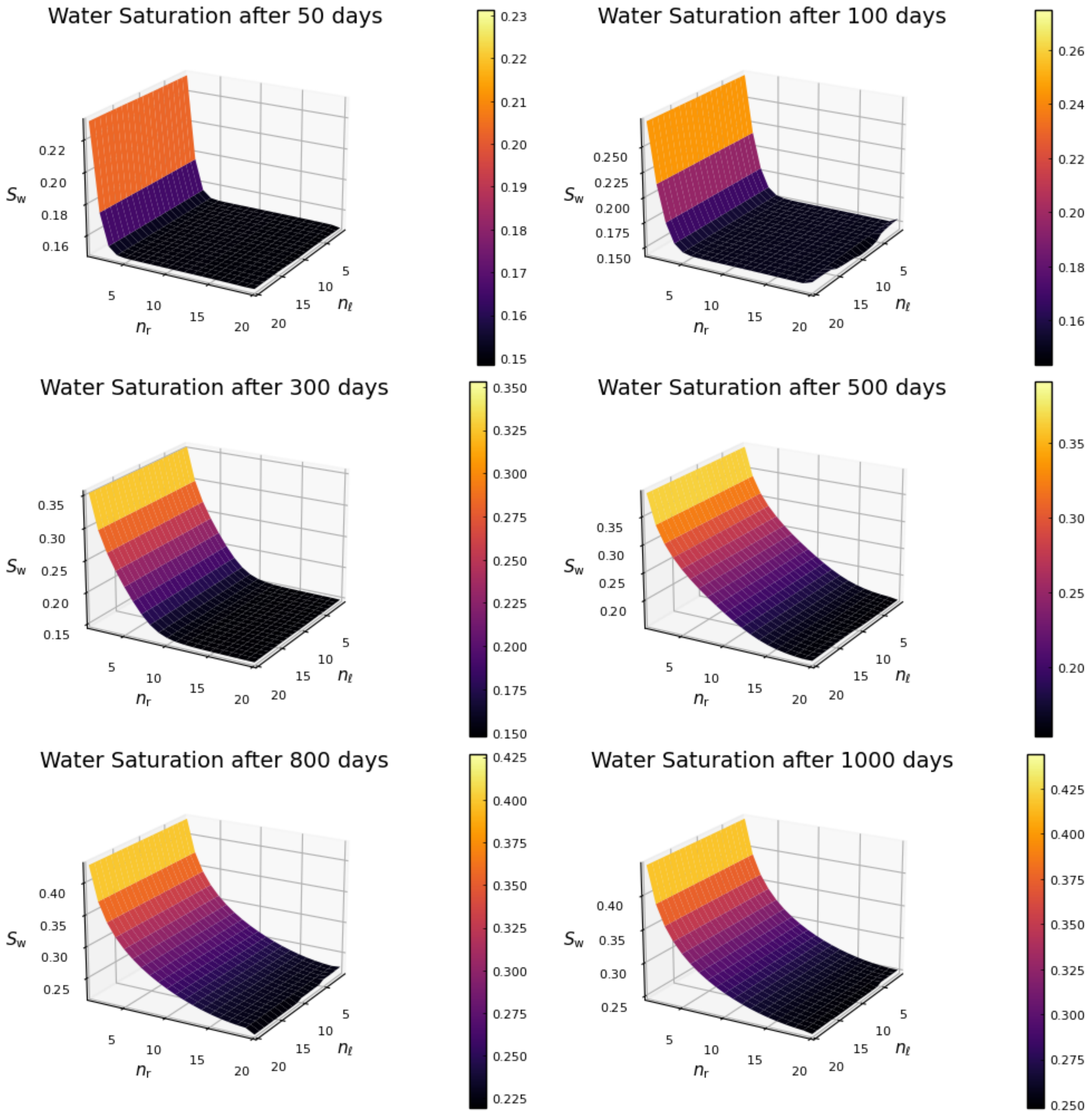

Figure B.2: Saturation profile for model with PI controller.

B.6.1 Pressure and water saturation profiles after implementation of PI controller.

B.6.2 Water saturation and permeability data

S_w	$k_\mathrm{rel,w}$	$k_\mathrm{rel,o}$
0.65	0.2250708	0.00869836
0	0	1
0.0165	0	0.9394007
0.025	0	0.9080903
0.033	0	0.879282
0.0495	0	0.8239987
0.05	0	0.8223931
0.066	0	0.7731554
0.075	0	0.7470281
0.0825	0	0.7260146
0.099	0	0.6819126
0.1	0	0.6793211
0.1155	0	0.6403207
0.125	0	0.6173504
0.132	0	0.6008349
0.1485	0	0.5631531
0.15	0	0.5598066
0.165	0.001805274	0.5270542
0.175	0.002221468	0.5058771
0.1815	0.002527138	0.4923795
0.198	0.003437885	0.4590195
0.2	0.003562836	0.4550606
0.2145	0.004565692	0.426902
0.225	0.005409582	0.4070896
0.231	0.005940281	0.3959838
0.2475	0.007592825	0.3662437
0.25	0.007869965	0.3618399
0.264	0.009555825	0.3376765
0.275	0.01105311	0.3192857
0.2805	0.01186297	0.3102883
0.297	0.01454895	0.284093
0.3	0.01508133	0.27946
0.3135	0.01764925	0.2591083

S_w	$k_\mathrm{rel,w}$	$k_\mathrm{rel,o}$
0.65	0.2250708	0.00869836
0.325	0.02007374	0.2424207
0.33	0.02119994	0.2353535
0.3465	0.02523738	0.2128469
0.35	0.02616042	0.208235
0.363	0.02979794	0.1916038
0.375	0.03346337	0.1769545
0.3795	0.03491768	0.1716354
0.396	0.04063209	0.1529471
0.4	0.04211141	0.1486094
0.4125	0.04697568	0.135538
0.425	0.05222028	0.1231967
0.429	0.05398177	0.1194002
0.4455	0.06168213	0.1045188
0.45	0.06390718	0.1006752
0.462	0.07010683	0.09087132
0.475	0.07727275	0.08096951
0.4785	0.07928404	0.07842837
0.495	0.08923999	0.06715384
0.5	0.09241477	0.06396118
0.5115	0.09999903	0.05700542
0.525	0.1094148	0.04950738
0.528	0.1115839	0.04793525
0.5445	0.124016	0.03989057
0.55	0.1283522	0.0374265
0.561	0.1373164	0.03281457
0.575	0.1492979	0.02752656
0.5775	0.1515063	0.02664707
0.594	0.1666087	0.02132539
0.6	0.1723319	0.01958671
0.6105	0.1826498	0.01678503
0.625	0.1975458	0.01338899
0.627	0.1996613	0.01296043
0.6435	0.217683	0.009785629
0.66	0.2367663	0.007194854
0.675	0.2550908	0.005292373
0.6765	0.2569781	0.005123079
0.693	0.2784065	0.003506498
0.7	0.2878918	0.002942531
0.7095	0.3011662	0.002282941
0.725	0.3238897	0.001438291

S_w	$k_\mathrm{rel,w}$	$k_\mathrm{rel,o}$
0.65	0.2250708	0.00869836
0.726	0.325406	0.001392237
0.7425	0.3513151	0.000776531
0.75	0.3637058	0.00057226
0.759	0.3791262	0.00038058
0.775	0.4081596	0.000157206
0.7755	0.4091031	0.000152041
0.792	0.4414735	$4.18 \cdot 10^{-5}$
0.8	0.4581766	$1.62 \cdot 10^{-5}$
0.8085	0.4761313	$4.63 \cdot 10^{-5}$
0.825	0.5100219	0
0.85	0.5661953	0
0.875	0.6266545	0
0.9	0.6915901	0

S_w	$k_\mathrm{rel,w}$	$k_\mathrm{rel,o}$
0.65	0.2250708	0.00869836
0.925	0.7611952	0
0.95	0.8356658	0
0.975	0.9152003	0
1	1	0